Theses and Dissertations

5-2014

Multi-Physics Modeling of Terahertz and Millimeter-Wave Devices

Mohammad Ali Khorrami
University of Arkansas, Fayetteville

Follow this and additional works at: http://scholarworks.uark.edu/etd

Part of the Engineering Physics Commons

Recommended Citation

Khorrami, Mohammad Ali, "Multi-Physics Modeling of Terahertz and Millimeter-Wave Devices" (2014). *Theses and Dissertations.*
2309.
http://scholarworks.uark.edu/etd/2309

Multi-Physics Modeling of Terahertz and Millimeter-Wave Devices

Multi-Physics Modeling of Terahertz and Millimeter-Wave Devices

A dissertation submitted in partial fulfillment
of the requirements for the degree of
Doctor of Philosophy in Electrical Engineering

By

Mohammad Ali Khorrami
Ferdowsi University of Mashhad
Bachelor of Science in Electrical Engineering, 2004
Amir Kabir University of Technology
Master of Science in Electrical Engineering, 2008

May 2014
University of Arkansas

The dissertation is approved for recommendation to the Graduate Council.

_____
Dissertation Director
Prof. Samir El-Ghazaly

_____   _____
Committee Member   Committee Member
Prof. Greg Salamo   Prof. Hameed Naseem

_____
Committee Member
Dr. Shui-Qing Yu

ABSTRACT

In recent years, there have been substantial efforts to design and fabricate millimeter-wave and terahertz (THz) active and passive devices. Operation of microwave and photonic devices in THz range is limited due to limited maximum allowable electron velocity at semiconductor materials, and large dimensions of optical structures that prohibit their integration into nano-size packages, respectively. In order to address these issues, the application of surface plasmons (SPs) is mostly suggested to advance plasmonic devices and make this area comparable to photonics or electronics.

In this research, the feasibility of implementing THz and millimeter-wave plasmonic devices inside different material platforms including: two-dimensional electron gas (2DEG) layers of hetero-structures, silicon wafers and graphene, are elaborated. To this end, an analytical model is developed to describe the propagation of two-dimensional plasmons along electron gas layers of biased hetero-structures. Using this analytical model, the existence of new plasmonic modes along the biased electron gas is reported for the first time. For an independent verification, a novel multi-physics simulator is developed to analyze active terahertz plasmonic structures. It is also anticipated that the solver can offer novel ideas for guiding the SPs inside the future plasmonic circuits.

In a different approach to design plasmonic devices in a widely used material platform, silicon, a THz modulator is proposed. Using a full wave simulator, it is shown that plasmonic wave can propagate along an indented n-type doped silicon wafer (which is later covered with a metallic layer) with large attenuations. However, the signal losses can be prohibited by applying bias voltages onto the metal as the thickness of the depletion layer between the metal and silicon increases.

At the end, an effective method to couple incident waves onto an infinitely thin graphene mono-layer is presented. As will be illustrated, the surface waves along a corrugated metal can efficiently transit into graphene and successfully launch plasmons.

ACKNOWLEDGEMENTS

Firstly, I would like to thank Prof. Samir El-Ghazaly for encouraging me to perform to the best of my abilities. The author is very grateful for his genuine support, advice and in-depth understanding in every aspect of this research throughout the duration of this dissertation.

The author also wishes to express heartfelt thanks to his other committee members, Prof. Hameed Naseem, Prof. Greg Salamo, and Dr. Shui-Qing Yu for all their advice given towards this dissertation. Also, special thanks go out to the faculty and staff at the University of Arkansas for their commitment to the University and to the students.

DEDICATION

I dedicate my dissertation work especially to my family. A special feeling of gratitude to my loving parents, Mahmood Khorrami and Nahid Rahimi whose words of encouragement and push for tenacity ring in my ears. My wife and my love Maryam Ashgharpour have never left my side and being there for me throughout the doctorate program.

TABLE OF CONTENTS

LIST OF PAPERS

[1] M. A. Khorrami, S. El-Ghazaly, S. Q. Yu, H. Naseem, "Analytical modeling of THz wave propagation inside ungated two dimensional electron gas layers", Int. IEEE Microw. Symp., Baltimore, Jun. 2011.

[2] M. A. Khorrami, S. El-Ghazaly, S. Q. Yu, H. Naseem, "THz plasmon amplification using two-dimensional electron-gas layers", J. Appl. Phys., vol. 111, pp.094501(1)094501-(7), May 2012.

[3] M. A. Khorrami, S. El-Ghazaly, "2D plasmon propagation inside a two-dimensional electron gas layer with a low loss metallic gate," *IEEE Photonic Conference* (IPC 2012), pp. 895-896, San Francisco, Sep. 2012.

[4] M. A. Khorrami, S. El-Ghazaly, H. Naseem, S. Q. Yu, "Global modeling of active terahertz plasmonic devices," *IEEE Trans. Terahertz Sci. Technol.,* vol. 4, no. 1, pp. 101-109.

[5] M. A. Khorrami, S. El-Ghazaly, H. Naseem, S. Q. Yu, "Compact terahertz surface plasmon switch inside a two dimensional electron gas layer," *IEEE International Microwave Symposium* (IMS2012)*,* Montreal, Canada, Jun. 2012.

[6] M. A. Khorrami, S. El-Ghazaly, "Design and analysis of silicon-based terahertz plasmonic switch," *Optics Express,* vol. 21, pp. 25452-25466, Oct. 2013.

[7] M. A. Khorrami and S. El-Ghazaly, "Broadband excitation and active control of terahertz plasmons in graphene," IEEE International Microwave Symposium, Tampa, FL, Jun. 2014.

I. INTRODUCTION

A. TERAHERTZ GAP

Terahertz (THz) frequency band (see Fig. 1), located between microwave and optical ranges (300 GHz – 3 THz), is a gifted but still unknown section of electromagnetic spectrum. THz signal has been utilized in laboratories to find its applications in security and medical areas. For example, it has been employed to demonstrate and recognize explosive materials and weapons, and identify cancer cells and tooth decays [1]. In spite of several unique characteristics and the laboratory level demonstrations, practical application of THz radiation is still challenging. The industrial usage of THz signal is majorly prohibited due to the absence of room-temperature active and passive devices such as sources, detectors, modulators and waveguides. In recent years, there have been considerable studies aiming to close the so called "Terahertz Gap" by designing THz active and passive devices fabricated inside semiconductor and novel materials as graphene [2]-[10]. Operation of semiconductor microwave devices in THz range is physically constrained by the maximum achievable electron velocity. Therefore the design and fabrication of transistors with operating frequencies in THz range is challenging. Traditionally, THz signal is generated by successive multiplication of lower frequency waves obtained by using readily available solid-state power amplifiers [10]. However, this multiplication results into a poor efficiency and therefore a significant loss of the input power. On the other hand, approaching the THz range from photonics is challenging because of the low photon energy (2 meV at 1 THz) and relatively long wavelength (300 μm at 1 THz) that make the nano-fabrication of the room temperature operating photonic devices difficult.
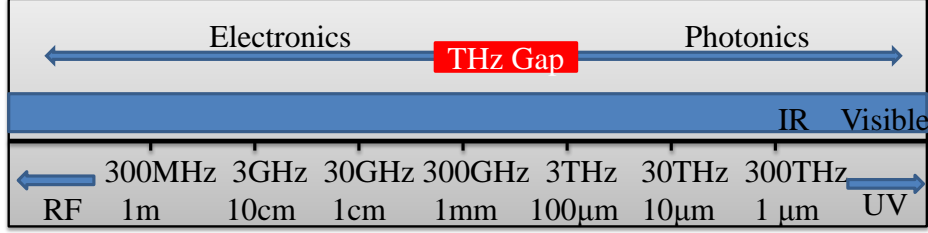
Fig. 1. A representation of the location of THz gap inside electromagnetic spectrum.

B. SURFACE PLASMON AT THE DIELECTRIC/METAL INTERFACE

Surface Plasmons (SPs) are electromagnetic (EM) surface waves propagating at the interface between a dielectric and a conductor, evanescently confined in the perpendicular direction [11]. These surface waves are resulted from the coupling of the EM waves to the electron plasma oscillations of the metal.

The simplest geometry supporting SPs is a flat interface between a dielectric ($z > 0$) and an adjacent metal ($z < 0$) as depicted in Fig. 2. It is assumed that the dielectric and metal are infinitely long in the y and x axis. The dielectric is represented by a relative dielectric constant ε_{r2}. The relative permittivity of the metal is described by using Drude model as $\varepsilon_{r1} = 1 - \omega_p^2/(\omega^2 - j\omega/\tau)$ where ω, j, ω_p and τ are angular frequency, imaginary number, the plasma frequency and the momentum relaxation time of the metal, respectively. The plasma frequency is estimated by $\omega_p = \sqrt{Nq^2/\varepsilon_0 m^*}$, $\varepsilon_0 = 8.85 \times 10^{-12} (F/m)$ where N, m^* and q are electron density, effective mass and unit charge, respectively. Drude model for noble metals has been validated by Johnson and Christy [12] experimentally.

A surface wave on the interface with an evanescent nature along z is described by the wave function:

$$\psi = \begin{cases} \phi_1 \exp\left(j\omega t - \gamma x - \delta_1 z\right) & z \geq 0 \\ \phi_2 \exp\left(j\omega t - \gamma x + \delta_2 z\right) & z < 0 \end{cases} \tag{1}$$

where, $\gamma = \alpha + j\beta$ is the propagation constant. α and β are the attenuation and the phase constants, respectively. To confine the mode along the interface, the real parts of δ_1 and δ_2 must be positive. It is known that the SPs only exist for Transverse Magnetic (TM^x) mode [13]; therefore, the solution of this mode is only considered here.

Dielectric ε_2

H_{y2}

$\otimes$ E_{x2} →

$\otimes$ E_{x1} →

H_{y1}

Metal ε_1
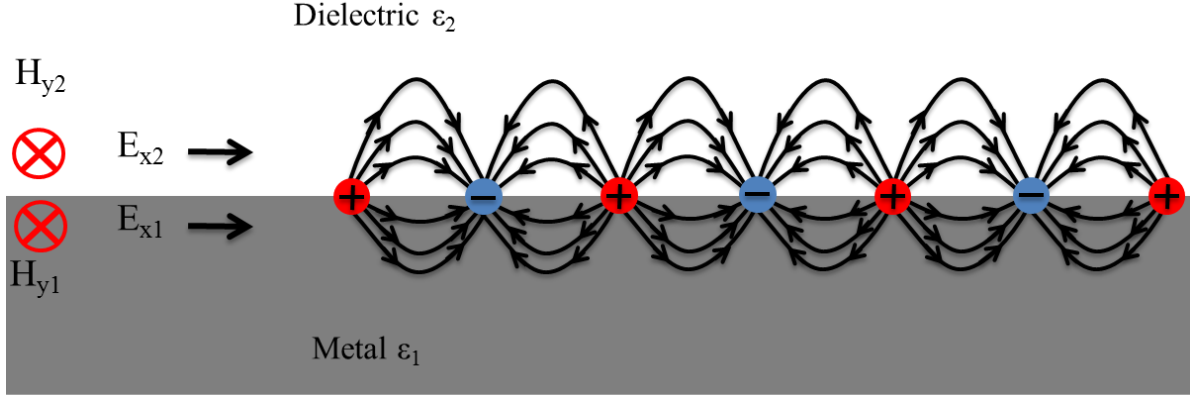
Fig. 2: A geometry showing SPs propagation along the metal/dielectric interface.

An analytical solution of Maxwell equations for the TM^x mode with the wave function (1) will provide the field distribution along the interface. Boundary conditions on the interface are the continuity of tangential component of magnetic and electric fields which result into:

$$\frac{\varepsilon_2}{\varepsilon_1} = -\frac{\delta_2}{\delta_1}. \tag{2}$$

Using (2), It is understood that the real part of ε_{r1} should be negative since ε_{r2} and the real part of δ_2 and δ_1 are positive. This requirement can be satisfied only if the operating frequency is lower than the plasma frequency of the metal. Combining the wave equation (also called Helmholtz equation) $\gamma^2 + \delta_{1,2}^2 + \omega^2\varepsilon_{r1,2}/c^2 = 0$ and (2) yields the dispersion relation of the SPs:

$$\gamma = j\frac{\omega}{c}\sqrt{\frac{\varepsilon_{r1} \times \varepsilon_{r2}}{\varepsilon_{r1} + \varepsilon_{r2}}}. \tag{3}$$

The dispersion relations of SPs on the metal/air interface and the radiative mode counterpart inside the air ($\beta = \omega/c$) are depicted in Fig. 3. As calculating the dispersion relation in Fig. 3,

4

electron scatterings inside the metal are considered negligible ($\omega \times \tau \gg 1$). In this manner, the dispersion relation is obtained from (3) as $\varepsilon_{r2} = 1$, $\varepsilon_{r1} = 1 - (\omega_p / \omega)^2$ and $\gamma = j \times \beta$.

As presented in Fig. 3, SPs gain very large phase constants in the vicinity of the cut-off frequency ($\omega_c = \omega_p / \sqrt{1 + \varepsilon_2}$). Therefore, the plasmons propagate with very small wavelength, compared to the radiating mode counterpart, in these frequency ranges. More details on the characteristics of SPs can be found in [13].
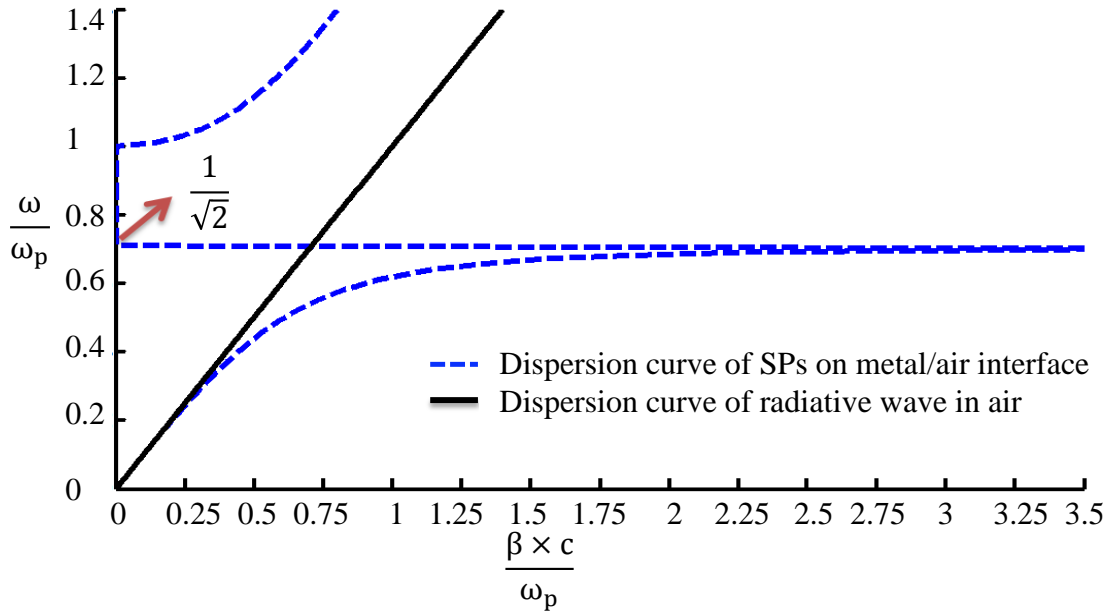
Fig. 3. Dispersion curves of the SPs (dash line) and its radiating mode counterpart inside the dielectric (solid line). We are interested in lower non-radiative section of the SPs' dispersion curve $\omega < \omega_p / \sqrt{1 + \varepsilon_2}$. Large momentum mismatch between SPs and the radiative mode is observed at higher frequencies. Application of specific techniques such as metal gratings or prism coupling is required to excite SPs due to the momentum mismatch.

C.   TWO-DIMENSIONAL PLASMONS

SPs are able to confine EM fields along the interface of a metal and a dielectric over length scales significantly smaller than the wavelength. However, this localization occurs as long as the field oscillates at frequencies close to the described cut-off frequency which is related to ω_p. The

plasma frequency is proportional to the free carrier density N which is in the order of 10^{23} cm^{-3}. This suggests that the plasma frequency is located in the visible range. For typical metals such as gold and silver, SPs are not localized along the interface in THz frequencies and are extended over several wavelengths into the dielectric space above the interface. In order to use SPs in THz frequencies, engineering the surface of the metals by appropriate array of holes [14] or using highly doped semiconductors instead of the metallic surfaces [13] are suggested. In semiconductors, the plasma frequency can be easily controlled by altering the electron density using thermal, optical and electrical gating techniques. This ability can help engineers to design future active plasmonic devices such as modulators. However, SP propagation along doped semiconductors faces large attenuations which is due to electron scatterings. Therefore, the scattering is mostly avoided by employing Two Dimensional Electron Gas (2DEG) layers of hetero-structures or graphene. It is interesting that 2D plasmons inside electron sheets can offer very small wavelengths λ_{2D}, compared to their free space counterparts λ_0 ($\lambda_{2D} < \lambda_0 / 700$) [15], and astonishing field improvements in THz frequencies [16].

   Recently, two-dimensional plasmons along 2DEG layers of High Electron Mobility Transistors (HEMTs) have been employed to fabricate sources and detectors [2]-[10]. These detectors are very promising in terms of performance and integration into compact sizes compared to the other modern ones designed by different concepts [3]. In spite of these advances in the fabrication of THz plasmonic detectors, crystals [16], these structures are still un-matured compared to other photonic and electronic devices and require more advanced techniques for manipulating and amplifying surface wave signals.

D.   ANALYTICAL MODELING OF TWO-DIMENSIONAL PLASMONS

In Fig. 4, two-dimensional plasmons which can propagate along the electron gas layer of the AlGaAs/GaAs HEMT are depicted. The plasmons are excited by a –z going plane wave illuminating the transistor. However, this excitation is possible due to the presence of the metallic gate on the top surface of the structure. The diffracted waves from the metallic gate obtain enough momentum (phase constant) to excite the plasmons.
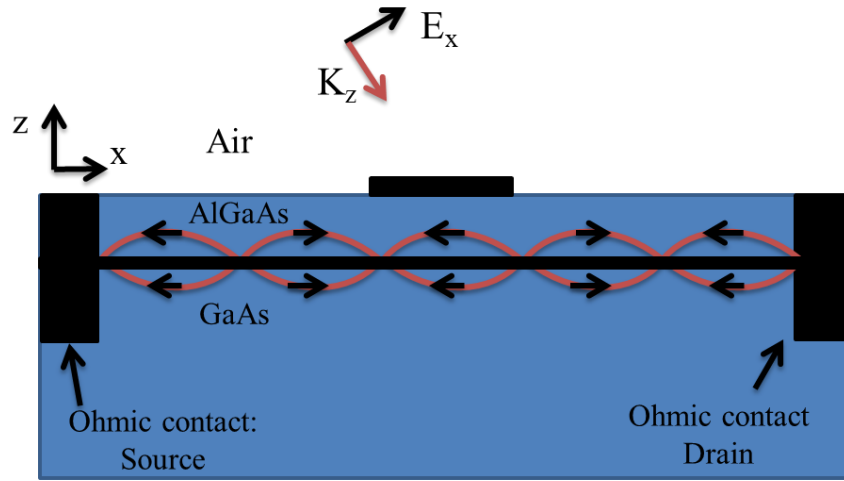
Fig. 4. Two-dimensional plasmons are propagating symmetrically along *x* axis out of the metallic gate. The presence of the Ohmic contacts allows us to apply external bias voltage on the channel and therefore change the properties of the plasmons accordingly.

The presence of two-dimensional plasmons along 2D conductors has been first theoretically predicted and modeled in [17]. To this end, the dispersion relation of the plasmons and its dependence on the conductivity of the conductor has been detailed. Later, similar results with different notations and more in-depth analysis have been presented in [18]. In these analytical formulations [17]-[18], Maxwell equations are solved after applying required boundaries. In this manner, the properties of the plasmons propagating along the 2D conductor are calculated. Later, the real and imaginary conductivity of a two-dimensional electron gas layer of a HEMT at cryogenic temperatures has been measured in [19]. Moreover, a novel distributed lumped

element representation of the electron gas has been proposed in [19]. The distributed model has been employed to describe the properties of the plasmons propagating on the electron gas [19].

In the mentioned researches, the presence of the bias electric field along the channel that can exist as applying the bias voltage has been disregarded. However, it is critical to consider the effects of the applied bias voltage on the properties of plasmons in order to design future plasmonic sources and active detectors. To this end, a solution of Poisson, continuity and Euler equations has been presented in [20]-[21] to include the effects of electron drift velocity, accelerated by an applied bias voltage, in the modeling of modern plasmonic detector and sources. It has been shown analytically that the steady-state dc current in a FET can lead to un-stabilities which can result into plasma oscillations in terahertz frequency range [20]-[21]. Additionally, it has been claimed that this mechanism can lead to the design and fabrication of terahertz and infrared plasmonic sources and detectors [20].

In [22], a small signal analysis of Euler equation (or the so called momentum conservation equation) and continuity equations are employed to include the effects of electron average drift velocity v_0 into the calculated surface conductivity (σ) of 2D electron gas layers as:

$$\sigma = \frac{n_0 q^2}{m^*} \frac{j\omega}{\left(j\omega - v_0\gamma\right)\left(j\omega - v_0\gamma + \dfrac{1}{\tau_m}\right)}, \tag{4}$$

where, n_0, q, m^*, and τ_m are electron: surface density, unit charge, effective mass, and momentum relaxation time, respectively. The detailed calculation of (4) is presented in Appendix I, section A, as it is assumed that the plasmons follow the variations in (1).

In [23], we employed the electron velocity dependent conductivity (4) to calculate the dispersion relation of two-dimensional plasmons along biased electron gas layers. To this end, appropriate boundary conditions are applied and the dispersion relation is obtained as:

8

$$A_1\gamma^4 + A_2\gamma^3 + A_3\gamma^2 + A_4\gamma + A_5 = 0 \qquad (5)$$

Where [23],

$$A_1 = v_0^4, \quad A_2 = -\frac{2v_0^3}{\tau_m} - 4j\omega v_0^3$$

$$A_3 = -6\omega^2 v_0^2 + \frac{v_0^2}{\tau_m^2} + \frac{6j\omega v_0^2}{\tau_m} + 4a^2$$

$$A_4 = 4jv_0\omega^3 + \frac{6v_0\omega^2}{\tau_m} - \frac{2jv_0\omega}{\tau_m^2}$$

$$A_5 = \omega^4 - \frac{\omega^2}{\tau_m^2} - \frac{2j\omega^3}{\tau_m} + \frac{4a^2\omega^2\varepsilon_r}{c^2}$$
$$\qquad (6)$$

As is presented in (5), four new plasmonic modes can propagate along the channel. This is in contrary to other predictions that have assumed that the surface modes along a biased 2D conductor don't change even if there is an external bias electric field. One of the major achievements in this solution is the prediction of an available growing mode along the biased 2D conductor which can lead to the design of a plasmonic terahertz amplifier, if certain impedance matching conditions are implemented [23]-[24].

Although the analytical method presented in [23]-[24] is able to correctly characterize wave propagation along biased 2D conductors, it is still limited by several restrictions. For example, the wave reflections from Ohmic contacts have been disregarded. To obtain a complete picture of electron-wave interactions inside modern plasmonic devices, a more complex model with very limited assumptions is required.

E.   GLOBAL MODELING OF ACTIVE TERAHERTZ PLASMONIC DEVICESs

Global modeling has been previously utilized in the design and analysis of microwave transistors [25]-[27]. Moreover, it has been recently used in the modeling of silicon conductivity in terahertz frequency range [28]. This modeling technique is based on a self-consistent solution of wave propagation and electronic transport equations. In [25]-[27], this is performed by a full

9

wave solution of Maxwell and moments of Boltzmann equations. In this manner, high frequency effects of these devices are completely considered into the simulator. Similar to microwave transistors, the characteristics of wave propagation and the motion of electrons are completely inter-related inside active terahertz plasmonic devices. Therefore, global modeling can also be employed in the analysis and design of modern active plasmonic devices [29].

The wave propagation in a homogenous material can be described by Maxwell equations, with constant material properties ε (permittivity) and µ (permeability) throughout the medium, as:

$$\nabla \times \vec{H} = \varepsilon \frac{\partial \vec{E}}{\partial t} + \vec{J}$$
$$\nabla \times \vec{E} = -\mu \frac{\partial \vec{H}}{\partial t} \qquad (7)$$

In (7), $\vec{E}$ and $\vec{H}$, and $\vec{J}$ are electric and magnetic fields, and electric current density respectively. In [29], we employed finite difference time domain technique to solve (7) with appropriate boundary conditions inside an active terahertz plasmonic device. To estimate the electrons' behavior with respect to an applied external voltage, we utilized moments of Boltzmann equation and Poisson equation. In this manner, the electric current density $\vec{J}$ can be updated at each time step. The numerical schemes employed to solve the electronic transport equations have been listed in Appendix II. In order to couple these two solvers (full wave and electronic transport simulators), physical properties should be transformed properly from one to the other. This becomes possible by feeding the full wave solver with calculated current density by the electronic transport simulator. Additionally, updated electric and magnetic fields are inserted into the electronic transport solver at each time step. This concept is depicted in Fig. 5. Using this numerical solver, the presence of periodic metallic grating of top of the device is characterized in [29]. Moreover, we designed and simulated a novel, fast and efficient terahertz

10

plasmonic switch inside a hetero-structure in [30]. This plasmonic switch is able to operate effectively in THz frequencies with small control voltage.

E, H

| FDTD simulator | Electron Transport solver |

J
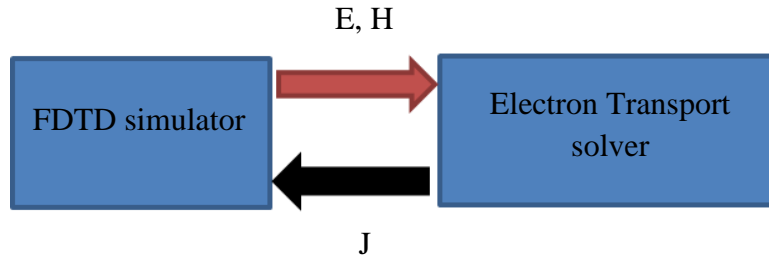
Fig. 5. A schematic of the basics of global modeling simulator employed in the analysis of active plasmonic devices.

F.   SILICON-BASED PLASMONIC TERAHERTZ MODULATOR

Application of modern active devices is critical in the emerging plasmonic area, since these plasmonic components combine low optical losses with high mode confinements [13]. "Active plasmonic" term has been coined first in a paper in 2004 [31], in which a compact active switch has been implemented on the interface of Ga/Au. It has been shown that the propagation of plasmonic waves along the interface can be controlled by applying heat [31]. This is due to the changes in the electrical properties of Ga that happens as the operating temperature varies. However, this methodology is not very promising since heat cannot be applied on a specific surface with an acceptable level of speed. To circumvent the operating speed, other types of modern plasmonic switches with an additional optical source have been developed [32]. In this manner, the material properties of the plasmonic waveguide can be controlled by applying an intense optical source. Similar ideas have been engaged in the design of plasmonic based terahertz modulators on the surface of semiconductors in [33]-[35]. Additionally, the application of electro-optic materials, such as nematic liquid crystals with electrically controllable properties has been introduced in the plasmon-based modulators [36]. However, it is very challenging to employ liquid crystals in modern compact plasmonic devices [36]. Moreover, in terms of

11

integrating electronics and photonics, it would be highly favorable to develop a plasmonic component with the same materials as the rest of a photonic system. In this manner, existing Si and III-V based processing can be used in the fabrication of plasmonic devices [37].

In order to design a plasmonic modulator, there is a need to design an optimized waveguide that can handle and localized waves in THz frequency range. As previously mentioned in section C, surface waves are not bounded to the dielectric/metal interface, in Fig. 2, at this frequency range. Therefore, doped-semiconductors are mostly employed as plasmonic waveguides in this range. Recently, the application of a metallic structure with a periodic array of grooves is proposed in [38] to guide localized plasmons in THz frequencies. In this manner, the effective permittivity of the corrugated metallic surface can be controlled by changing the dimensions and repetition rate of the holes. These waves along the indented surface are mostly called Spoof Surface Plasmon Polaritons (SSPPs). SSPPs have been recently employed in terahertz lasers to focus the generated beam efficiently [39].

The idea of changing the material properties of a semiconductor by changing the depletion depth between the metal and semiconductor has been previously employed to control extraordinary terahertz transmission trough a metallic sheet with sub-wavelength holes [40]. In this manner, the enhanced THz transmission is modulated up to 52% by changing the applied bias voltage, on the Schottky contact between 0 to 16 volts [40]. Additionally, a voltage-controlled, a silicon-based electromagnetic meta-material operating between 75-110 GHz has been experimentally demonstrated in [41]. Similarly, the transmittance of the meta-material can be modulated by applying voltages onto the Schottky contact between the silicon substrate and the deposited gold layer [41].

In [37], we employed the same guiding methodology to design a fast and compact plasmonic

12

switch. This device is designed inside a corrugated lightly-doped silicon wafer covered with gold. In this manner, SSPPs can propagate along the corrugated structure. Moreover, the doping density of silicon wafer can be controlled after applying appropriate control voltages onto the gold layer and an Ohmic contact designed below the active structure. This design leads to a compact THz switch activated by a control voltage. The effectiveness of the plasmonic switch can be determined by considering its isolation in the OFF mode and its insertion loss in the ON state. It is shown that the plasmonic switch with the Schottky contact can obtain insertion losses below 5 dB and isolations above 15 dB between 260-315 GHz [37]. Finally, a more sophisticated design that employs a PIN diode to electrically modify the doping density of the silicon substrate is introduced in [37] which can vastly enhance the operation of the plasmonic switch. It is envisioned that the proposed switches may be useful in future all-integrated silicon-based THz plasmonic devices and communication systems. Specifically, the future generation of very large scale integration (VLSI) chips will pursue the combination of electronic processing and optical communications through fiber optic cables. In order to resolve the coupling problem between optical and electronic components and integrate photonic components with electronic devices in nano-scale dimensions, we proposed the application of the developed plasmonic waveguide and modulator.

G.   GRAPHENE-BASED TERAHERTZ PLASMONIC DEVICES

Graphene is a two-dimensional (2D) form of carbon in which the atoms are arranged in a honeycomb arrangement. Since its extraction from graphite compounds [42], it has attracted numerous researchers both in academia and industry due to its unique mechanical, thermal and electromagnetic properties [43]-[50]. Specifically, the tunability of its electrical conductivity by means of chemical and electrical doping has made graphene a prime candidate for applications in

nano-electronics and nano-photonics [44]. Graphene supports plasmons at terahertz and far-infrared frequency range (0.1-10 THz) [46]. Most importantly, graphene provides an exceptional possibility of plasmon tunability, unlike in metals, because of the mentioned control over its electrical properties. Therefore, graphene is widely being explored to construct future compact on-chip optical devices and circuits.

Fig. 6 depicts a 2D representation of a monolayer graphene linear band structure with different doping types and their related possible optical transitions. As shown in Fig. 6.(a), the Fermi energy level is located exactly in the middle of the conductance and valance band of intrinsic graphene (Dirac point). Moreover, the valance band is completely full of electrons while the conductance band is empty. In the intrinsic graphene, single-photon absorption (inter-band transition) can take place over a very wide frequency range. In Fig. 6.(b), the band structure of an n-doped graphene is depicted. As presented, the Fermi level is above the Dirac point in this case and photons with energy $\bar{h}\omega_2 > (2 \times E_F)$ can only be absorbed by graphene since there is no empty state below this level. The band-structure of a p-type graphene is also presented in Fig. 6.(c). As illustrated, the Fermi level is below the Dirac point in the p-type graphene. Under this condition, graphene cannot absorb photons with energies $\bar{h}\omega_2 < (2 \times E_F)$, since there is not any electron in the valance band above Fermi energy level.

14
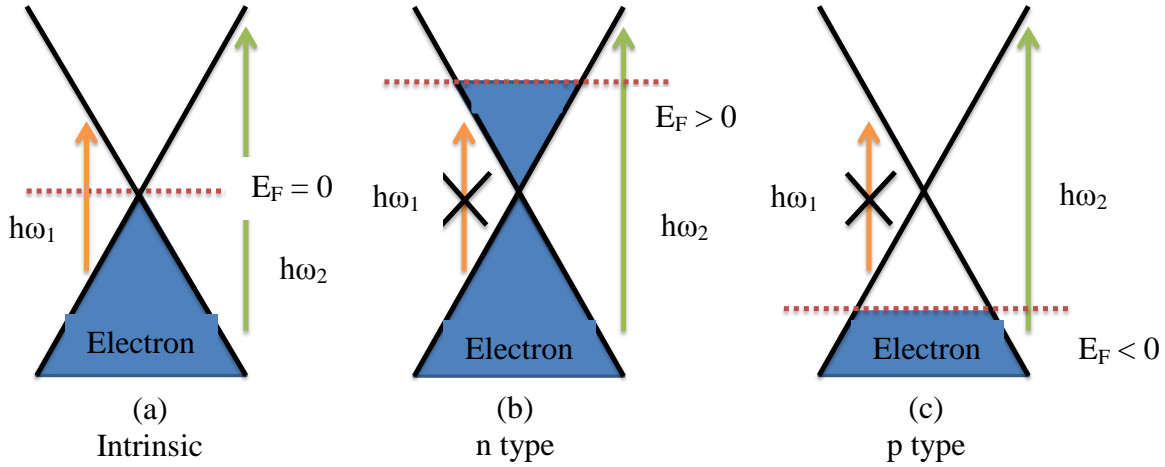
Fig. 6. A 2D schematic of (a) intrinsic, (b) n-type, and (c) p-type monolayer graphene band-structure and their possible optical transitions.

As mentioned, the Fermi energy level of a graphene sheet can be tuned electrically by applying perpendicular electric fields. One method to apply the required electric field is using a back gate as depicted in Fig. 7. To this end, graphene can be placed over an insulator such as silicon dioxide on top of a silicon wafer. An Ohmic contact can be established by depositing a metal on the graphene sheet and applying a bias voltage V_a between the top and back metals as illustrated Fig. 7. In this structure, the thickness and dielectric constant of the insulator are d and ε_r, respectively.
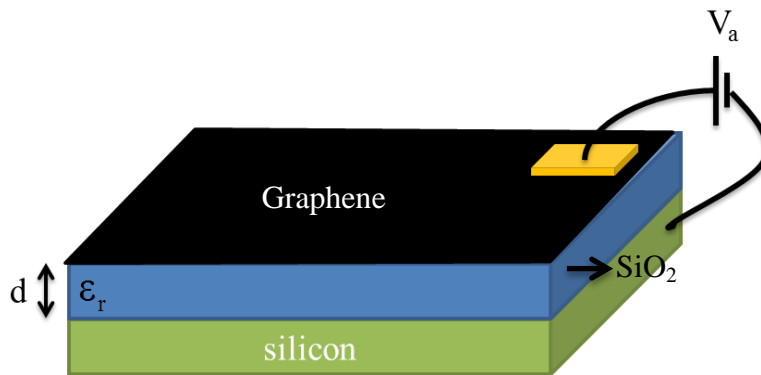
Fig. 7. A simple method to apply perpendicular electric fields on a graphene sheet to electrically control its Fermi energy level.

As detailed in [51], the required control voltage V_a to achieve a specific Fermi energy level E_F

can be calculated from:

$$V_a = \frac{2qd}{\pi \varepsilon_r \varepsilon_0 \bar{h}^2 v_F^2} \int_0^\infty \varepsilon \times \left(F(\varepsilon) - F(\varepsilon + 2E_F) \right) d\varepsilon, \tag{8}$$

where, q (= 1.60216×10^{-19} C), ε, $\bar{h}$ (= 1.054×10^{-34} J.s), and v_F = 10^6 (m / s) are electron unit charge, energy, reduced Planck constant, and graphene Fermi velocity, respectively. In (8), Fermi-Dirac distribution function:

$$F(\varepsilon) = \frac{1}{1 + \exp\left((\varepsilon - E_F)/kT \right)} \tag{9}$$

is used, as k (= 1.38×10^{-23} m^2.kg.s^{-2}.K^{-1}) and T are Boltzmann constant and operating temperature, respectively. To provide an insight into the controllability of the chemical potential of graphene by changing the applied voltage, the required perpendicular electric field for various practical Fermi levels are calculated from (8)-(9) and depicted in Fig. 8 as T = 300 (K) and ε_r = 1 (F / m). As presented, graphene can change from a p-type material to an n-type one by altering the perpendicular electric field. It can be seen that the Fermi energy level can be practically tuned from –1 eV to 1 eV by applying typical values of bias electric fields as the insulator thickness "d" is below one micrometer. The application of larger fields is possible by using thinner insulators. It is worthy to mention that the chemical potential of doped graphene is related to the charge density
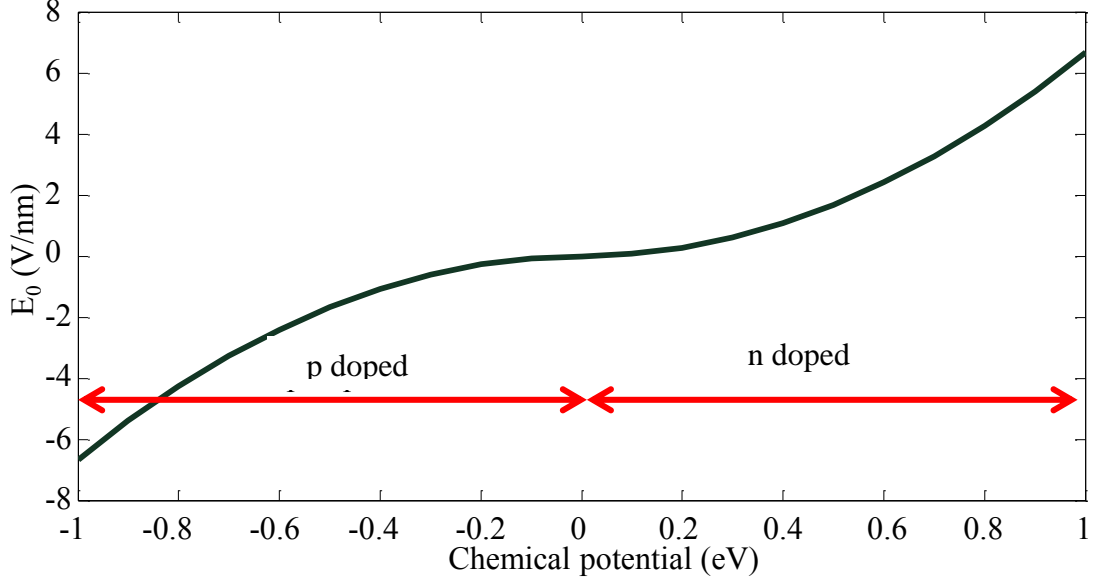
Fig. 8. Fermi level of graphene versus applied perpendicular electric field.

The surface electrical conductivity σ of graphene can be calculated from Kubo formalism [51]. It is famous that the conductivity is affected by two major contributions, namely inter-band σ_{inter} and intra-band σ_{intra} transitions ($\sigma = \sigma_{intra} + \sigma_{inter}$). Using Kubo formalism, it can be calculated that:

$$\sigma_{Intran} = -j\frac{q^2 kT}{\pi \bar{h}^2 (\omega - j2\Gamma)}\left(\frac{E_F}{k_B T} + 2\ln\left(\exp\left(-\frac{E_F}{kT}\right)+1\right)\right)$$

$$\sigma_{Inter} = -\frac{jq^2(\omega - j2\Gamma)}{\pi \bar{h}^2}\int_0^\infty \left[\left(F(-\varepsilon)-F(\varepsilon)\right)\bigg/\left((\omega - j2\Gamma)^2 - 4\left(\varepsilon/\bar{h}\right)^2\right)\right]d\varepsilon \tag{10}$$

where, $\Gamma = 1 / (2 \times \tau)$ and τ is electron momentum relation time. As seen in (10), both inter-band and intra-band conductivities are closely correlated with the chemical potential of graphene and the frequency of the propagating wave. As seen in Fig. 6.(a), intra-band transitions don't exist in pristine graphene since there are not any electron and empty energy level in the conductance and the valance band, respectively. Additionally, the intra-band part will only be relevant in terahertz frequency range as $2E_F > \bar{h}\omega$.

Plasmons along graphene are of described two-dimensional type. The TM^x mode along a graphene mono-layer, which is assumed to be infinite along x and y axis, and located at $z = 0$ plane follows the wave-function:

$$\psi = \begin{cases} \phi_1 \exp\left(j\omega t - \gamma x - \delta z \right) & z \geq 0 \\ \phi_1 \exp\left(j\omega t - \gamma x + \delta z \right) & z < 0 \end{cases} \tag{11}$$

where, γ and δ are propagation constants along x axis and attenuation constant in z direction, respectively. It is assumed that the graphene sheet, with surface conductivity σ, is located in a homogenous material with permittivity ε_r. After solving Maxwell equations and satisfying boundary conditions along the graphene layer, 2D plasmon dispersion relation can be obtained as [23]:

$$\frac{-\sigma}{j\omega} = \frac{2\varepsilon}{\delta} . \tag{12}$$

where, $\varepsilon = \varepsilon_r \times \varepsilon_0$ and ($\varepsilon_0 = 8.85 \times 10^{-12}$ F / m).Using (10), (12) and Helmholtz equation, the dispersion relation of the plasmonic mode can be calculated.

In spite of the mentioned advantages of graphene over conventional metals in THz plasmonic devices, the challenge is how to effectively couple long-wavelength terahertz wave onto an infinitesimally sheet of graphene. This problem specially persists due to the very large mismatch between the wavelengths of the incident radiating waves and the surface waves on graphene. To address this critical challenge, electrically generated surface acoustic waves have been employed to form a diffraction grating [48]. In this manner, the plasmons along graphene are launched without the need to use complicated optical near-field techniques such as those based on scatterings from an atomic force microscope tip. However, this method still relies on an extra acoustic source. In [49], an etched silicon wafer is employed to implement diffractive gratings on which a mono-layer graphene can be later deposit. It is shown that there exists a sharp notch on

the normal incident transmission spectra of the structure as the incident optical wave couples to the graphene plasmonic wave [49]. However, the described methodology is only effective in a narrow frequency bandwidth which is related to the grating period of the etched silicon wafer. Therefore, an urgent need to effectively launch the propagating plasmonic mode along graphene layers in a wide frequency range still exists.

Recently, we have proposed to initially excite electromagnetic wave along a more sophisticated plasmonic structure as a periodically grooved metallic surface. Next, the graphene sheet can be deposited onto the structured metal to transfer the electromagnetic energy to the ultra-thin waveguide [52]. Next, the effectiveness of this method is proved [52] using a full-wave simulation and analytical model.

H.   DISSERTATION STRUCTURE

This dissertation is composed of seven previously published papers. It is an acceptable format by the Graduate school and it is approved by the dissertation chair and the committee before beginning the project. All requirements with regard to this type of submission are elaborated in the official document of the graduate school "The University of Arkansas Graduate School Guide to Preparing Doctoral Dissertations", page 11.

In chapter two, the analytical modeling of plasmon propagation along gated and un-gated electron gas layers is elaborated. This chapter includes three published papers as listed as follows.

[1] M. A. Khorrami, S. El-Ghazaly, S. Q. Yu, H. Naseem, "Analytical modeling of THz wave propagation inside ungated two dimensional electron gas layers", Int. IEEE Microw. Symp., Baltimore, Jun. 2011.

19

[2] M. A. Khorrami, S. El-Ghazaly, S. Q. Yu, H. Naseem, "THz plasmon amplification using two-dimensional electron-gas layers", J. Appl. Phys., vol. 111, pp.094501(1)094501-(7), May 2012.

[3] M. A. Khorrami, S. El-Ghazaly, "2D plasmon propagation inside a two-dimensional electron gas layer with a low loss metallic gate," *IEEE Photonic Conference* (IPC 2012), pp. 895-896, San Francisco, Sep. 2012.

In [1], a summary of different analytical models, found in the literature, which describe the surface wave propagation along un-gated electron gas layers are listed. Besides, an analytical model is developed to characterize 2D plasmon properties along biased electron gas layers of hetero-structure. This representation is based on the solution of Maxwell and Hydrodynamic equations. It is shown that the application of bias voltage drastically changes the characteristics of the surface wave and divides two symmetrical modes into four new asymmetrical ones. Besides, the wave impedances of each mode are illustrated. At last, a simple matching network is introduced that can be useful to effectively launch plasmons along the electron gas.

In [2] an analytical model to investigate the possibility of steering and amplifying terahertz plasmons in gated and un-gated two dimensional electron gas layers by applying a bias electric field is reported. The proposed representation involves a solution of Maxwell and semi-classical electronic transport equations inside the biased structure simultaneously. In [2], the possibility of achieving a plasmonic amplifier inside the un-gated electron gas layer is illustrated. It is shown that certain impedance matching requirements needs to be satisfied before reaching an efficient THz amplifier. Since the properties of the asymmetrical modes along the biased device can be controlled via biasing, proposals of new plasmonic devices such as modulators and switches are also elaborated in [2]. The mentioned analytical investigation is repeated for un-gated electron

gas layers, which similarly shows the division of symmetrical modes inside unbiased device into two asymmetrical ones as the bias electric field is applied. Unlike the un-gated electron gas sheet, it is shown that the amplifying mode may not propagate along the gated one for different bias electric fields.

In [3], perturbation theory is employed to analytically characterize 2D plasmon propagation along gated two dimensional electron gas layers as the attenuations due to the presence of lossy gate are included. In this manner, extra Ohmic losses introduced by the non-ideal metallic gate are taken into account.

In chapter three, the details of the global modeling of active THz plasmonic devices are presented. This chapter includes two published papers as listed as follows.

[4] M. A. Khorrami, S. El-Ghazaly, H. Naseem, S. Q. Yu, "Global modeling of active terahertz plasmonic devices," *IEEE Trans. Terahertz Sci. Technol.,* vol. 4, no. 1, pp. 101-109.

[5] M. A. Khorrami, S. El-Ghazaly, H. Naseem, S. Q. Yu, "Compact terahertz surface plasmon switch inside a two dimensional electron gas layer," *IEEE International Microwave Symposium* (IMS2012)*,* Montreal, Canada, Jun. 2012.

In [4], global modeling is employed to characterize the wave propagation along un-gated biased electron gas layers. In this manner, the existence of new asymmetrical plasmonic modes presented in biased electron gas layers is proved using an independent verification. Moreover, the properties of the plasmons in a biased electron gas beneath a periodic metallic grating are described.

In [5], a fast and compact THz plasmonic switch is designed and simulated using global modeling. It is shown that the switch can provide very high signal isolations with a small control voltage.

In chapter four, the details of the silicon-based THz plasmonic modulator is presented. This chapter includes one published paper as listed as follows.

[6] M. A. Khorrami, S. El-Ghazaly, "Design and analysis of silicon-based terahertz plasmonic switch," *Optics Express,* vol. 21, pp. 25452-25466, Oct. 2013.

In [6], a novel THz plasmonic modulator inside a silicon wafer is designed and simulated. The structure is implemented inside an n-type doped silicon which is periodically corrugated and covered by a gold layer. In this manner, the attenuation of the plasmons, propagating along the indented metallic layer can be controlled by applying control voltages onto the metal and a back-gate that can established beneath the modulator. The application of voltage can change the width of the depletion layer to a great extent. Therefore, THz signal can propagate without large attenuations inside the depleted area.

In chapter five, the details of an efficient method to launch 2D plasmons along graphene is described. This chapter includes one published paper as listed as follows.

[7] M. A. Khorrami and S. El-Ghazaly, "Broadband excitation and active control of terahertz plasmons in graphene," IEEE International Microwave Symposium, Tampa, FL, Jun. 2014.

In [7], a broadband methodology to effectively excite 2D plasmons along a graphene mono-layer at THz frequency range is presented. For this purpose, the plasmon transition from periodically corrugated metals to suspended graphene is investigated. It is shown that the wave transition from one plasmonic waveguide to the next one can be successfully handled in a wide THz frequency range. The analysis is based on a transmission line (TL) representation of two plasmonic waveguides which are connected in series. The accuracy of the TL model is verified by a full-wave numerical solver.

This dissertation includes two appendices. Appendix A includes the details of dispersion

relation calculation of plasmons along un-gated 2D electron gas layers in [2]. In Appendix B, the

discretization details of electronic transport equations in [4] are presented.

References:

[1]   C. M. Armstrong, "The truth about terahertz," *IEEE Spectr.* Vol. 49, no. 9, pp. 36–41, 2012.

[2]   S. J. Allen, D. C. Tsui, and R. A. Logan "Observation of the Two-Dimensional Plasmon in Silicon Inversion Layers," *Phys. Rev. Lett.*, vol. 38, pp. 980-983, March 1977.

[3]   G. C. Dyer, G. R. Aizin, J. L. Reno, E. A. Shaner and S. J. Allen, "Novel tunable millimeter-wave grating-gated plasmonic detectors," *IEEE J. Sel. Topics Quantum Electron.*, vol. 17, no. 1, pp. 85-91, Feb. 2011.

[4]   T. A. Elkhatib, V. Y. Kachorovskii, W. J. Stillman, D. B. Veksler, K. N. Salama, X. Zhang and M. Shur, "Enhanced plasma wave detection of terahertz radiation using multiple high electron-mobility transistors connected in series," *IEEE Trans. Microw. Theory & Tech.*, vol. 58, no. 2, pp. 331-339, 2010.

[5]   V. V. Popov, D. M. Ermolaev, K. V. Maremyanin, N. A. Maleev and V. E. Zemlyakov, "High-responsivity terahertz detection by on-chip InGaAs/GaAs field-effect-transistor array", *Appl. Phys. Lett.*, vol. 98, pp. 153504(1)-153504(3), April 2011.

[6]   J. K. Choi, V. Mitin, R. Ramaswamy, V. A. Pogrebnyak, M. Pakmehr, A. Muravjov, M. Shur, J. Gill, I. Mehdi, B. S. Karasik, and A. Sergeev, "THz Hot-Electron Micro-Bolometer Based on Low-Mobility 2DEG in GaN Heterostructure", *IEEE Sensors Journal*, vol. 13, no. 1, pp. 80-88, Jan. 2013.

[7]   B. Sensale-Rodrigues, L. Liu, P. Fay, D. Jena, and H. Grace, "Power amplification at THz via plasma wave exciation in RTD-gated HEMTs," *IEEE Trans. THz Sci. Technol.*, vol. 3, no. 2, Mar. 2013.

[8]   T. Otsuji, T.Watanabe, S. A. B. Tombet, A. Satou, W. M. Knap, V. V. Popov, M. Ryzhii, and V. Ryhzhii, "Emission and detection of terahertz radiation using two-dimensional electrons in III-V semiconductors and graphene," *IEEE Trans. THz Sci. Technol.*, vol. 3, no. 1, Jan. 2013.

[9]   J. Mateos and T. Gonzalez, "Plasmsa enhanced terahertz rectification and noise in InGaAs HEMTs," *IEEE Trans. THz Sci. Technol.*, vol. 2, no. 5, pp. 562–569, Sep. 2012.

[10]   V. Radisic, K. M. K. H. Leong, X. Mei, S. Sarkozy, W. Yoshida, and W. R. Deal, "Power Amplification at 0.65 THz Using InP HEMTs", *IEEE Trans. Microw. Theory Techn.*, vol. 60, no. 3, March 2012.

[11]   E. Ozbay, "Plasmonics: Merging photonics and electronics at nanoscale dimensions," *Science*, vol. 311, pp. 189-193, Jan. 2006.

[12]   P. B. Johnson and R. W. Christy, "Optical constants of nobel metals," *Phys. Rev. B,* vol. 6, pp. 4370-4379, Jul. 1972.

[13]   S. A. Maier, *Plasmonics: Fundamentals and applications,* Springer, 2007.

[14]   J. B. Pendry, L. Martin-Moreno, F. J. Garcia-vidal, "Mimicking surface plasmons with structured surfaces", *Science,* vol. 305, pp. 847-848, Aug. 2004.

[15]   W. F. Andress, H. Yoon, K. Y. M. Yeung, L. Qin, K. West, L. Pfeiffer and D. Ham, "Ultra-subwavelength two-dimensional plasmonic circuits", Nano Lett., vol. 12, pp. 2272-2277, Apr. 2012.

[16]   H. Yoon, K. Y. M. Yeung, V. Umansky and D. Ham, "A Newtonian approach to extraordinary strong negative refraction", nature, vol. 488, pp. 65-69, Aug. 2012.

[17]   F. Stern, "Polarizability of a two-dimensional electron gas," *Phys. Rev. Lett.,* vol. 18, no. 14, Apr. 1967.

[18]   M. Nakayama, "Theory of surface waves coupled to surface carriers," *J. of the Phys. Soc. of Japan*, vol. 36, no. 2, Feb. 1974.

[19]   P. J. Burke, I. B. Spielman, J. P. Eisenstein, and L. N. Pfeiffer, "High frequency conductivity of the high-mobility two-dimensional electron gas," App. Phys. Lett., vol. 76, no. 6, pp. 745–747, Feb. 2000.

[20]   M. Dyakonov, and M. Shur, "Shallow water analogy for a ballistic field effect transistor: new mechanism of plasma wave generation by dc current," *Phys. Rev. Lett.,* vol. 71, no. 15, pp. 2465-2468, Oct. 1993.

[21]   M. Dyakonov and M. Shur, "Detection, mixing, and frequency multiplication of Terahertz radation by two-dimensional electron fluid," *IEEE Trans. Electron Devices*, vol. 43, no. 3, pp. 380–387, Mar. 1996.

[22]   S. A. Mikhailov, "Plasma instability and amplification of electromagnetic waves in low-dimensional electron systems," Phys. Rev. B, vol. 58, no. 3, pp. 1517–1532, Jul. 1998.

[23]   M. A. Khorrami, S. El-Ghazaly, S. Q. Yu, H. Naseem, "THz plasmon amplification using two-dimensional electron-gas layers", J. Appl. Phys., vol. 111, pp.094501(1)094501-(7), May 2012.

[24]   M. A. Khorrami, S. El-Ghazaly, S. Q. Yu, H. Naseem, "Analytical modeling of THz wave propagation inside ungated two dimensional electron gas layers", Int. IEEE Microw. Symp., Baltimore, Jun. 2011.

[25]   M. A. Alsunaidi, S. M. S. Imtiaz and S. El-Ghazaly, "Electromagnetic wave effects on microwave transistors using a full-wave high-frequency time-domain model", *IEEE Trans. Microw. Theory,* vol. 44, no. 6, pp. 779-808, Jun. 1996.

[26]   R. O. Grondin, S. El-Ghazaly and S. Goodnick, "A review of global modeling of charge transport in semiconductors and full-wave electromagnetics", *IEEE Trans. Microw. Theory & Tech.,* vol. 47, no. 6, pp. 817-829, Jun. 1999.

[27] S. M. Sohel Imtiaz and S. M. El-Ghazaly, "Global modeling of millimeter-wave circuits: Electromagnetics simulation of amplifiers," IEEE Trans. Microwave Theory Tech, vol. 45, pp. 2208–2216, Dec. 1997

[28] K. J. Willis, S. C. Hagness and I. Knezevic, "Terahertz conductivity of doped silicon calculated using the ensemble Monte Carlo/finite-difference time-domain simulation technique", *Appl. Phys. Lett.*, vol. 96, p. 062106, Feb. 2010.

[29] M. A. Khorrami, S. El-Ghazaly, H. Naseem, and S. Q. Yu, "Global modeling of active terahertz plasmonic devices," *IEEE Trans. on THz Sci. & Technol.*, vol. 4, no. 1, pp. 101-109, Jan. 2014.

[30] M. A. Khorrami, S. El-Ghazaly, S. Q. Yu, H. Naseem, "A novel THz plasmonic switch," *2012 IEEE Int. Microwave Symp. Dig.*, Montreal, Canada, Jun. 2012.

[31] A. V, Krasavin, and N. Zheludev, "Active plasmonics: Controlling signals in Au/Ga waveguide using nanoscale structural transformations," *Appl. Phys. Lett.,* vol. 84, pp. 1416-1418, Nov. 2004.

[32] K. F. MacDoland, Z. L. Samson, M. I. Stockman, and N. I. Zheludev, "Ultrafast active plasmonics," *Nature Photonics,* vol. 3, pp. 55-58, Dec. 2009.

[33] J. Gomez Rivas, J. A. Sanchez-Gil, M. Kuttge, P. H. Bolivar, and H. Kurz, "Optically switchable mirrors for surface plasmon polaritons propagating on semiconductor surfaces," *Phys. Rev. B,* vol. 74, p. 245324, Dec. 2006.

[34] J. A. Sanchez-Gil, and J. G. Rivas, "Thermal switching of the scattering coefficients of terahertz surface plasmon polaritons impinging on a finite array of subwavelength grooves on semiconductor surfaces," *Phys. Rev. B.,* vol. 73, p. 205410, May 2006.

[35] E. Hendry, M. J. Lockyear, J. Gomez Rivas, L. Kuipers, and M. Bonn, "Ultrafast optical switching of the THz transmission through metallic subwavelength hole arrays," *Phys Rev. B,* vol. 75, p. 235305, Jun. 2007.

[36] K. Song, and P. Mazmuder, "Active terahertz spoof surface plasmon polariton switch comprising the perfect conductor metamaterial," *IEEE Trans. on Elect. Devices,* vol. 56, p. 2792, Nov. 2009.

[37] M. A. Khorrami, and S. El-Ghazaly, "Design and analysis of a silicon-based terahertz plasmonic switch," *Optics Express*, vol. 21, no. 21, pp. 25452-25466, Oct. 2013.

[38] J. B. Pendry, L. Martin-Moreno, and F. J. Garcia-Vidal, "Mimicking plasmons with structured surfaces," *Science,* vol. 35, pp. 847-848, Jul. 2004.

[39] N. Yu, Q. J. Wang, M. A. Kats, J. A. Fan, S. P. Khanna, L. Li, A. Giles Davis, E. H. Linfield, and F. Capasso, "Designer spoof surface plasmon structures collimate terahertz laser beams," *nature materials,* vol. 9, pp. 730-735, Aug. 2010.

[40] H. T. Chen, H. Lu, A. K. Azad, R. D. Averitt, A. C. Gossard, S. A. Trugman, J. F. O'Harra and A. J. Taylor, "Electric control of extraordinary terahertz transmission through subwavelength metal hole arrays", *Opt. Exp.*, vol. 16, no.11, pp. 7641-7648, May 2008.

[41] Y. Urzhumov, J. S. Lee, T. Tyler, S. Dhar, V. Nguyen, N. M. Jokerst, P. Schmalenberg, and D. R. Smith, "Electronically reconfigurable metal-on-silicon metamaterial," *Phys. Rev. B.,* vol. 86, p. 075112, Aug. 2012.

[42] K. S. Novoselov, A. K. Geim, S. V. Morozov, D. Jiang, Y. Zhang, S. V. Dubonos, I. V. Grigorieva, and A. A. Firsov, "Electric field effect in atomically thin carbon films," *Science,* vol. 306, pp. 666-669, 2004.

[43] F. Schwierz, "Graphene transistors," *Nature Nanotechnologey,* vol. 5, pp. 487-496, Jul. 2010.

[44] L. Ju, B. Geng, J. Horng, C. Girit, M. Martin, Z. Hao, H. A. Bechtel, X. Liang, A. Zettl, Y. R. Shen and F. Wang "Graphene plasmonics for tunable terahertz metamaterials" Nature Nanotech., vol. 6, pp. 630-634, Sep. 2011.

[45] L. Vicarelli1, M. S. Vitiello1, D. Coquillat, A. Lombardo, A. C. Ferrari,W. Knap, M. Polini, V. Pellegrini and A. Tredicucci, "Graphene field-effect transistors as room-temperature terahertz detectors", Nature Materials, vol. 11, pp. 865-871, April 2012.

[46] J. S. Gomez-Diaz, and J. Perruisseau-Carrier, "Graphene-based plasmonic switches at near infrared frequencies," *Optics Exp.,* vol. 21, pp. 15490-15504, Jun. 2013.

[47] V. W. Brar, M. S. Jang, M. Sherrott, J. J. Lopez, and H. A. Atwater, "Highly confined tunable mid-infrared plasmonics in graphene nanoresonators", *Nano Lett.,* Apr. 2013.

[48] J. Schiefele, J. Pedros, F. Sols, F. Calle, and F. Guinea, "Coupling light into graphene plasmons through surface acoustic waves," *Phys. Rev. Lett.*, vol. 111, p. 237405, Dec. 2013.

[49] W. Gao, J. Shu, C. Qiu, and Q. Xu, "Excitation of plasmonic waves in graphene by guided-mode resonances," *ACS Nano,* vol. 6, no. 9, pp. 7806-7813, Aug. 2012.

[50] W. Gao, G. Shi, Z. Jin, J. Shu, Q. Zhang, R. Vajtai, P. M. Ajayan, J. Kono, and Q. Xu, "Exciation and active control of propagating surface plasmon polaritins in graphene," Nano Lett., vol. 13, pp. 3698-3702, Jul. 2013.

[51] G. W. Hanson, "Dyadic Green's function for an anistropic non-local model of biased graphene," *IEEE Trans. on Antenas. Propag.*, vol. 56, no. 3, pp. 747-757, Mar. 2008.

[52] M. A. Khorrami and S. El-Ghazaly, "Broadband excitation and active control of terahertz plasmons in graphene," *IEEE International Microwave Symposium,* Tampa, FL, Jun. 2014.

II.   THZ PLASMON PROPAGATION ALONG TWO DIMENSIONAL ELECTRON-GAS LAYERS

A.   ANALYTICAL MODELING OF THZ WAVE PROPAGATION INSIDE UN-GATED TWO DIMENSIONAL ELECTRON GAS LAYERS

Int. IEEE Microw. Symp., Baltimore, Jun. 2011.

Abstract:

   Plasma wave propagation along an un-gated two Dimensional Electron Gas (2DEG) layer of a hetero-structure is studied. It is shown that the wave can be useful in amplification of THz signals. An analytical solution of Maxwell and Hydrodynamic equations is presented. This method provides an insight into electromagnetic modes allowed to propagate along the 2DEG as electrons are in motion with constant average drift velocity. Besides, wave impedances of the modes are illustrated. Afterwards, a simple matching network design for input and output ports of the 2DEGs is developed.

Introduction:

Detection and generation of THz signals with the aid of plasma waves inside two Dimensional Electron Gas (2DEG) layers of High Electron Mobility Transistors (HEMTs), have been observed in several experiments [1]-[2]. Also, several theoretical models have been proposed to describe these observations [3]-[5]. In [3], plasma wave and shallow water equations are compared and a THz wave generation is predicted in a gated 2DEG layer of a HEMT with open and short circuited drain and source, respectively. The model is used to explain the THz wave generation and (resonant and non-resonant) detection in gated 2DEG of HEMT. Recently, a room temperature THz source implemented in an AlGaN/GaN based HEMT, tunable with gate voltage between 0.75 to 2.1 THz, has been reported [2]. On the other hand, plasma wave resonances in un-gated 2DEG layers have also been proposed in [4] with the same boundary conditions as in [3].

In [3] and [4], modeling of the plasma wave propagation is executed by solving Poisson and Hydrodynamic equations (Euler and continuity). This solution is correct because the wavelength of the plasma wave and the device dimensions are much smaller than transverse electromagnetic wavelength at the same frequency [5]. However, it is not able to describe the mechanism of the wave amplification exactly because no in depth field analysis is performed. Therefore, the specific boundary conditions are introduced to establish the energy transfer from the bias source to the plasma wave. Besides, a simple and direct design procedure is not viable through the method.

In this paper, the plasma wave propagation along an un-gated 2DEG in the presence of drift current is studied. A method based on a solution of Maxwell equations coupled with the Hydrodynamic one is used to define the wave characteristics. To this end, the 2DEG is treated as

a charge sheet positioned at the interface of two wide and narrow band-gap semiconductors. Next, the coupling of the 2DEG carriers to plasma waves is simply taken into account by introducing surface currents on the sheet as Maxwell equations are satisfied. To consider drift motions of electrons induced by bias source, linearization of Hydrodynamic equations is used to reflect the movement into the surface conductivity. This helps us perform an exact propagation mode analysis and define required conditions for the wave amplification. Also, a propagation impedance investigation is done that facilitates further design of a matching network required for an efficient THz amplifier.

Dispersion relation calculation in the presence of drift current:

Consider a 2DEG layer placed at $z = 0$ plane and embedded inside a semi-infinite hetero-structure as in Fig. 1. There is also a constant motion of electrons along the 2DEG toward $+x$, characterized by the average electron drift velocity v_0.
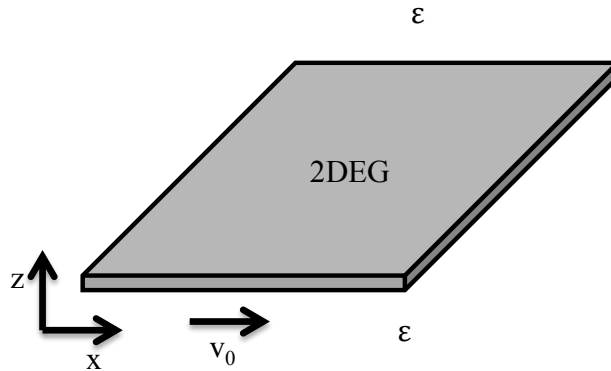
Fig. 1. Schematic view of a 2DEG layer implemented in a hetero-structure (not shown) with a constant average drift electron velocity

While developing the solution for the plasma wave propagation along x axis, it has been shown that TE^x mode does not exist if the 2DEG surface and the surrounding media are isotropic [6]. Therefore, electromagnetic field equations and the related dispersion relations are presented just for non-radiative TM^x case. Here, relative permittivities of the wide and narrow band-gap

semiconductors are assumed to be equal ε_r.

Accordingly, wave function and field formulations for $z \geq 0$ part are:

$$\psi = \phi \exp\left(j\omega t - \gamma x - \delta z\right) \tag{1}$$

where $\gamma = \alpha + j\beta$ and

$$E^x = -\frac{\delta^2}{j\omega\varepsilon}\psi, \; E^z = \frac{\gamma\delta}{j\omega\varepsilon}\psi, \; H^y = -\delta\psi \tag{2}$$

$$E^y = H^z = H^x = 0.$$

From Helmholtz equation, it is obtained that:

$$\delta^2 + \gamma^2 + \frac{\varepsilon_r \omega^2}{c^2} = 0 \tag{3}$$

where $\varepsilon = \varepsilon_0 \varepsilon_r$ ($\varepsilon_0 = 8.85 \times 10^{-12} \, F/m$, $c = 3 \times 10^8 \, m/s$). Continuity of tangential component of the electric field along the interface $E^x\big|_{z=0}$ is the first boundary condition. Second boundary condition is simply acquired by relating surface current $J^x = \hat{z} \times \left(H^y\big|_{z=0^+} - H^y\big|_{z=0^-}\right)$ to the tangential electric field by $J^x = \sigma E^x\big|_{z=0}$, where σ is the xx component of surface conductivity tensor. Considering the boundary conditions, it is derived that:

$$-\frac{\sigma}{j\omega} = \frac{2\varepsilon}{\delta}. \tag{4}$$

In [6], the surface conductivity approximation from Drude model $\sigma = \frac{n_0 q^2}{j\omega m^*}$ is replaced into (3) and the dispersion relation of a normal mode of propagation is attained from (3) and (4) as:

$$\gamma = \pm j \frac{\omega^2}{2a} \tag{5}$$

Where $a = \frac{n_0 q^2}{4\varepsilon m^*}$.

Here, in order to take the electron motion into consideration a new surface conductivity but not the value from Drude model approximation is employed. To this end, the surface conductivity model developed in [7] is used. In [7], linearization of Hydrodynamic equations (Euler and continuity) is performed to include the carrier movement. Hydrodynamic equations are well known to be valid as the mean-free path for electron-electron collision is smaller than the device length and the mean-free path for scatterings from phonons and impurities [3]. Electrons in the 2DEG layers simply satisfy these two conditions. Conductivity of the 2DEG layer in the presence of the electrons motion has been obtained with the aid of the linearization in [7] as:

$$\sigma = \frac{n_0 q^2}{m^*} \frac{j\omega}{\left(j\omega - v_0\gamma\right)\left(j\omega - v_0\gamma + \dfrac{1}{\tau}\right)} \tag{6}$$

where m^*, n_0, q and τ are electron effective mass, 2DEG electron density at steady state condition, unit charge ($q = 1.6 \times 10^{-19} C$) and momentum relaxation time, respectively.

In a collision-less case ($\gamma v_0 \gg \dfrac{1}{\tau}$), by replacing (4) and (6) into (3):

$$\gamma^2 + \frac{1}{4a^2}\left(j\omega - v_0\gamma\right)^4 + \frac{\omega^2 \varepsilon_r}{c^2} = 0 \tag{7}$$

is derived. In the THz frequencies, (7) can be reduced to:

$$-4a^2\gamma^2 = \left(j\omega - v_0\gamma\right)^4 \tag{8}$$

and therefore, four different modes with dispersion relations of:

$$\gamma_{1,2} = j\frac{\left(a + v_0\omega\right) \pm \sqrt{a^2 + 2av_0\omega}}{v^2_0}$$

$$\gamma_{3,4} = j\frac{\left(-a + v_0\omega\right) \pm \sqrt{a^2 - 2av_0\omega}}{v^2_0}. \tag{10}$$

are obtained. It means that the normal TM^x mode of propagation along the surface of the 2DEG, with the dispersion relation (5), is divided into four different modes as electrons are moving with the constant average drift velocity. It can be shown that the collision-less condition is not a critical one, and the four modes still can exist with slight changes as collisions are also included. From now to the end, only the collision less case is explained and the collision effects will be covered in a separate paper.

To finish the analysis, the wave impedance along the 2DEG $Z^x = -\dfrac{E^z}{H^y}$ is also calculated for each mode as:

$$Z_{1,\dots,4}{}^x = \frac{\gamma_{1,\dots,4}}{j\omega\varepsilon}. \tag{11}$$

Characteristics of each mode

It is obvious (from (10)) that for frequencies lower than $\omega_{bf} = a/2v_0$ (named breaking frequency afterwards) all four modes are purely propagating since their propagation constants are imaginary. With typical value of a and v_0, first two modes are propagating toward $+x$ while the other two are moving in the opposite direction. Also, it can be shown that the second mode has a similar behavior to the normal mode as the electron drift is not included. For frequencies above ω_{bf}, the propagation constants of the third and fourth modes are complex numbers and have attenuation constant (positive or negative). In other words, as a plasma wave is launched properly along the 2DEG at frequency ranges above ω_{bf}, energy is being transferred between the bias source and the electromagnetic wave as being amplified or attenuated. It is obvious that ω_{bf} can be controlled by changing the 2DEG charge density and the electron drift velocity. Obviously, the mechanism of energy transfer still needs more investigations. Perhaps, a complete

analysis based on a time domain full wave model in conjunction with Boltzmann equations should be performed for better understanding.

The separation of the normal mode into four new modes is very similar to what has been proposed in travelling wave tubes [8]. A traveling wave tube is basically composed of a slow wave structure as a helix and an electron beam. As the electron beam is passed through the helix, the normal propagation mode is divided into three different modes of growing, attenuating and propagating ones [8].

Discussion of a specific example

In this section, the characteristics of the four propagation modes is investigated for a 2DEG created at the interface of InGaAs/InP with $n_0 = 0.3 \times 10^{12} cm^{-2}, v_0 = 2 \times 10^7 \ cm/s$ and electron effective mass $0.042 m_0 \left(m_0 = 9.1 \times 10^{-31} kg \right)$. Besides, relative permittivity of both InGaAs and InP are assumed to be equal $\varepsilon_r = 12.6$.

With these values, calculated attenuation and phase constants (α and β) of the four modes are shown in Fig. 2 and Fig. 3 for frequency range of 300GHz up to 3 THz. As depicted in Fig. 2, the two first modes are propagating along the electron drift velocity $+x$ while the two last modes are in the opposite direction $-x$. As shown in Fig. 3, the first and second modes are merely propagating ones but the third and fourth modes can have attenuation term as soon as operating frequency is higher than ω_{bf}. From the propagation direction of each mode and the sign of the attenuation constants, it is clear that the third mode is an attenuating mode while the fourth one is an amplifying mode.

In Fig. 4, phase velocity of each mode normalized to the drift velocity is shown. As depicted, the first mode is the slowest and the second one is the fastest. Also, notice that ω_{bf} is the point

which the phase velocities of the third and the fourth modes become equal to the drift velocity.

Next, magnitude of real part of wave impedances normalized to vacuum wave impedance $Z_0 = 377\Omega$, are illustrated in Fig. 5. As shown in Fig. 5, the real parts of the third and fourth modes are equal at the frequencies higher than ω_{bf}.

In Fig. 6, imaginary part of the wave impedances normalized to Z_0 are presented. As seen, the first two modes do not have imaginary part. Additionally, last two modes have complex wave impedance for frequencies above ω_{bp}. After this point, third mode has inductive impedance while the fourth one is highly capacitive considering that they both propagate toward $-x$.
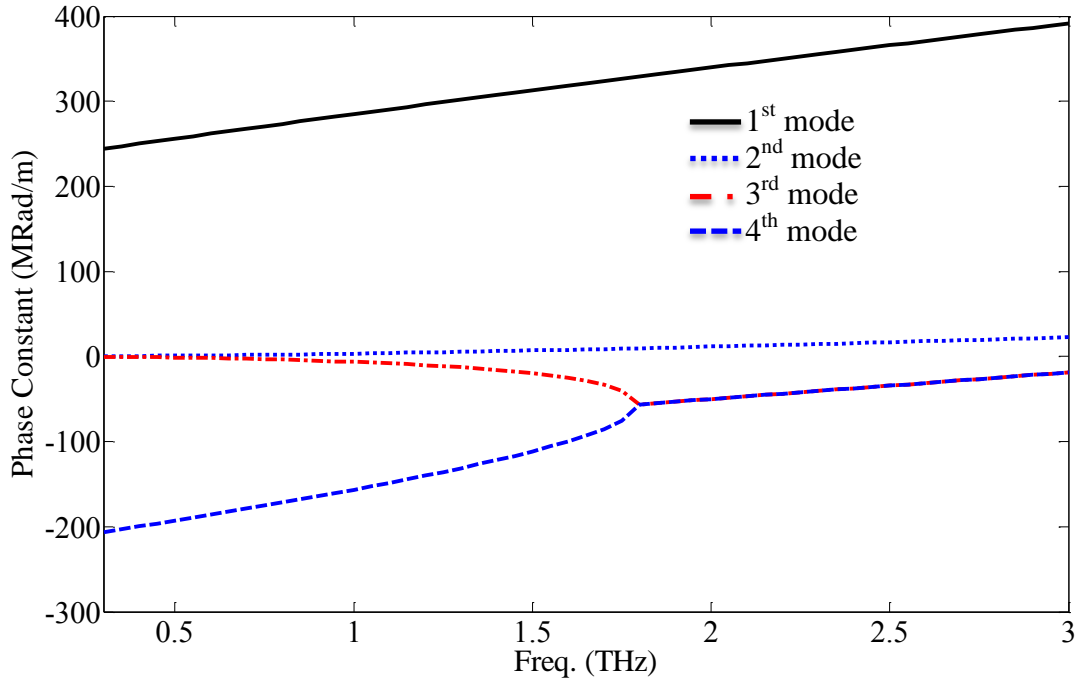
Fig. 2. Phase constants of the four modes versus frequency
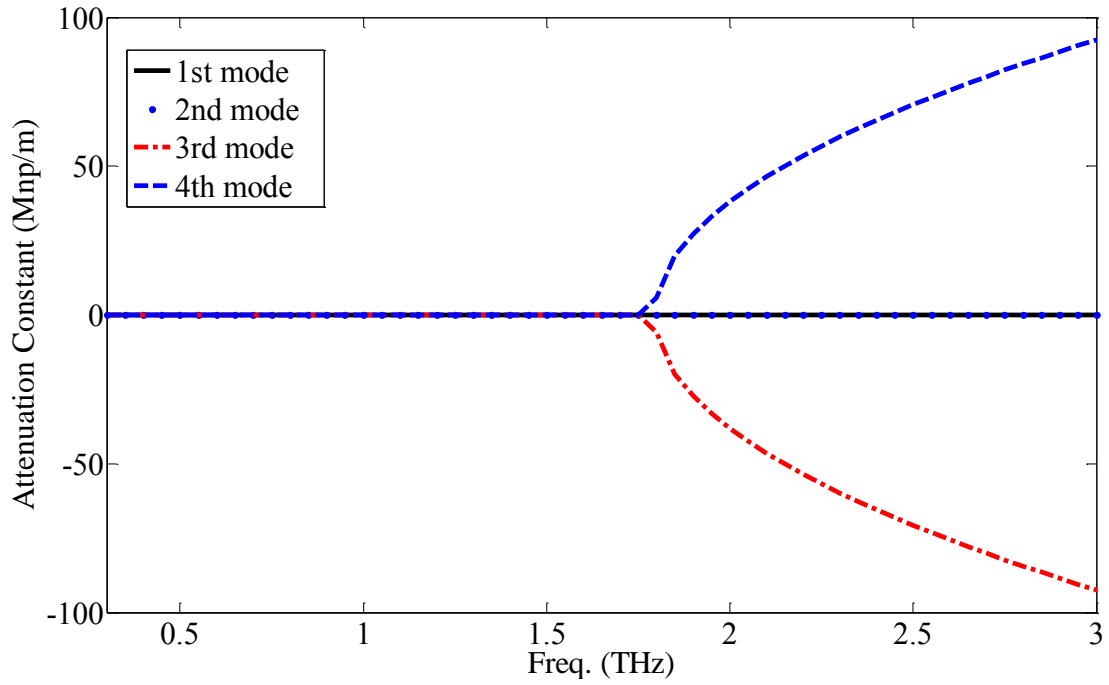
Fig. 3. Attenuation constant of each mode versus frequency
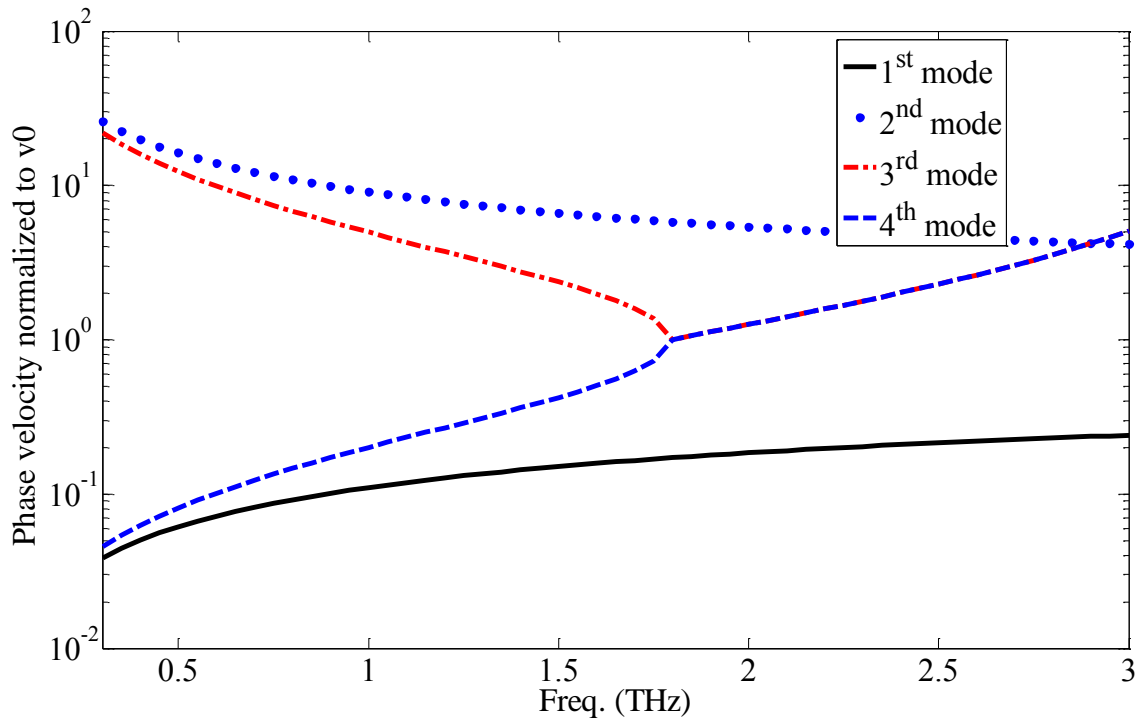
Fig. 4 Phase velocity of each mode normalized to the constant electron drift velocity versus frequency in a logarithmic plot
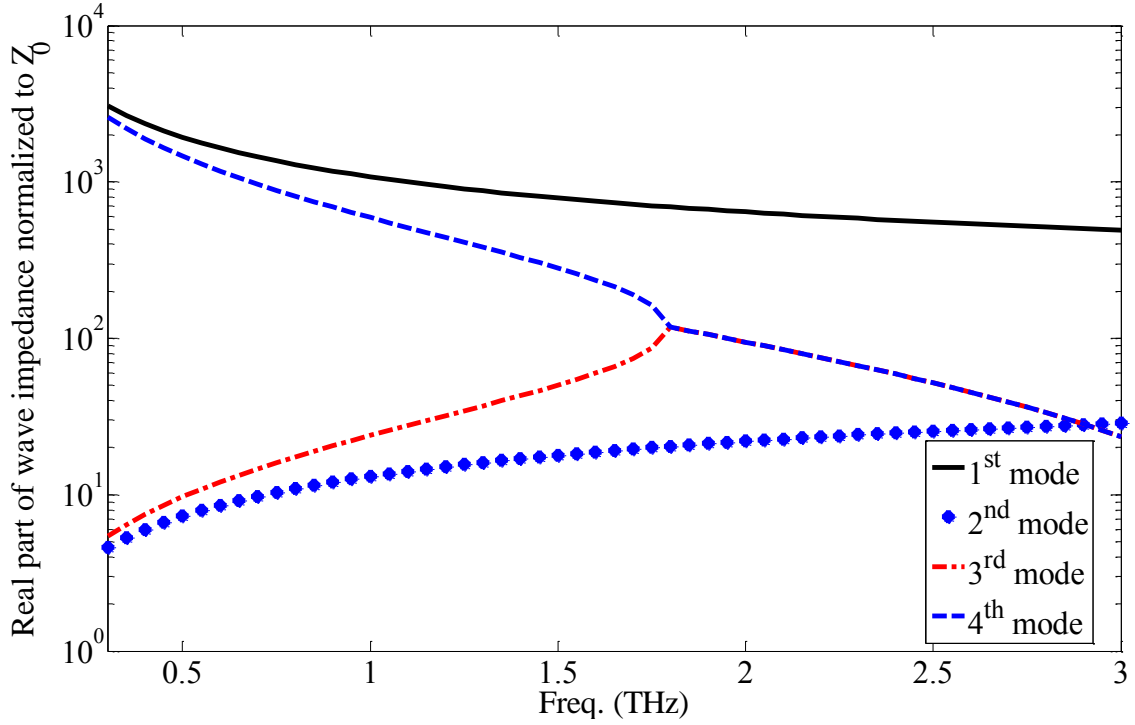
Fig. 5   Real part of each mode's wave impedance normalized to wave impedance in vacuum in a logarithmic plot
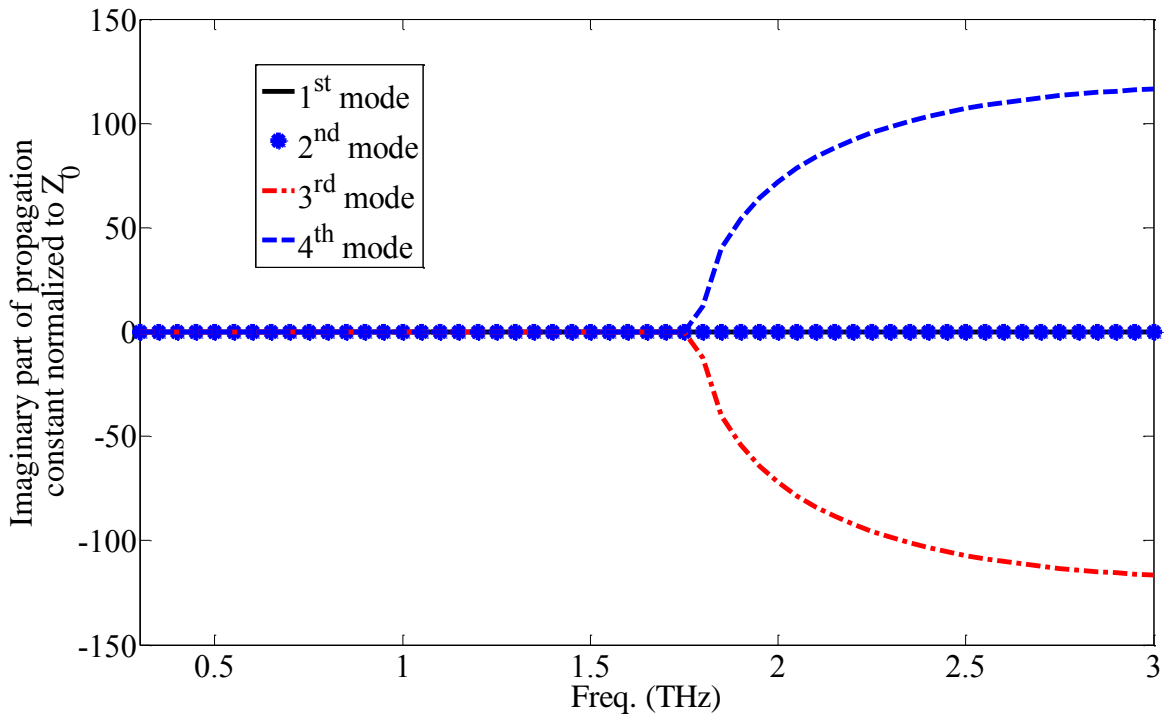
Fig. 6   Imaginary part of wave impedance normalized to wave impedance in vacuum

After considering the appropriate sign for the wave impedances, a simple matching network

36

shown in Fig. 7 is proposed. Notice that to couple the wave from the signal source placed at $x = L$ to the plasma wave with fourth mode properties, a matching network with highly inductive output impedance is required. The same matching network is also required for the load placed at $z = 0$ to handle the mismatch between the load and the wave impedance. It is obvious that further investigations and designs are needed to be done to improve the THz wave coupling to 2DEG.
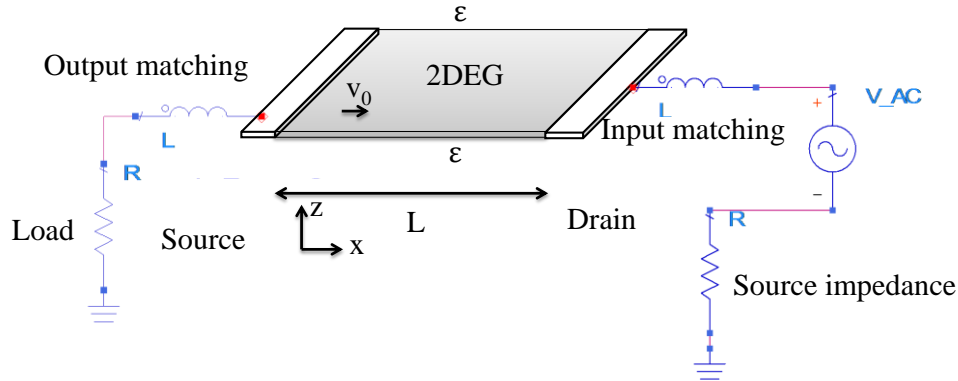
Fig. 7 A simple matching network placed at both ports (Bias circuit is not included).

Conclusion

An analytic method is proposed to study plasma wave modes along 2DEG layers of hetero-structures in the presence of carrier motion. The electrons movement causes the normal mode separation into four new modes with one being a growing mode at THz frequency ranges. Therefore, an amplification of plasma waves in this range is predicted and also, a need for sophisticated matching network designs is addressed. It is pointed out that for better understanding and more accurate designs, application of a full wave time domain method satisfied by Boltzmann equation is inevitable.

References:

[1]   T. A. Elkhatib, V. Y. Kachorovskii, W. J. Stillman, D. B. Veksler, K. N. Salama, X. Zhang and M. Shur, "Enhanced plasma wave detection of terahertz radiation using multiple high electron-mobility transistors connected in series," *IEEE Trans. Microwave Theory & Tech.,* vol. 58, no. 2, pp. 331-339, February 2010.

[2]   A. El Fatimy, N. Dyakonova, Y. Meziani, T. Otsuji, W. Knap, S. Vandenbrouk, K. Madjour, D. Theron, C. Gaquiere, M. A. Poisson, S. Delage, P. Prystawko and C. Skierbiszewski, "AlGaN/GaN high electron mobility transistors as a voltage-tunable room temperature terahertz source," *J. of Appl. Phys.,* vol. 107, pp. 024504-024507, January 2010.

[3]   M. Dyakonov and M. Shur, "Shallow water analogy for a ballistic field effect transistor: New mechanism of plasma wave generation by dc current," *Physical Review Letter,* vol. 71, no. 15, pp. 2465-2468, October 1993.

[4]   M. Dyakonov and M. Shur, "Current instability and plasma waves generation in ungated two-dimensional electron layers," *Applied Phys. Letters.,* vol. 87, pp. 111501, 2005.

[5]   V. V. Popov, O. V. Polischuk and M. S. Shur "Resonant excitation of plasma oscillations in a partially gated two-dimensional electron layer," *J. of Appl. Phys.,* vol. 98, pp. 033510-033517, 2005.

[6]   M. Nakayama, "Theory of surface waves coupled to surface carriers," *J. of the Physical Society of Japan.,* vol. 36, no. 2, pp. 393-398, February 1974.

[7]   S. A. Mikhailov, "Plasma instability and amplification of electromagnetic waves in low-dimensional electron systems," *Physical Rev. B,* vol. 58, no. 3, pp. 1517-1532, July 1998.

[8]   L. J. Chu and J. D. Jackson, "Field theory of traveling-wave tubes," *Proceeding of the I.R.E.,* pp. 853-863, 1948.

APPENDIX I:

UNIVERSITY OF ARKANSAS

College of Engineering
Department of Electrical Engineering

May 17, 2014

To whom it may be concerned,

I certify that Mr. Mohammadali Khorrami is the first author of the paper titled "Analytical modeling of THz wave propagation inside un-gated two dimensional electron gas layers," presented in International IEEE Microwave Symposium in June 2011. Mr. Khorrami completed the majority (more than 51 percent) of this research and writings of this paper.

Dr. Samir El-Ghazaly
Distinguished Professor
Electrical Engineering
Office: 3169 Bell Engineering Center
Phone: (479) 575-6048
Email: elghazal@uark.edu

3217 Bell Engineering Center • Fayetteville, AR 72701 • 479-575-3005 • Fax: 479-575-7967 • www.uark.edu
The University of Arkansas is an equal opportunity/affirmative action institution.

39

APPENDIX II:

Copyright Clearance Center

RightsLink®

Home | Create Account | Help

IEEE
Requesting permission to reuse content from an IEEE publication

Title: Analytical modeling of THz wave propagation inside ungated two dimensional electron gas layers

Conference Proceedings: Microwave Symposium Digest (MTT), 2011 IEEE MTT-S International

Author: Khorrami, M.A.; El-Ghazaly, S.; Shui-Qing Yu; Naseem, H.

Publisher: IEEE

Date: 5-10 June 2011

Copyright © 2011, IEEE

User ID

Password

☐ Enable Auto Login

LOGIN

Forgot Password/User ID?

If you're a copyright.com user, you can login to RightsLink using your copyright.com credentials. Already **a RightsLink user** or want to learn more?

Thesis / Dissertation Reuse

The IEEE does not require individuals working on a thesis to obtain a formal reuse license, however, you may print out this statement to be used as a permission grant:

Requirements to be followed when using any portion (e.g., figure, graph, table, or textual material) of an IEEE copyrighted paper in a thesis:

1) In the case of textual material (e.g., using short quotes or referring to the work within these papers) users must give full credit to the original source (author, paper, publication) followed by the IEEE copyright line © 2011 IEEE.
2) In the case of illustrations or tabular material, we require that the copyright line © [Year of original publication] IEEE appear prominently with each reprinted figure and/or table.
3) If a substantial portion of the original paper is to be used, and if you are not the senior author, also obtain the senior author's approval.

Requirements to be followed when using an entire IEEE copyrighted paper in a thesis:

1) The following IEEE copyright/ credit notice should be placed prominently in the references: © [year of original publication] IEEE. Reprinted, with permission, from [author names, paper title, IEEE publication title, and month/year of publication]
2) Only the accepted version of an IEEE copyrighted paper can be used when posting the paper or your thesis on-line.
3) In placing the thesis on the author's university website, please display the following message in a prominent place on the website: In reference to IEEE copyrighted material which is used with permission in this thesis, the IEEE does not endorse any of [university/educational entity's name goes here]'s products or services. Internal or personal use of this material is permitted. If interested in reprinting/republishing IEEE copyrighted material for advertising or promotional purposes or for creating new collective works for resale or redistribution, please go to http://www.ieee.org/publications_standards/publications/rights/rights_link.html to learn how to obtain a License from RightsLink.

If applicable, University Microfilms and/or ProQuest Library, or the Archives of Canada may supply single copies of the dissertation.

BACK | CLOSE WINDOW

B.   TERAHERTZ PLASMON AMPLIFICATION USING TWO-DIMENSIONAL ELECTRON-GAS LAYERS

Abstract

   In this study, we propose an analytical model to investigate the possibility of guiding and amplifying terahertz (THz) plasmons in a Two Dimensional Electron Gas (2DEG) layer of a hetero-structure by applying a bias electric field. This analytical model solves Maxwell equations and semi-classical electronic transport equations inside the biased hetero-structure simultaneously. It is shown that the two dimensional plasmon's properties alter vastly as the electrons are accelerated by the bias field. Four asymmetric plasmonic modes can propagate inside the un-gated 2DEG layer of the biased hetero-structure. One of these modes in the un-gated 2DEG layer is a growing mode which can be useful in the implementation of THz amplifiers. Since the characteristics of these modes can be controlled via biasing, design of new plasmonic devices such as modulators and switches is possible by this approach. Similar analysis has been performed in a gated 2DEG layer that shows clear changes in the two dimensional plasmon properties due to the biasing. Unlike the un-gated 2DEG layer, our efforts to find a growing mode in the gated 2DEG layer have failed. These multi-physics models lead to a better understanding of THz plasmonic sources and detectors as well as proposals on new plasmonic devices. Besides, they provide a physical insight into the electron-wave interactions inside the biased hetero-structure.

Introduction

In recent years, there have been substantial efforts to close the so called "THz Gap" by proposing all solid state devices aiming to generate and detect THz signals. Operation of microwave devices at THz frequencies is inherently limited by the electron velocity maximum inside semiconductors. Conversely, lower frequency edge of photonics is about 20 THz [1] and also the integration of optical devices into dimensions that are smaller than the wavelength of the photons in the free space, is limited by diffraction [2]. Recently, surface waves coupled to the motion of the surface carriers (after this shortened as SWC) also called two dimensional plasmons, have been employed increasingly to localize EM waves within nano-size distances. This high field localization only happens when the operating frequency is close to the plasma frequency of the carriers. Highly doped semiconductors with lower plasma frequencies offer localized plasmon propagation in the THz frequency range [3]. SWCs inside Two Dimensional Electron Gas (2DEG) layers with small propagation loss are very promising for THz plasmonic applications [1]. SWCs propagate in the 2DEG layers with phase velocities even ten times higher than the electron drift velocity maximum, while offering wavelengths that are orders of magnitude smaller than the radiative mode counterpart. To this end, many researchers in this area have focused on implementing THz sources and detectors using SWCs in: the inversion layer of Metal-Oxide-Silicon (MOS) structures [4]-[6], the 2DEG layer of High Electron Mobility Transistors (HEMTs) [7]-[12] and graphene [13]. Lately, novel plasmonic detectors inside 2DEG layers of hetero-structures have been implemented [9]-[10] that are comparable to the other state of the art THz detectors. Furthermore, different experiments [11]-[12] have indicated potentials of THz wave radiation from the 2DEG layers. As an example, room temperature THz emissions from an AlGaN/GaN based HEMT, tunable with gate voltage between 0.75 to 2.1 THz, has been

43

observed [11].

Emissions of THz signals from the structures are mostly interpreted as a consequence of the radiative decay of the SWCs thermally excited by hot electrons [5]-[6] or plasma wave resonances due to reflections from the device boundaries [11]-[12] and [14]-[15]. In [14], a solution of Poisson equation and Hydrodynamic (HD) equations, including continuity and Euler equations, are employed to characterize the motion of electrons inside the gated section of the 2DEG layer of a HEMT. Afterward, specific boundary conditions (short circuit at source and open circuit at drain) are utilized to represent the gated 2DEG as a plasmonic resonant cavity and a gain medium which allows exponential SWC growth in THz range. Following the same procedure, similar SWC instabilities have been predicted in an un-gated 2DEG layer [15]. Nevertheless, it should be mentioned that the models [14]-[15] are not able to describe any type of energy transfer from the bias voltage to the SWCs or any exponential growth of the surface waves without considering the boundary conditions.

In this paper, a complete wave characterization of the SWCs in the gated and the un-gated 2DEG layers of biased hetero-structures is presented. To this end, an analytical solution of HD equations and Maxwell equations inside a non-degenerate electron gas is performed. In the search of a possible plasmonic amplifier, the analysis is focused on finding surface wave modes that can exist and grow exponentially. This mode analysis is similar to the one performed for helix-type traveling wave tubes in [16]. Incorporating Maxwell equations into our model allows us to perform an inclusive mode analysis compared to the other methods [14]-[15] which simply employed Poisson equation for the field calculations. Also, this method enables us to illustrate several interesting wave parameters such as phase velocities, wave impedances and admittances of the SWCs. Here, the effects of the hetero-structure's end contacts and the corresponding

boundary conditions on the wave propagation are ignored. This assumption allows us to first examine the ability of the 2DEG layer to handle a growing SWC mode before any resonant cavity is assigned inside the structure. It is shown that the wave properties of the normal symmetrical SWC modes along an un-biased 2DEG will drastically change as a bias voltage is applied onto the2DEG ends. In the biased device, the symmetry of the right and left going SWC of the unbiased 2DEG is completely broken. This can explain unsuccessful experiments designed to search for resonant behaviors of the 2DEG conductance due to the SWCs inside biased devices, while there are several reports as [4] and [8] showing the plasmon-induced resonant characteristics in transmission spectroscopy response of un-biased 2DEG layers. In spite of several benefits of this analytical method, a numerical solution of complete form of electronic transport equations coupled to a full wave simulator is still required to obtain a comprehensive picture of plasmon-electron energy interactions. A perfect candidate for this purpose is the multi-physics numerical solver in [17] that was first introduced for the analysis of high frequency transistors.

Analytical modeling of the SWCs propagation in a biased un-gated 2DEG layer

Fig. 1 shows the schematic diagram of the simulated structure, including an infinitely wide (along y-axis) 2DEG sheet with equilibrium surface charge density n_0 positioned at $z = 0$. It is assumed that the 2DEG layer is confined inside two lossless semi-infinite (along z axis) semiconductors with similar permittivities $\varepsilon = \varepsilon_r \times \varepsilon_0$, $\varepsilon_0 = 8.85 \times 10^{-12}$ (F/m). The motion of the electrons along the z-axis is quantized with a ground state wave function spread of about 10nm. The spread is smaller than the SWCs decay length along z axis. Therefore, the 2DEG is represented as a zero thickness sheet of electrons in our analytical model. It is assumed that electrons are only allowed to move along x axis. An external bias electric field E_0 causes the

45

electrons to move toward $+x$ with an average electron drift velocity v_0. The bias electric field is applied by inserting a dc voltage onto Ohmic contacts (source and drain) located at both ends. It is assumed that the contacts are extremely far from each other compared to the SWCs wavelengths so that their effects are not included.
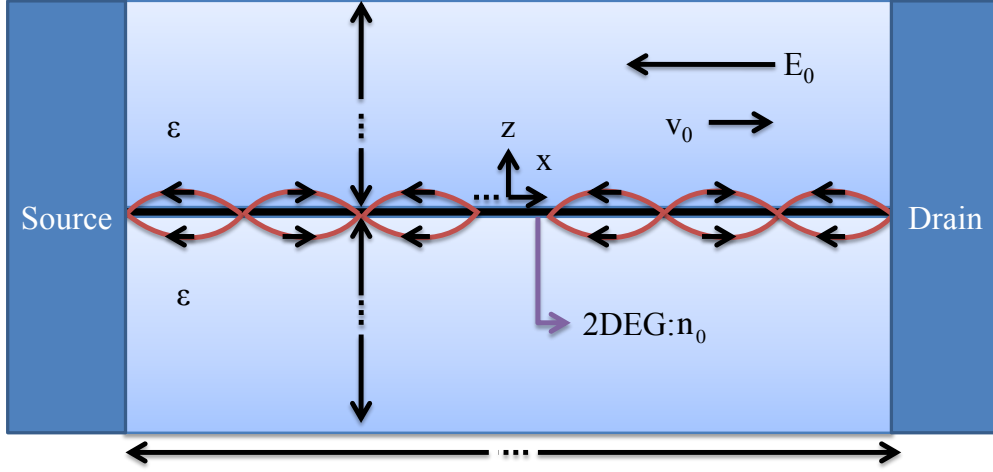
Fig. 1. A front view of the structure considered in the analytical model. The infinite electron sheet is confined inside two dielectrics. Electrons are moving as a consequence of the sum of two electric fields; the large bias electric field E_0 and the weak SWC time varying one.

As previously proved in [18]-[19], TE^x mode is not permitted to propagate along the 2DEG layers of the hetero-structures with isotropic semiconductors. Therefore, only a TM^x mode solution along the 2DEG layer is presented here. To this end, a magnetic vector potential $\vec{A} = \hat{x}\psi$ (refer to [20]-[21] for the definition) with a wave function

$$\psi = \begin{cases} \phi_1 \exp\left(j\omega t - \gamma x - \delta z \right) & z \geq 0 \\ \phi_2 \exp\left(j\omega t - \gamma x + \delta z \right) & z < 0 \end{cases} \tag{1}$$

along x axis with a unit vector $\hat{x}$ is considered. Inside the wave function, a propagation constant $\gamma = \alpha + j\beta$ is assumed that t, ω andα and β are time, radial frequency and attenuation and phase constants along x axis, respectively. Also, δ is the attenuation constant along z direction. The corresponding wave equation can be written as:

$$\delta^2 + \gamma^2 + \frac{\varepsilon_r \omega^2}{c^2} = 0 \qquad (2)$$

where $c = 1/\sqrt{\mu_0 \varepsilon_0}$ and $\mu_0 = 4\pi \times 10^{-7}$ (H/m). The TM^x mode solution of Maxwell equations

provides wave components

$$E_x = \frac{1}{j\omega\varepsilon}\left(\frac{\partial^2 \psi}{\partial^2 x} + \frac{\varepsilon_r \omega^2}{c^2}\psi\right), \; E_z = \frac{1}{j\omega\varepsilon}\frac{\partial^2 \psi}{\partial x \partial z}$$

$$H_y = \frac{\partial \psi}{\partial z}, \; E_y = H_z = H_x = 0. \qquad (3)$$

Boundary conditions applied on the surface of the 2DEG are the continuity of tangential

component of the electric field $E_x|_{z=0^+} = E_x|_{z=0^-}$ and the presence of surface current density $J_x^S =$

$H_y|_{z=0^+} - H_y|_{z=0^-}$. The surface current is related to the electric field through $J_x^S = \sigma E_x|_{z=0}$ where σ

is the *xx* component of the surface conductivity tensor [19]. Using this relation, the previously

mentioned boundary conditions and the wave equation (2), it is concluded that $\varphi_1 = \varphi_2$ and

$$-\frac{\sigma}{j\omega} = \frac{2\varepsilon}{\delta}. \qquad (4)$$

In order to consider the electronic transport effects of the active plasmonic structure into the

surface conductivity component, a small signal analysis of HD equations [22] is incorporated

into our model. For this purpose, HD equations including electron continuity relation

$$\frac{\partial n}{\partial t} + \nabla.(n\vec{v}) = 0 \qquad (5)$$

and Euler equation (also called simplified form of momentum conservation equation)

$$\frac{\partial \vec{v}}{\partial t} + \vec{v}.(\nabla \vec{v}) = -\frac{q}{m^*}\vec{E}_{total} - \frac{\vec{v}}{\tau_m} \qquad (6)$$

are linearized. In (5)-(6), n, v, m*, q and τ_m are electron: density, velocity, effective mass, unit

charge (q = 1.6×10^{-19}C) and momentum relaxation time, respectively. Since electrons are only

allowed to move along *x* direction, *x* component of the electron velocity v_x and the total applied

47

electric field $E^{total}{}_x = E_0 + E_x$ are considered. These transport equations (5)-(6) are well known to correctly predict the low field behaviors of electronic devices [14].

In our small signal analysis, electron velocity and charge density are $v_x = v_0 + v_x{}^{ss} \times \exp(j\omega t - \gamma x - \delta z)$ and $n = n_0 + n^{ss} \times \exp(j\omega t - \gamma x - \delta z)$, respectively. After linearizing (5)-(6) and considering that $J_x{}^s = -qnv_x$; the surface conductivity is obtained as:

$$\sigma = \frac{n_0 q^2}{m^*} \frac{j\omega}{(j\omega - v_0\gamma)\left(j\omega - v_0\gamma + \dfrac{1}{\tau_m}\right)}.$$ (7)

Substituting (7) into (4) and using the wave equation (2); it is concluded that:

$$A_1\gamma^4 + A_2\gamma^3 + A_3\gamma^2 + A_4\gamma + A_5 = 0.$$ (8)

where,

$$A_1 = v^4{}_0, \quad A_2 = -\frac{2v^3{}_0}{\tau_m} - 4j\omega v^3{}_0$$

$$A_3 = -6\omega^2 v^2{}_0 + \frac{v^2{}_0}{\tau_m{}^2} + \frac{6j\omega v^2{}_0}{\tau_m} + 4a^2$$

$$A_4 = 4jv_0\omega^3 + \frac{6v_0\omega^2}{\tau_m} - \frac{2jv_0\omega}{\tau_m{}^2}$$ (9)

$$A_5 = \omega^4 - \frac{\omega^2}{\tau_m{}^2} - \frac{2j\omega^3}{\tau_m} + \frac{4a^2\omega^2\varepsilon_r}{c^2}$$

and $a = \dfrac{n_0 q^2}{4\varepsilon m^*}$. Solving the fourth order equation (8), four SWC modes with different dispersion relations are obtained. In order to verify our solution, a specific case with small bias voltage or negligible electron drift velocity ($v_0 \approx 0$) and low scattering rate ($\omega \gg 1/\tau_m$) is considered. Under these conditions, (8) simplifies into $\gamma = \pm j\sqrt{\omega^4 + 4a^2\omega^2\varepsilon_r/c^2}/2a$ which is identical to the dispersion relations calculated in [18]-[19]. These two SWC modes inside the unbiased 2DEG are divided into four different modes resulted from (8), as the bias voltage is applied.

Under the conditions of small bias voltage ($v_0 \approx 0$) and non-negligible scattering rate, (8) reduces to:

$$\gamma = \pm \frac{j}{2a} \sqrt{\omega^4 - \frac{\omega^2}{\tau_m^{\,2}} - \frac{2j\omega^3}{\tau_m} + \frac{4a^2\omega^2\varepsilon_r}{c^2}}.$$

(10)

Also, a solution of (8) can be obtained in a biased 2DEG layer with low scattering rate ($\omega \gg 1/\tau_m$) as:

$$\gamma_{1,2} = j \frac{(a + v_0\omega) \pm \sqrt{a^2 + 2av_0\omega}}{v^2_{\,0}}$$

$$\gamma_{3,4} = j \frac{(-a + v_0\omega) \pm \sqrt{a^2 - 2av_0\omega}}{v^2_{\,0}}.$$

(11)

Considering the dispersion relations of the 3rd and the 4th modes in (11); it is understood that the propagation constants of these modes are complex as $\omega \geq a\,/\,2v_0$. Following [23], the special frequency $f_{br} = a\,/\,4\pi v_0$ is named breaking frequency. A SWC mode with a complex propagation constant (nonzero attenuation constant) can represent a growing or an attenuating mode depending on the signs of its propagation and attenuation constants. Hence, the possibility of finding a growing mode should be considered in each specific case. If the scattering effect is not negligible, a numerical solution of (8) is required for the complete mode characterization.

To examine the energy interaction between the electromagnetic waves and electrons, wave admittance of each mode along the perpendicular direction z is defined as:

$$Y_{1,...,4}^{\;\;z} = -\frac{H^y}{E^x} = -\frac{j\omega\varepsilon}{\delta}.$$

(12)

With this definition, positive conductance is interpreted as the transfer of energy from the waves to the electrons and negative conductance represents an opposite power exchange [16] that leads

to the SWC amplification. It is expected that the energy of the growing mode is due to the reduction of the total kinetic energy of the electron stream.

Another interesting parameter is the wave impedance along x axis

$$Z^x_{1,...,4} = \frac{\gamma_{1,...,4}}{j\omega\varepsilon},$$

(13)

that can be useful in the design of matching networks. These networks are required to effectively match the input and output of the 2DEG layer to other sections of a future plasmonic circuit.

Discussion of the SWCs propagation in an un-gated 2DEG layer

Here, a mode analysis of the SWCs in the un-gated 2DEG layer of an AlGaAs/GaAs heterostructure is performed in a broad THz frequency range using the analytical method proposed in section II. A 2DEG layer with equilibrium charge density $n_0 = 10^{11} \text{cm}^{-2}$ located inside the heterostructure with electron effective mass $0.0623 m_0$ ($m_0 = 9.1 \times 10^{-31}$ kg) and electron momentum relaxation time $\tau_m = 1$ps is considered. It is assumed that a bias voltage has induced an electric field along the 2DEG layer that has accelerated the electrons toward $+x$ with the average drift velocity $v_0 = 10^7$ cm/s. Also, the relative permittivities of the semiconductors confining the 2DEG are assumed to be equal $\varepsilon_r = 12.6$.

In Fig. 2, the SWCs phase constants in the 2DEG layer in the biased (8) and the un-biased (10) cases are shown. Because of the symmetry of the SWC modes in the un-biased case, one of the SWC modes is only considered here. As depicted (see Fig. 2), there exist vast differences between the SWCs phase constants in the biased and the unbiased cases. These changes are related to the presence of the electron drift motion. This clearly emphasizes that the electron drift movement must be considered into the models of active plasmonic devices. As illustrated, phase constants of the 1st and the 4th modes are positive and hence; these modes are allowed to propagate toward $+x$. The 2nd and the 3rd modes propagate toward $–x$ due to their negative phase
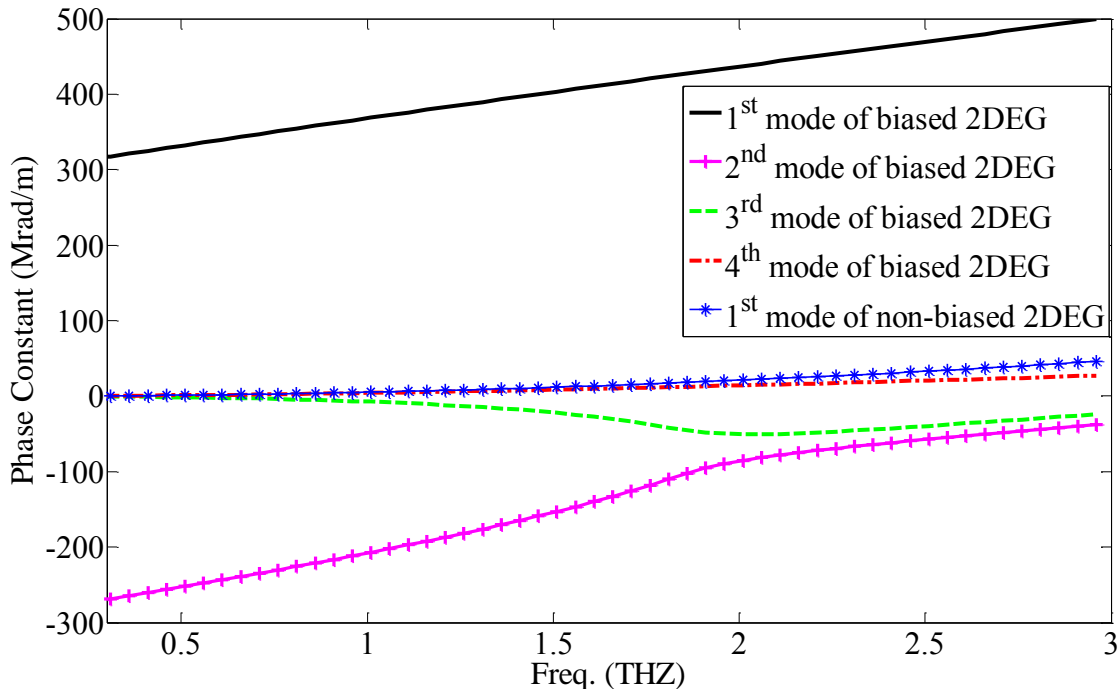
50

constants.

Fig. 2. Phase constants of the SWC modes in the un-gated 2DEG layer for the biased and the un-biased cases in the frequency range 300GHz to 1.5THz.
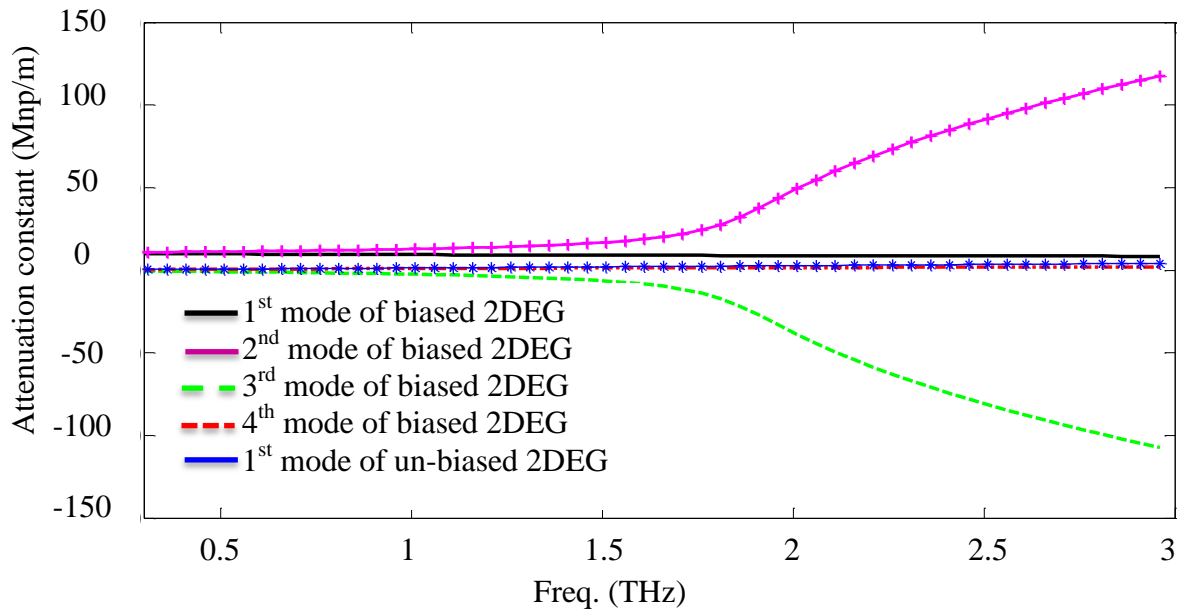

Fig. 3. Attenuation constants (along x axis) of the SWC modes in the un-gated 2DEG layer for the biased and the un-biased cases in the frequency range 300GHz to 1.5THz.
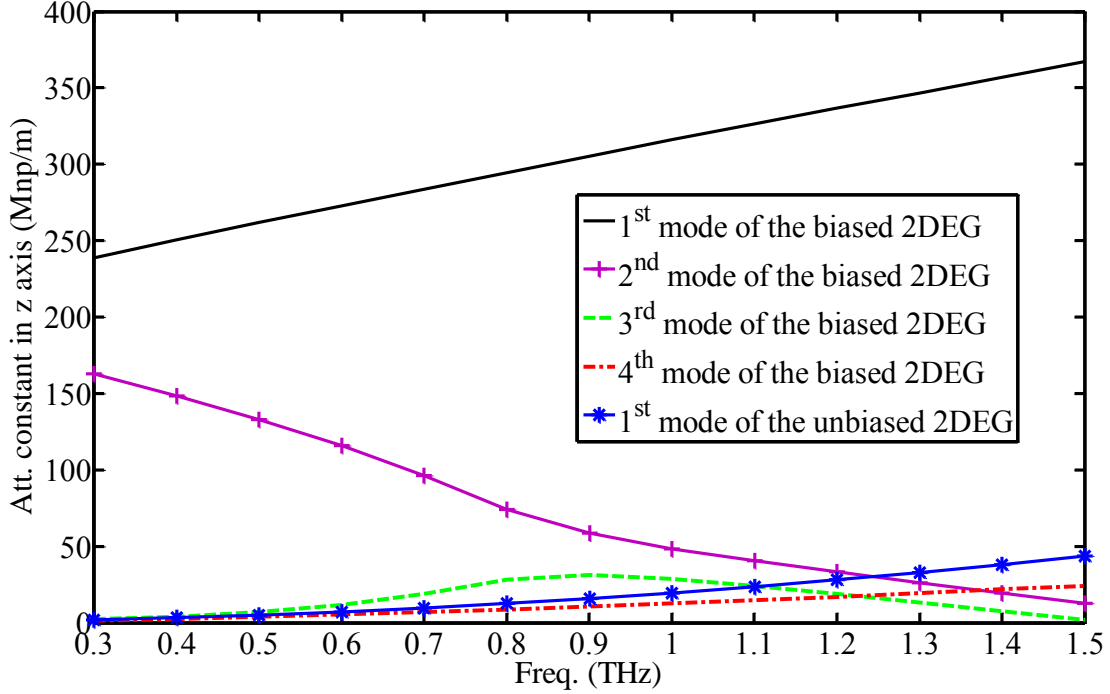
Fig. 4. Attenuation constants (along *z* axis) of the SWC modes in the un-gated 2DEG layer for the biased and the unbiased cases in the frequency range 300 GHz to 1.5 THz.

In Fig. 3, the attenuation constants of the SWC modes in the biased and un-biased cases are shown. In the following, the attenuation constants are reported in the unit of mega Nepers per meter. Large modifications in the attenuation constants of the SWC modes are similarly observed as electrons are accelerated by the bias field. The 1st and the 4th modes are able to propagate with small attenuations while the 2nd and the 3rd modes have comparatively large attenuation constants in the frequencies higher than $f_{br} = 0.8$THz. Considering the direction of propagation (Fig. 2) and the sign of the attenuation constant (Fig. 3) of each mode, it is concluded that the 2nd mode is a growing mode. This means that if this mode is properly launched along the 2DEG, SWCs will grow exponentially as they propagate. This growth can continue until the point that the presented small signal analysis reaches its limit. This unidirectional SWC amplification can be useful in the design of wideband THz amplifiers inside hetero-structures. As mentioned, the SWCs growth rate is small in lower frequencies while it increases in higher frequency ranges. This frequency

dependent behavior should be considered in the design of the THz amplifiers to reach the highest possible gain in the interested frequency range. As shown in Fig. 2, the SWCs have large phase constants or equivalently very small wavelengths in most part of the frequency range. This justifies the assumption of infinitely long 2DEG layer compared to the SWCs wavelengths. As an incident radiating THz electromagnetic field is exciting the amplifier; the application of special coupling mechanism such as diffraction based gratings is required to compensate the phase mismatch between the SWCs and the incident wave. As the amplifier input signal is provided by another circuit such as a plasmonic waveguide, the wave impedance of the waveguide should match the amplifier wave impedance (13). Similar impedance matching is also required in the output of the amplifier to avoid any unwanted instabilities and transferring the maximum portion of the amplified signal to the terminating circuit. Because of the unidirectional behavior of the growing mode, implementation of a THz oscillator inside the same structure may be challenging. However, using an external feedback circuit connected to the plasmonic amplifier can make the implementation of a THz oscillator in the 2DEG layer achievable.

From Fig. 2 and Fig. 3, it can be concluded that the 3rd mode is facing large attenuations as propagating. This specific mode may be employed in the design of novel electrically controlled plasmonic switches.

In Fig. 4, the attenuation constants δ of the SWCs along the perpendicular direction z are illustrated. As depicted, all modes are showing relatively large attenuations in this direction in a broad frequency range. This means that the SWCs are mostly localized around the 2DEG in these frequencies. Considering the high field concentration along the 2DEG layer, the assumption of infinitely thick dielectric around the 2DEG is justified. This high field attenuation also suggests that if the grating coupler is employed to launch the SWCs, the 2DEG should be

53

located close enough to the surface so that the diffracted fields can strongly excite the SWCs.
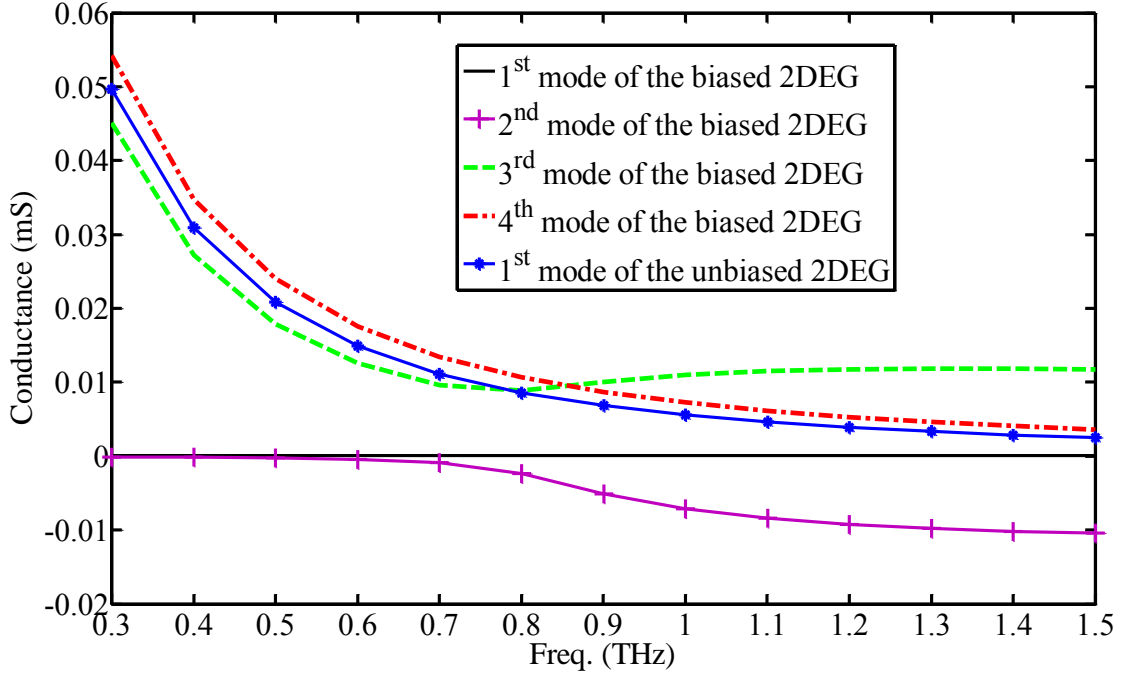
Fig. 5. Real part of the wave admittance of the SWC modes (along *z* axis) in the un-gated 2DEG layer for the biased and the un-biased cases in the frequency range 300 GHz to 1.5 THz.

In Fig. 5, the real part of the wave admittance calculated in the perpendicular direction *z* (12) is presented. With our definition of the admittance, negative conductance is interpreted as the transfer of energy from the electron stream to the wave. As shown, all modes have positive conductance in the frequency range except the 2nd mode that experiences large negative conductance specifically as the operating frequency is above f_{br}. Since the breaking frequency is dependent on the equilibrium charge density n_0 and the drift velocity v_0, it is clear that the gain bandwidth of the amplifier can be controlled by changing n_0 and v_0. As depicted in Fig. 5, the 1st mode of the biased 2DEG shows comparatively negligible positive conductance in the frequency range.

In Fig. 6, phase velocities of the SWC modes normalized to v_0 are illustrated. As illustrated, all four modes have slow wave nature. It is also interesting to notice that the growth starts as soon as

the phase velocity of the amplifying mode becomes very close to the drift velocity.
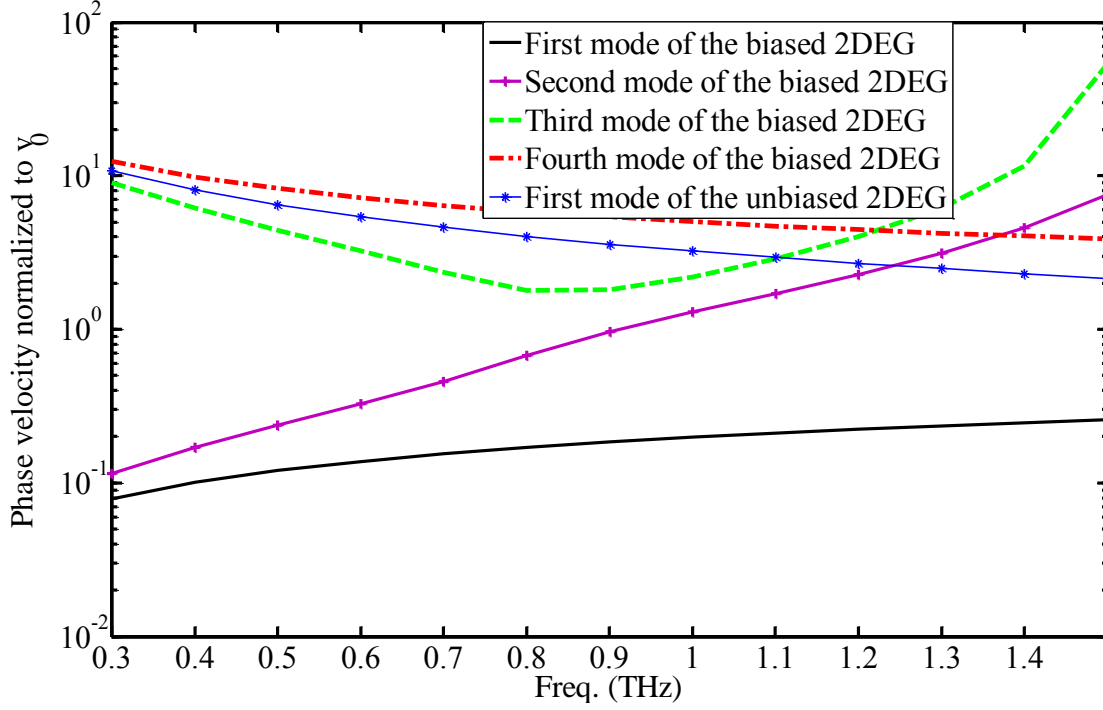
Fig. 6. Phase velocities of the SWC modes in the un-gated 2DEG layer for the biased and the unbiased cases in the frequency range 300GHz to 1.5THz in a logarithmic plot.

Analytical modeling of the SWCs propagation in a biased gated 2DEG layer

Here, similar mode analysis of the SWCs inside a gated 2DEG layer is performed. Similarly, the possibility of finding a growing SWC mode is investigated in this structure. Consider the same structure in Fig. 1 but with an infinitely long (along +z) perfect electric conductor positioned at z = d as a gate. In this case, the corresponding wave function of the TM^x mode is described as:

$$\psi = \begin{cases} \phi_1 \exp\left(j\omega t - \gamma x + \delta z \right) & z \leq 0 \\ \phi_2 \exp\left(j\omega t - \gamma x \right) \sin \delta \left(z - d \right) & 0 < z \leq d \,. \\ 0 & z > d \end{cases} \qquad (14)$$

After solving Maxwell equation and inserting the wave function (14) into the solution (3), wave components in the areas below the gate (z < d) are obtained as:

$$E_x = \frac{-\delta^2}{j\omega\varepsilon}\psi, \; H_x = H_z = E_y = 0$$

$$H_y =$$

$$\begin{cases} \delta \times \phi_1 \exp(j\omega t - \gamma x + \delta z) & z \leq 0 \\ \delta \times \phi_2 \exp(j\omega t - \gamma x)\cos\delta(z-d) & 0 < z \leq d \end{cases} \tag{15}$$

$$E_z =$$

$$\frac{-\gamma\delta}{j\omega\varepsilon} \times \begin{cases} \phi_1 \exp(j\omega t - \gamma x + \delta z) & z \leq 0 \\ \phi_2 \exp(j\omega t - \gamma x)\cos\delta(z-d) & 0 < z \leq d \end{cases}.$$

The wave components above the gate are equal to zero. After applying similar boundary conditions $\left(E_x\big|_{z=0^+} = E_x\big|_{z=0^-} \text{ and } J^s_x = H_y\big|_{z=0^+} - H_y\big|_{z=0^-}\right)$, it is concluded that:

$$\begin{cases} \phi_1 = -\phi_2 \sin(\delta d) \\ J_x = -\delta \times (\phi_2 \cos(\delta d) - \phi_1) \times \exp(j\omega t - \gamma x) \end{cases} \tag{16}$$

Incorporating the relation between the surface current density and the x component of the ac electric field $J^s_x = \sigma \times E_x\big|_{z=0}$ into (16), it can be calculated that:

$$1 + \cot(\delta d) = \frac{-\delta\sigma}{j\omega\varepsilon}. \tag{17}$$

This result is consistent with the relation calculated in [24] for the same structure. It can be shown that the small signal analysis of the electronic transport equations (4)-(5) inside the gated 2DEG layer also leads to the similar surface conductivity (6). By substituting (6) into (17) and considering a tightly screened 2DEG ($\delta \times d \ll 1$); it is concluded that:

$$\left(v^2_0 - 4ad\right)\gamma^2 - \left(\frac{v_0}{\tau} + 2j\omega v_0\right)\gamma - \omega^2 + \frac{j\omega}{\tau} = 0. \tag{18}$$

In this manner, the dispersion relations of the SWCs in the gated 2DEG layer of biased hetero-structures are attained as:

$$\gamma_{1,2} = \frac{\left(\dfrac{v_0}{\tau} + 2jv_0\omega\right) \pm \Delta}{2\left(v_0^2 - 4ad\right)},$$

$$\Delta = \sqrt{\frac{v_0^2}{\tau^2} - 16 \times ad\omega^2 + 16j\frac{\omega ad}{\tau}}.$$

(19)

The propagation constants calculated in (19) are complex and hence; SWC mode characteristics should be calculated in each specific hetero-structure. We have tried several hetero-structures with their nominal values to examine the possibility of finding a growing mode. However, the resulting propagation constants only showed attenuating modes.

If the drift velocity and the scattering effects are ignored, famous shallow plasma wave dispersion relation is obtained:

$$\gamma_{1,2} = \pm\frac{j\omega}{2\sqrt{ad}}.$$

(20)

In the collision-less case (ω, $\gamma v_0 \gg 1/\tau$), the dispersion relation (19) simplifies to $\gamma_{1,2} = j\omega / (v0 \pm 2\sqrt{ad})$ which is similar to the relation employed in [14]. In this case, the propagation constants are purely imaginary and therefore; the amplification or the attenuation of SWC modes is not expected.

Challenges and Summary

In this paper, we have characterized the SWC modes in 2DEG layers of biased hetero-structures at THz frequencies to investigate the possibility of controlling and amplifying SWCs in these structures. In this analysis, an analytical method consisting of a modal solution of Maxwell equations and HD equations is introduced. This investigation clearly highlights several important changes that the SWCs in both gated and un-gated structures face as the electrons are accelerated by the bias electric field. In the un-gated 2DEG layer, a growing SWC mode can exist which may lead to the amplification of SWCs. Several obstacles are to be overcome before

the growing mode can be useful in the implementation of THz amplifiers. Due to the non-radiative nature of the plasmons, a diffraction based structure such as a grating coupler is required to excite the SWC mode. Also, it is important to only excite the growing mode along the 2DEG to obtain an efficient amplifier. Besides, reflections of the plasmons from the coupler and the Ohmic contacts should be considered to avoid unwanted instabilities. The electron heating has not been addressed in this work and therefore possible hot electron effects need to be investigated separately.

The growing mode has not been observed inside the gated 2DEG layers. However, active control of the SWCs in the gated 2DEG layers by external bias voltages can provide new opportunities to design and implement novel plasmonic switches and modulators.

References

[1]   M. Lee and M C. Wanke, "Searching for a solid-state terahertz technology," *Science*, vol. 316, pp. 64-65, Apr. 2007.

[2]   E. Ozbay, "Plasmonics: Merging photonics and Electronics," *Science,* vol. 311, pp. 189-193, Jan. 2006.

[3]   S. A. Maier, *Plasmonics: Fundamentals and applications.* (Springer, UK, 2007).

[4]   S. J. Allen, D. C. Tsui and R. A. Logan, "Observation of the two-dimensional plasmon in silicon inversion layers," *Phys., Rev. Lett*., vol. 38, no. 17, pp. 980-983, Apr. 1977.

[5]   D. C. Tsui, E. Gornik and R. A. Logan, "Far infrared emission from plasma oscillation of Si inversion layers," *Solid State Commun.,* vol. 35, pp. 875-877, (1980).

[6]   R. A. Hopfel, E. Vaas and E. Gornik, "Thermal excitation of two-dimensional plasma oscillations," *Phys. Rev. Lett.,* vol. 49, no. 22, pp. 1667-1671, Nov. 1982.

[7]   T. A. Elkhatib, V. Y. Kachorovskii, W. J. Stillman, D. B. Veksler, K. N. Salama, X. Zhang and M. Shur, "Enhanced plasma wave detection of terahertz radiation using multiple high electron-mobility transistors connected in series," *IEEE Trans. Microw. Theory & Tech.,* vol. 58, no. 2, pp. 331-339, Feb. 2010.

[8]   H. Saxena, R. E. Peale and W. R. Buchwald, "Tunable two-dimensional plasmon resonances in an InGaAs/InP high electron mobility transistor," *J. Appl. Phys.,* vol. 105, p. 113101, Jun. 2009.

[9]   G. C. Dyer, G. R. Aizin, J. L. Reno, E. A. Shaner and S. J. Allen, "Novel tunable millimeter-wave grating-gated plasmonic detectors," *IEEE J. Sel. Topics Quantum Electron.,* vol. 17, no. 1, pp. 85-91, Jan. 2011.

[10]   V. V. Popov, D. M. Ermolaev, K. V. Maremyanin, N. A. Maleev and V. E. Zemlyakov, "High-responsivity terahertz detection by on-chip InGaAs/GaAs field-effect-transistor array," *Appl. Phys. Lett.*, vol. 98, p. 153504, Apr. 2011.

[11]   A. El Fatimy, N. Dyakonova, Y. Meziani, T. Otsuji, W. Knap, S. Vandenbrouk, K. Madjour, D. Theron, C. Gaquiere, M. A. Poisson, S. Delage, P. Prystawko and C. Skierbiszewski, "AlGaN/GaN high electron mobility transistors as a voltage-tunable room temperature terahertz sources," *J. of Appl. Phys.*, vol. 107, p. 024504, Jan. 2010.

[12]   W. Knap, J. Lusakowski, T. Parenty, S. Bollaert, A. Cappy, V. V. Popov and M. S. Shur, "Terahertz emission by plasma waves in 60 nm gate high electron mobility transistors," *Appl. Phys. Lett.,* vol. 84, p. 2331, Mar. 2004.

[13]   J. Khoury, B. Haji-Saeed, W. Buchwald, C. Woods, S. Wentzell, B. Krejca and J. Kierstead, "Electrically tunable surface plasmon source for THz applications," *IEEE J. Sel. Topics Quantum Electron.*, vol. 17, no. 1, pp. 138-145, Jan. 2011.

[14]   M. Dyakonov and M. Shur, "Shallow water analogy for a ballistic field effect transistor: New mechanism of plasma wave generation by dc current," *Phys. Rev. Lett.*, vol. 71, no. 15, pp. 2465-2468, Oct. 1993.

[15]   M. Dyakonov and M. Shur, "Current instability and plasma waves generation in ungated two-dimensional electron layers," *Appl. Phys. Lett.*, vol. 87, p. 111501, Sep. 2005.

[16]   L. J. Chu and J. D. Jackson, "Field theory of traveling-wave tubes," *Proceeding of the I.R.E.,* vol. 36, no. 7, pp. 853-863, Jul. 1948.

[17]   R. O. Grondin, S. El-Ghazaly and S. Goodnick, "A review of global modeling of charge transport in semiconductors and full-wave electromagnetics," *IEEE Trans. Microw. Theory & Tech.,* vol. 47, no. 6, pp. 817-829, Jul. 1999.

[18]   F. Stern, "Polarizability of a two-dimensional electron gas," *Phys. Rev. Lett.*, vol. 18, no. 14, pp. 546-548, Apr. 1967.

[19]   M. Nakayama, "Theory of surface waves coupled to surface carriers," *Phys. Soc. of Japan,* vol. 36, no. 2, pp. 393-398, Jan. 1974.

[20]   C. A. Balanis, *Advanced Engineering Electromagnetics* (John Wiley & Sons, Inc, USA).

[21]   J. D. Jackson*, Classical Electrodynamics*(John Wiley & Sons, Inc, USA)

[22]   S. A. Mikhailov, "Plasma instability and amplification of electromagnetic waves in low-dimensional electron systems," *Phys. Rev. B*, vol. 58, no. 3, pp. 1517-1532, Jul. 1998.

[23]   M. A. Khorrami, S. El-Ghazaly, S. Q. Yu, H. Naseem, "Analytical modeling of THZ wave propagation inside ungated two dimensional electron gas layers," *Int. IEEE Microw. Symp.,* Baltimore, 2011.

[24]   A. Eguiluz, T. K. Lee. J. J. Quinn and K. W. Chiu, "Interface excitations in metal-insulator-semiconductor structures," *Phys. Rev. B*, vol. 11, no. 12, pp. 4989-499, Jun. 1975.

APPENDIX I:

A. SURFACE CONDUCTIVITY OF A BIASED TWO-DIMENSIONAL CONDUCTOR

Here, the small signal analysis of Hydrodynamic equations (momentum conservation and continuity equations) is performed to obtain the surface conductivity of a biased electron gas. In general, continuity equation:

$$\partial n / \partial t + \nabla.\left(n\vec{v}\right) = 0 \tag{1}$$

and simplified form of momentum conservation relation:

$$\partial \vec{v} / \partial t + \vec{v}.\left(\nabla \vec{v}\right) = -\frac{q}{m^*}\vec{E}_{total} - \frac{\vec{v}}{\tau_m} \tag{2}$$

are sufficient to represent the electron motion along a biased semiconductors as the electron velocity is below the saturation velocity (low field behavior) [1]. In (1)-(2), n, v, m^*, q, τ_m and E_{total} are electron: density, velocity, effective mass, unit charge (q = 1.6 × 10^{-19}C), momentum relaxation time, and total electric field, respectively. Here, it is assumed that the infinitesimal 2D conductor with surface electron density n_0 is located at the $z = 0$ plane. Additionally, the electron sheet is infinite along y axis, and electrons are not able to move in the perpendicular direction z due to the quantum confinement. Therefore, electric field component and electron velocity along y direction are disregarded. Moreover, it is assumed that a biased electric field E_0 externally applied on the electrons is able to move them with an average drift velocity v_0.

In our small signal analysis, it is presumed that the total electric applied on the 2D sheet ($z = 0$) is:

$$E^x_{total} = E_0 + E^x_{ss} \exp\left(j\omega t - \gamma x\right). \tag{3}$$

Due to direct dependency of electron density and velocity on the electric field value, they can be considered as $v_x = v_0 + v_x{}^{ss} \times \exp(j\omega t - \gamma x)$ and $n = n_0 + n^{ss} \times \exp(j\omega t - \gamma x)$, respectively. Inserting the electron density and velocity, and electric field into (1), it is obtained that:

$$\frac{\partial n}{\partial t} + \frac{\partial}{\partial x}\left(n_0 \times v_0 + n_0 \times v^{ss}{}_x \exp(j\omega t - \gamma x) + v_0 \times n^{ss} \exp(j\omega t - \gamma x) + v^{ss} \times n^{ss} \exp(2(j\omega t - \gamma x))\right) = 0 \tag{4}$$

as $z > 0$. After disregarding the last element of (4) with amplitude $v^{ss} \times n^{ss}$ and eliminating the exponential terms, it is obtained that $j\omega n^{ss} = \gamma \times \left(n_0 \times v^{ss}{}_x + v_0 \times n^{ss}\right)$ or:

$$v^{ss}{}_x = n^{ss} \times \frac{j\omega - v_0\gamma}{\gamma n_0}. \tag{5}$$

Inserting the electron density and velocity, and electric field into (2) yields:

$$j\omega v^{ss} \exp(j\omega t - \gamma x) + \left(v_0 + v^{ss} \exp(j\omega t - \gamma x)\right) \times$$
$$\frac{\partial}{\partial x}\left(v_0 + v^{ss} \exp(j\omega t - \gamma x)\right) = -\frac{q}{m^*} \times \tag{6}$$
$$\left(E_0 + E^x{}_{ss} \exp(j\omega t - \gamma x)\right) - \frac{v_0 + v^{ss} \exp(j\omega t - \gamma x)}{\tau_m}.$$

Separating harmonic and non-harmonic parts of (6) leads to:

$$\begin{cases} j\omega v^{ss} - \gamma v^{ss} v_0 = -\dfrac{q}{m^*} E^{ss} - \dfrac{v_{ss}}{\tau_m} \\ v_0 = -\dfrac{q\tau_m}{m^*} E_0 \end{cases}. \tag{7}$$

Additionally, surface current density of the 2D sheet $J = -(q \times n \times v)$ and the electrical conductivity σ are related as: $J = \sigma \times E$. Using the considered electron density and velocity, it can be easily shown that:

$$\sigma E^{ss} = -q\left(v_0 n^{ss} + n_0 v^{ss}\right). \tag{8}$$

Using (5) and (7)-(8), the surface conductivity of the biased electron sheet can be calculated as:

$$\sigma = \frac{n_0 q^2}{m^*} \frac{j\omega}{\left(j\omega - v_0\gamma\right)\left(j\omega - v_0\gamma + \dfrac{1}{\tau_m}\right)}. \tag{9}$$

B. TWO-DIMENSIONAL PLASMONS ALONG AN UN-GATED ELECTRON GAS

Here, the dispersion relation of 2D plasmons along a biased un-gated electron gas sheet is calculated. As mentioned in chapter 2, the solution of Maxwell equations with appropriate boundary conditions leads to:

$$-\frac{\sigma}{j\omega} = \frac{2\varepsilon}{\delta}. \tag{10}$$

Using (9)-(10) to define δ in terms of ω and γ, it can be calculated that:

$$\delta = \frac{-2\varepsilon m^*}{n_0 q^2}\left(j\omega - v_0\gamma\right)\left(j\omega - v_0\gamma + \frac{1}{\tau}\right). \tag{11}$$

Inserting (11) into the wave equation $\delta^2 + \gamma^2 + \dfrac{\varepsilon_r \omega^2}{c^2} = 0$, it is obtained that:

$$\gamma^2 = \frac{-1}{4a^2}\left(j\omega - v_0\gamma\right)^2\left(j\omega - v_0\gamma + \frac{1}{\tau}\right)^2 - \frac{\omega^2 \varepsilon_r}{c^2}, \tag{12}$$

where, $a = n \times q^2 / (4 \times \varepsilon \times m)$. Arranging (12) in term of γ lead to the following dispersion relation:

$$A_1\gamma^4 + A_2\gamma^3 + A_3\gamma^2 + A_4\gamma + A_5 = 0 \tag{13}$$

where:

$$A_1 = v^4_0, \quad A_2 = -\frac{2v^3_0}{\tau_m} - 4j\omega v^3_0$$

$$A_3 = -6\omega^2 v^2_0 + \frac{v^2_0}{\tau_m{}^2} + \frac{6j\omega v^2_0}{\tau_m} + 4a^2$$

$$A_4 = 4jv_0\omega^3 + \frac{6v_0\omega^2}{\tau_m} - \frac{2jv_0\omega}{\tau_m{}^2}$$

$$A_5 = \omega^4 - \frac{\omega^2}{\tau_m{}^2} - \frac{2j\omega^3}{\tau_m} + \frac{4a^2\omega^2\varepsilon_r}{c^2}$$

$$(14)$$

References:

[1]   S. M. Sze, K. K. Ng, Physics of Semiconductor Devices, *John Wiley & Sons, Inc.*, 3rd Edition, 2007.

APPENDIX II:

UNIVERSITY OF
ARKANSAS

College of Engineering
Department of Electrical Engineering

May 17, 2014

To whom it may be concerned,

I certify that Mr. Mohammadali Khorrami is the first author of the paper titled "Terahertz plasmon amplification using two-dimensional electron gas layers," published in Journal of Applied Physics, in May 2012. Mr. Khorrami completed the majority (more than 51 percent) of this research and writings of this paper.

Dr. Samir El-Ghazaly
Distinguished Professor
Electrical Engineering
Office: 3169 Bell Engineering Center
Phone: (479) 575-6048
Email: elghazal@uark.edu

3217 Bell Engineering Center • Fayetteville, AR 72701 • 479-575-3005 • Fax: 479-575-7967 • www.uark.edu
The University of Arkansas is an equal opportunity/affirmative action institution.

APPENDIX III:

AIP PUBLISHING LLC LICENSE
TERMS AND CONDITIONS

Apr 15, 2014

All payments must be made in full to CCC. For payment instructions, please see information listed at the bottom of this form.

License Number	3370530737606
Order Date	Apr 15, 2014
Publisher	AIP Publishing LLC
Publication	Journal of Applied Physics
Article Title	Terahertz plasmon amplification using two-dimensional electron-gas layers
Author	Mohammad Ali Khorrami, Samir El-Ghazaly, Shui-Qing Yu, et al.
Online Publication Date	May 1, 2012
Volume number	111
Issue number	9
Type of Use	Thesis/Dissertation
Requestor type	Author (original article)
Format	Print and electronic
Portion	Excerpt (> 800 words)
Will you be translating?	No
Title of your thesis / dissertation	Multi-Physics Modeling of Terahertz and Millimeter-wave Devices
Expected completion date	May 2014
Estimated size (number of pages)	150
Total	0.00 USD

Terms and Conditions

AIP Publishing LLC -- Terms and Conditions: Permissions Uses

AIP Publishing LLC ("AIPP") hereby grants to you the non-exclusive right and license to use and/or distribute the Material according to the use specified in your order, on a one-time basis, for the specified term, with a maximum distribution equal to the number that you have ordered. Any links or other content accompanying the Material are not the subject of this license.

1. You agree to include the following copyright and permission notice with the reproduction of the Material:"Reprinted with permission from [FULL CITATION]. Copyright [PUBLICATION YEAR], AIP Publishing LLC." For an article, the copyright and permission notice must be printed on the first page of the article or book chapter. For photographs, covers, or tables, the copyright and permission notice may appear with the Material, in a footnote, or in the reference list.
2. If you have licensed reuse of a figure, photograph, cover, or table, it is your responsibility to ensure that the material is original to AIPP and does not contain the copyright of another entity, and that the copyright notice of the figure, photograph, cover, or table does not indicate that it was reprinted by AIPP, with permission, from another source. Under no circumstances does AIPP, purport or intend to grant permission to reuse material to which it does not hold copyright.
3. You may not alter or modify the Material in any manner. You may translate the Material into another language only if you have licensed translation rights. You may not use the Material for promotional purposes. AIPP reserves all rights not specifically granted herein.

4. The foregoing license shall not take effect unless and until AIPP or its agent, Copyright Clearance Center, receives the Payment in accordance with Copyright Clearance Center Billing and Payment Terms and Conditions, which are incorporated herein by reference.

5. AIPP or the Copyright Clearance Center may, within two business days of granting this license, revoke the license for any reason whatsoever, with a full refund payable to you. Should you violate the terms of this license at any time, AIPP, AIP Publishing LLC, or Copyright Clearance Center may revoke the license with no refund to you. Notice of such revocation will be made using the contact information provided by you. Failure to receive such notice will not nullify the revocation.

6. AIPP makes no representations or warranties with respect to the Material. You agree to indemnify and hold harmless AIPP, AIP Publishing LLC, and their officers, directors, employees or agents from and against any and all claims arising out of your use of the Material other than as specifically authorized herein.

7. The permission granted herein is personal to you and is not transferable or assignable without the prior written permission of AIPP. This license may not be amended except in a writing signed by the party to be charged.

8. If purchase orders, acknowledgments or check endorsements are issued on any forms containing terms and conditions which are inconsistent with these provisions, such inconsistent terms and conditions shall be of no force and effect. This document, including the CCC Billing and Payment Terms and Conditions, shall be the entire agreement between the parties relating to the subject matter hereof.

This Agreement shall be governed by and construed in accordance with the laws of the State of New York. Both parties hereby submit to the jurisdiction of the courts of New York County for purposes of resolving any disputes that may arise hereunder.

If you would like to pay for this license now, please remit this license along with your payment made payable to "COPYRIGHT CLEARANCE CENTER" otherwise you will be invoiced within 48 hours of the license date. Payment should be in the form of a check or money order referencing your account number and this invoice number RLNK501279204. Once you receive your invoice for this order, you may pay your invoice by credit card. Please follow instructions provided at that time.

Make Payment To:
Copyright Clearance Center
Dept 001
P.O. Box 843006
Boston, MA 02284-3006

For suggestions or comments regarding this order, contact RightsLink Customer Support: customercare@copyright.com or +1-877-622-5543 (toll free in the US) or +1-978-646-2777.

Gratis licenses (referencing $0 in the Total field) are free. Please retain this printable license for your reference. No payment is required.

C.   2D PLASMON PROPAGATION INSIDE A TWO-DIMENSIONAL ELECTRON GAS LAYER WITH A LOW LOSS METALLIC GATE

IEEE Photonic Conference, pp. 895-896, San Francisco, Sep. 2012.

Abstract:

We have used perturbation theory to analytically characterize 2D plasmons' propagation inside gated two dimensional electron gas layers of hetero-structures. Using this analysis, the attenuations due to Ohmic losses of the metallic gate are calculated.

Introduction:

Two dimensional plasmons also called surface waves coupled to surface carriers (named SWC hereafter) have attracted a great interest in the area of microwave and terahertz (THz) devices because of strong field confinement and promises of novel THz devices such as sources, detectors and switches [1]-[4]. In spite of very attractive properties of SWC, their applications in room temperature devices have been limited due to large propagation losses caused by electron scatterings. However, the use of novel plasmonic materials such as graphene [5] and high quality

hetero-structures [1] has provided new paths toward modern THz plasmonic circuits. Although, the propagation losses due to limited electron mobilities of plasmonic materials have been extensively considered in different works (see [4] and its references), the Ohmic losses of adjacent metallic layers has always been disregarded by considering the metal as a Perfect Electric Conductor (PEC). With the advent of the novel plasmonic materials with acceptable level of electron scatterings, a complete investigation of the SWCs' attenuations due to the Ohmic losses is required.

In this paper, the effects of a low loss metal in the proximity of a two dimensional electron gas (2DEG) layer on the propagation characteristics of the SWCs are considered.

Analytical modeling of the SWC propagation along a 2DEG layer in the proximity of a low metallic gate:

Consider an infinitely wide (in y axis) and long (in x axis) 2DEG layer sheet with equilibrium charge density n_0 positioned at $z = 0$. It is assumed that the 2DEG layer is located inside a semi-infinite dielectric with permittivities $\varepsilon = \varepsilon_r \times \varepsilon_0$, $\varepsilon_0 = 8.85 \times 10^{-12}$ (F/m) extending from $z = d$ to $z = -\infty$. Here, SWCs' attenuations originated from lossy dielectrics and electron scatterings of the 2DEG layer are disregarded. In this manner, the wave attenuations caused only by the Ohmic losses are considered. To this end, a thick metallic layer with electrical conductivity σ_m is considered at $z = d$ parallel to the 2DEG layer. The metallic layer is assumed very thick compared to the skin depth so that it is assumed that it extends to $z = +\infty$. Considering the large conductivity value that is normal for metals such as gold and aluminum in THz frequencies, a TM^x mode wave can propagate along the 2DEG layer. Considering negligible mode variations from the ideal case with a PEC gate, the field values become:

68

$$E_x = \frac{-\delta^2}{j\omega\varepsilon}\psi, \; H_x = H_z = E_y = 0$$

$$H_y =$$

$$\begin{cases} \delta \times \phi_1 \exp\left(j(\omega t - \beta x) + \delta z\right) & z \le 0 \\ \delta \times \phi_2 \exp\left(j(\omega t - \beta x)\right)\cos\delta(z - d) & 0 < z \le d \end{cases} \qquad (1)$$

$$E_z =$$

$$\frac{-\gamma\delta}{j\omega\varepsilon} \times \begin{cases} \phi_1 \exp\left(j(\omega t - \beta x) + \delta z\right) & z \le 0 \\ \phi_2 \exp\left(j(\omega t - \beta x)\right)\cos\delta(z - d) & 0 < z \le d \end{cases}$$

where, ω, β and δ and are angular frequency, phase constant along x axis and attenuation constant in the perpendicular direction (z axis), respectively. Applying the boundary conditions at $z = 0$, it is concluded that $1 + \cot(\delta d) = \frac{-\delta\sigma}{j\omega\varepsilon}$ and $\varphi_1 = -\varphi_2 \sin(\delta d)$ [4] where σ is the surface conductivity of the 2DEG layer. Substituting the surface conductivity from simple Drude model $\sigma = \frac{-jn_0 q^2}{\omega m^*}$, the dispersion relation of the SWCs becomes $\beta = \pm\omega \times \sqrt{\frac{\varepsilon m^*}{n_0 q^2 d}}$ where, q and m^* are electron: unit charge 1.6×10^{-19} (c) and effective mass. In order to calculate the attenuation constant of the SWC due to Ohmic losses, the average power carried along x axis is first computed:

$$P = \int_{-\infty}^{d} \bar{S}_x dz, \; \bar{S}_x = -\frac{1}{2}\text{Re}\left\{E_z \times H_y^*\right\} \qquad (2)$$

that leads to:

$$P = \frac{\beta\delta}{4\omega\varepsilon}\phi_2^2 \sin^2(\delta d) + \dots$$

$$\frac{\beta\delta^2}{4\omega\varepsilon}\phi_2^2 \times \left(d + \frac{1}{2\delta}\sin(2\delta d)\right). \qquad (3)$$

Next, the Ohmic power losses induced by the wave attenuations at the surface of the low loss metal z = d from x = 0 to x = l (l is an arbitrary location) is calculated as:

$$P_c \mid_{x=l} = \frac{R_s}{2} \int_0^l J_s . J_s^* \, dx, \ J_s = \hat{n} \times H \mid_{z=d} \tag{4}$$

where the metal surface resistance $R_s = \sqrt{\omega\mu_0 / 2\sigma_m}$, $\mu_0 = 4\pi \times 10^{-7}$ (F/m). Considering the

definition of the attenuation constants due to power losses [6] $\alpha_c = P_c \mid_{x=l} / 2lP$, it is concluded

that:

$$\alpha_c = \frac{\delta\omega\varepsilon R_s}{\beta \sin^2(\delta d) + \beta\delta \times \left(d + \dfrac{1}{2\delta} \sin(2\delta d) \right)} . \tag{5}$$

Results and discussion:

Here, a wide band characterization of the SWCs' attenuations due to Ohmic losses in a specific

structure is performed. It is assumed that a 2DEG layer with surface charge density $n_0 = 10^{12}$

(cm^{-2}) is located inside an AlGaAs/GaAs hetero-structure with dielectric constant $\varepsilon_r = 12$. The

electron effective mass along the 2DEG is $m = 0.063 \times m_0$ ($m_0 = 9.1 \times 10^{-31}$ kg). A thick

aluminum gate with conductivity $\sigma_m = 3.5 \times 10^7$ (S/m) is placed above the hetero-structure with
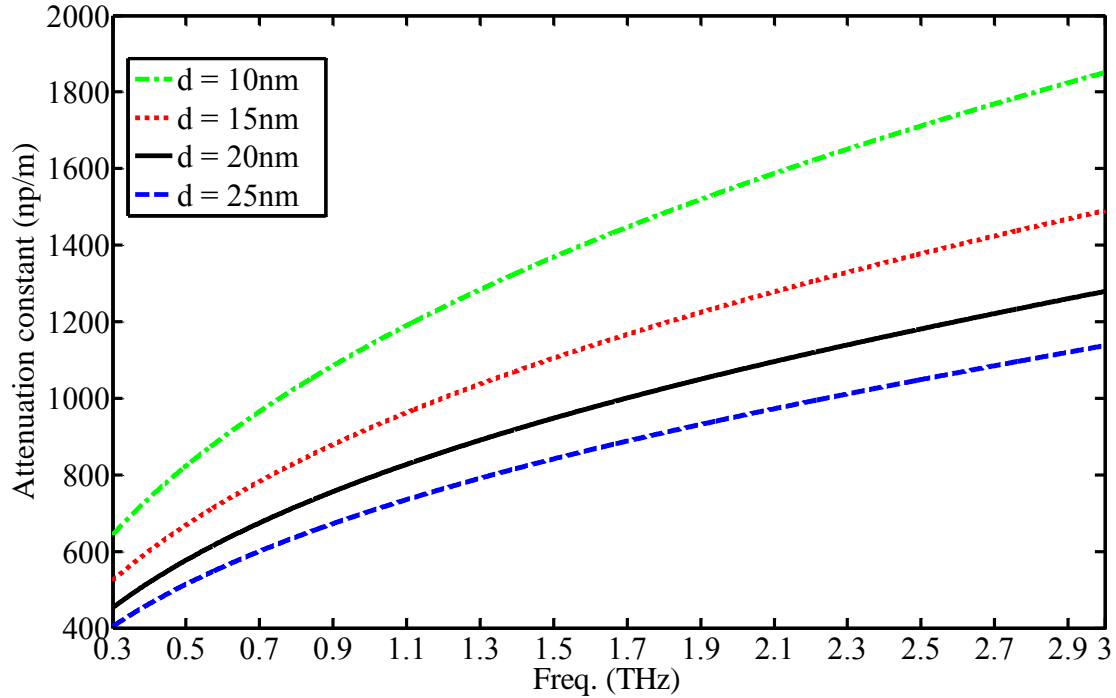
distance d from the 2DEG layer.

Fig. 1. SWCs' attenuation constants due to the Ohmic losses in THz frequency ranges.

In Fig. 1, the SWCs' attenuation constant due to the Ohmic losses calculated by the analytical method (5) is depicted in THz frequency ranges. As shown, the attenuation constant increases in higher frequencies. Besides, the Ohmic loss grows by decreasing the separation of the metallic gate and the 2DEG layer. This is clearly due to the enhanced field and metallic gate interactions. Considering the values of the calculated attenuation constants, it can be concluded that the Ohmic losses are negligible in the room temperature operation of recent plasmonic materials because of the substantially larger electron scatterings. However, the Ohmic losses effects become important in the cryogenic temperature operation of the plasmonic devices and also in the application of novel plasmonic materials as graphene with high electron mobilities even at room temperatures.

Conclusion:

An analytical method based on perturbation theory is presented to investigate the Ohmic losses

inside a gated 2D plasmonic waveguide. The analysis helps us to design optimized plasmonic circuits with acceptable level of losses in THz frequencies.

References:

[1]   W. F. Andress, H. Yoon, K. Y. M. Yeung, L. Qin, K. West, L. Pfeiffer and D. Ham, "Ultra-subwavelength two-dimensional plasmonic circuits", Nano Lett., vol. 12, pp. 2272-2277, Apr. 2012.

[2]   G. C. Dyer, G. R. Aizin, J. L. Reno, E. A. Shaner and S. J. Allen, "Novel tunable millimeter-wave grating-gated plasmonic detectors", IEEE J. Sel. Topics Quantum Electron., vol. 17, no. 1, pp. 85-91, Feb. 2011.

[3]   W. Knap, J. Lusakowski, T. Parenty, S. Bollaert, A. Cappy, V. V. Popov and M. S. Shur, "Terahertz emission by plasma waves in 60 nm gate high electron mobility transistors", Appl. Phys. Lett., vol. 84, pp. 2331-2333, Mar. 2004.

[4]   M. A. Khorrami, S. El-Ghazaly, S. Q. Yu, H. Naseem, "THz plasmon amplification using two-dimensional electron-gas layers", J. Appl. Phys., vol. 111, pp.094501(1)094501-(7), May 2012.

[5]   L. Ju, B. Geng, J. Horng, C. Girit, M. Martin, Z. Hao, H. A. Bechtel, X. Liang, A. Zettl, Y. R. Shen and F. Wang "Graphene plasmonics for tunable terahertz metamaterials" Nature Nanotech., vol. 6, pp. 630-634, Sep. 2011.

[6]   C. A. Balanis, Advanced Engineering Electromagnetics, New York: J. Wiley & Sons, 1989.

APPENDIX I:

UNIVERSITY OF ARKANSAS

College of Engineering
Department of Electrical Engineering

May 17, 2014

To whom it may be concerned,

I certify that Mr. Mohammadali Khorrami is the first author of the paper titled "2D plasmon propagation inside a two-dimensional electron gas layer with a low loss metallic gate," presented in *IEEE Photonic Conference*, at San Francisco. Mr. Khorrami completed the majority (more than 51 percent) of this research and writings of this paper.

Dr. Samir El-Ghazaly
Distinguished Professor
Electrical Engineering
Office: 3169 Bell Engineering Center
Phone: (479) 575-6048
Email: elghazal@uark.edu

3217 Bell Engineering Center • Fayetteville, AR 72701 • 479-575-3005 • Fax: 479-575-7967 • www.uark.edu
The University of Arkansas is an equal opportunity/affirmative action institution.

73

APPENDIX II:

Copyright Clearance Center

RightsLink®

Home   Create Account   Help

IEEE
Requesting permission to reuse content from an IEEE publication

Title: 2D plasmon propagation inside a two-dimensional electron gas layer with a low loss metallic gate

Conference Proceedings: Photonics Conference (IPC), 2012 IEEE

Author: Khorrami, M.A.; El-Ghazaly, S.

Publisher: IEEE

Date: 23-27 Sept. 2012

Copyright © 2012, IEEE

User ID

Password

☐ Enable Auto Login

LOGIN

Forgot Password/User ID?

If you're a copyright.com user, you can login to RightsLink using your copyright.com credentials. Already a RightsLink user or want to learn more?

Thesis / Dissertation Reuse

The IEEE does not require individuals working on a thesis to obtain a formal reuse license, however, you may print out this statement to be used as a permission grant:

Requirements to be followed when using any portion (e.g., figure, graph, table, or textual material) of an IEEE copyrighted paper in a thesis:

1) In the case of textual material (e.g., using short quotes or referring to the work within these papers) users must give full credit to the original source (author, paper, publication) followed by the IEEE copyright line © 2011 IEEE.
2) In the case of illustrations or tabular material, we require that the copyright line © [Year of original publication] IEEE appear prominently with each reprinted figure and/or table.
3) If a substantial portion of the original paper is to be used, and if you are not the senior author, also obtain the senior author's approval.

Requirements to be followed when using an entire IEEE copyrighted paper in a thesis:

1) The following IEEE copyright/ credit notice should be placed prominently in the references: © [year of original publication] IEEE. Reprinted, with permission, from [author names, paper title, IEEE publication title, and month/year of publication]
2) Only the accepted version of an IEEE copyrighted paper can be used when posting the paper or your thesis on-line.
3) In placing the thesis on the author's university website, please display the following message in a prominent place on the website: In reference to IEEE copyrighted material which is used with permission in this thesis, the IEEE does not endorse any of [university/educational entity's name goes here]'s products or services. Internal or personal use of this material is permitted. If interested in reprinting/republishing IEEE copyrighted material for advertising or promotional purposes or for creating new collective works for resale or redistribution, please go to http://www.ieee.org/publications_standards/publications/rights/rights_link.html to learn how to obtain a License from RightsLink.

If applicable, University Microfilms and/or ProQuest Library, or the Archives of Canada may supply single copies of the dissertation.

III. GLOBAL MODELING OF Active TERAHERTZ PLASMONIC DEVICES

A.   GLOBAL MODELING OF ACTIVE TERAHERTZ PLASMONIC DEVICES

IEEE Trans. THz Sci. Technol., vol. 4, no. 1, pp. 101-109, Jan. 2014.

Abstract:

   In this study, a full wave numerical technique is employed to characterize the propagation properties of 2D plasmons along Two Dimensional Electron Gas (2DEG) layers of biased hetero-structures at terahertz frequencies. This method is based on a coupled solution of Maxwell and hydrodynamic transport equations. In this manner, a complete description of carrier-wave interactions inside the 2DEG layer is obtained. Particularly, this simulator is employed to investigate the 2D plasmon variations initiated by the application of an external bias along the hetero-structure. Substantial changes in the plasmon characteristics such as wavelength and decay length are reported. It is also revealed that two symmetrical plasmonic modes along the un-biased 2DEG layer split into new asymmetrical ones after applying the bias voltage. The simulation has been performed in different structures to examine the effects of various electron

densities and the presence of periodic metallic gratings on the plasmon properties. Moreover, the 2D plasmon reflections from boundaries terminated by Ohmic contacts are separately studied. This research demonstrates the potentials of the 2D conductors in the design of novel active terahertz plasmonic devices as modulators and amplifiers while proposing a new approach for their modeling. The results of this simulation are verified independently with an analytical model.

Introduction:

  Recently, there has been a great interest among microwave and photonic research groups to exploit nano-plasmonics both in the visible and terahertz (THz) frequency ranges [1]-[3]. While Surface Plasmons (SPs) propagating on a dielectric-metal interface are suitable for localizing EM waves in nano-sized dimensions at optical frequencies, they are not confined to the interface at the lower part of the electromagnetic spectrum such as microwave and THz frequencies [4]. Therefore, the application of a highly doped semiconductor instead of the metal [4], engineering the metal electromagnetic (EM) properties by making holes and indentations on its surface to enhance carrier-wave interactions [5]-[6], or employing 2D conductors [7]-[10] have been proposed. Specifically, 2D conductors have become more interesting after the advent of graphene with very high charge mobilities even at room temperatures [11]-[12]. In 2D conductors, smaller numbers of electrons are affected by the EM waves compared to the metal-dielectric interface. Therefore, the collective plasma mode of the electrons gains significant amount of kinetic energy compared to the energy of the surrounding EM fields even at microwave and THz frequencies [13]. These plasma waves in 2D conductors are mostly called 2D plasmons or surface waves coupled to surface carries (shortened as SWC) [14]. They can propagate with velocities far lower than what is observed in SPs. Besides, 2D plasmon

wavelengths can be even 700 times smaller than the radiating mode wavelength in the free space [13]. Hence, 2D plasmons can be very useful in the fabrication of nano-sized microwave and THz devices. Specifically, 2D plasmons along the Two Dimensional Electron Gas (2DEG) layers of hetero-structures have been vastly employed in the design and fabrication of sources [15]-[16], resonant and non-resonant detectors [17]-[19], crystals and interferometers [13] and switches [20].

Mostly, the analysis of passive 2D plasmonic devices is performed using EM simulators as finite difference time domain (FDTD) [21] or distributed lumped element models [22]. These simulators represent conductors and doped semiconductors with the aid of Drude model as calculating field distributions and mode profiles within the devices. However, the analysis of modern active plasmonic circuits and devices as sources and detectors is not possible by simply using Drude model. This limitation exists since Drude approximation is a zero bias voltage model. Therefore, variations of the EM wave characteristic originated from the moving electrons accelerated by applied electric fields are disregarded. Besides, this model does not consider complex electron distributions inside the devices. Therefore, it is not able to provide a complete picture of electron-wave interactions. Non-linear effects such as electron velocity saturation due to electron heating are also not taken into account with this approximation. Previously, several analytical [8] and [23], and numerical [24] solutions of Poisson equation have been proposed to describe the THz wave propagation inside the 2D conductors. However, Poisson equation is not able to provide a fundamental insight into the electromagnetic wave propagation inside complex modern active plasmonic devices. For instance, wave impedances and transmitted power of each plasmonic mode is completely unknown while approximating the wave propagation using Poisson equation.

The rise of the active plasmonic area requires the development of a full wave simulator which enables the designer to completely capture the underlying physics of these devices. This simulator must provide a complete solution of coupled Maxwell and electronic transport equations. Previously, the necessity to characterize the carrier-wave interactions inside microwave transistors has led to the development of a similar numerical solver, mostly called global modeling [25]-[26]. Global modeling has also been employed at THz frequencies to characterize the electrical conductivities of silicon [27] and graphene layers [28]. In spite of the application of this modeling method in different high frequency applications, it has not been previously employed in the plasmonic area.

In this paper, we have employed the in-house global modeling simulator [25]-[26] to characterize the 2D plasmon propagation inside a non-degenerate 2DEG layer of a hetero-structure. This solver has been already validated through comparison of small-signal parameters and output voltages of similar microwave transistors with experimental results. This simulator solves a set of conservation equations, developed from the moments of Boltzmann transport equation, and Maxwell equations self-consistently. Here, global modeling is employed to investigate the possibility of guiding and amplifying THz plasmons in the 2DEG layer by applying a bias electric field. It is shown that the plasmon properties change vastly as the electrons are accelerated by the bias field. This type of investigation is able to provide real time information about electron density and velocity inside the plasmonic channel. In order to verify the results, the analytical model developed in [29]-[30] is employed. Compared to the analytical model in [29]-[30], this full wave simulator is able to consider the finite thicknesses of electron gas layers. Additionally, the influence of the wide band-gap semiconductor thickness on the properties of the 2D plasmons can be investigated. Moreover, the presence of Ohmic contacts on

the propagation characteristics of the surface waves can be examined using the global modeling method. Furthermore, the presence of metallic gratings, mostly fabricated on the device surface to excite a specific plasmonic mode may be taken into account using this technique.

Models and methods:

1. Electronic Transport model

Electron dynamics inside 2DEG layers of hetero-structures can be described by solving the moments of Boltzmann transport equation [25]. These strongly coupled highly non-linear set of partial differential equations relating volume electron density n_v and electron momentum $\vec{p}$ are:

1) Complete form of Momentum Conservation:

$$\frac{\partial(n_v p_x)}{\partial t} + \nabla.(n_v p_x \vec{v}) + \frac{\partial}{\partial x}(n_v k_B T) = \\ qn_v\left(E_x + \left(\vec{v}\times\vec{B}\right)_x\right) - \frac{n_v p_x}{\tau_m}$$

(1)

and

2) Continuity equations:

$$\frac{\partial n_v}{\partial t} + \nabla.(n_v \vec{v}) = 0$$

(2)

where, q, τ_m, T, and $\vec{v}$ are electron: unit charge, momentum relaxation time, temperature, and velocity, respectively. Moreover, k_B, $\vec{B}$ and $\vec{E}$ are Boltzmann constant, the magnetic flux and the electric field at the electron position, respectively. Additionally, the momentum conservation equation (1) can be similarly rewritten in other directions (*y* and *z*) too. Electronic current density $\vec{J}_v$ inside the 2DEG may be calculated at any time t as: $\vec{J}_v(t) = -qn_v(t)\vec{v}(t)$. Furthermore, the electron momentum and velocity are related through the electron effective mass m^* ($p = m^* \times v$). In general, a complete 1-D solution of the transport (continuity, momentum and energy conservations) equations can be performed. However, energy conservation equation (not

mentioned here) is not included in the solution presented in this paper. This does not change the validity of our analysis since the bias voltage and the ac incident electric fields are both chosen such that the device operates only in the linear section of the electron velocity-electric field curve [31].

2. Electromagnetic model

Maxwell equations can accurately characterize electromagnetic field propagation. In a uniform, isotropic and linear medium with relative permittivity ε_r and permeability μ_r, Maxwell equations are

$$\nabla \times \vec{H} = \varepsilon \frac{\partial \vec{E}}{\partial t} + \vec{J}_v \tag{3}$$

and

$$\nabla \times \vec{E} = -\mu \frac{\partial \vec{H}}{\partial t}. \tag{4}$$

In (3)-(4), $\vec{H} = \vec{B}/\mu$, $\varepsilon = \varepsilon_0 \times \varepsilon_r$ ($\varepsilon_0 \approx 8.85 \times 10^{-12}$ F / m) and $\mu = \mu_0 \times \mu_r$ ($\mu_0 \approx 4\pi \times 10^{-7}$ H / m)

are the magnetic field and the permittivity and the permeability of the corresponding medium, respectively. FDTD is a time domain solution of Maxwell equations using a mesh where the field components are arranged inside following Yee scheme [32]. The time and space derivatives in (3) and (4) are estimated using central differencing with the second order accuracy.

3. Coupling the EM and the electronic transport model

The EM solver calculates the field variations due to the moving charges while the electronic transport simulator updates charge properties altered by the applied fields. By passing physical parameters such as the fields and the current density between the two models, an appropriate link is established among the simulators. The initial state of the time-dependent calculation is obtained by solving Poisson equation ($\nabla^2 V = -q \left[N^+_D - n_v \right] / \varepsilon$ where N_D^+ is the ionized donor

density of the surrounding semiconductors) and electronic transport (continuity and momentum conservation) equations. This solution provides an initial electric field value for the FDTD simulation. At the steady state, Maxwell equations simplify to:

$$\nabla \times \vec{E}^{dc} = 0 \tag{5}$$

and:

$$\nabla \times \vec{H}^{dc} = J_v^{dc}. \tag{6}$$

Considering (6), it is suggested that the initial value of the magnetic field is introduced by the presence of $\vec{J}_v^{dc}$. Therefore, the magnetic field will be initiated properly by implementing the steady state current density inside the FDTD code.

As the initialization process ends, an ac excitation is applied. By defining total electric $\vec{E}^{total} = \vec{E}^{dc} + \vec{E}^{ac}$ and magnetic $\vec{H}^{total} = \vec{H}^{dc} + \vec{H}^{ac}$ fields and using Maxwell equations, it is concluded that:

$$\frac{\partial \vec{E}^{total}}{\partial t} = \frac{1}{\varepsilon}\left(\nabla \times \vec{H}^{ac} + \vec{J}_v^{dc} - \vec{J}_v^{total}\right) \tag{7}$$

$$\frac{\partial \vec{H}^{total}}{\partial t} = -\frac{1}{\mu}\nabla \times \vec{E}^{total} \tag{8}$$

where $\vec{J}_v^{total}$ is calculated by the device modeler after the ac excitation is applied. Therefore, the total electric and magnetic fields are updated at each time step by solving (8)-(9). These new values are fed to the device simulator to update the total current density at the same time step. Next, the updated total current density is used in the full wave solver to revise the fields at the following time step. This process continues until the set of equations satisfy each other self-consistently and the simulation becomes stable. A more detailed description of global modeling can be found in [25]-[26].

4. The simulated plasmonic structure and the simulation details

The 2-D schematic of the simulated active plasmonic structure is shown in Fig. 1. It is consisted of a hetero-structure (AlGaAs/GaAs) of thickness h_1 = 7.5 μm which is represented as a dielectric with ε_r = 12.6. Furthermore, a 2DEG layer of thickness d = 20nm is assumed at h_2 = 80nm underneath the surface. Ohmic contacts (named drain and source herein) at the device terminals are approximated as Perfect Electric Conductors (PECs) with fixed charge densities and very high electrical conductivities ($\approx 10^{10}$ S/m). This assumption is valid in most of the practical semiconductor devices due to very high surface recombination velocities at the contacts with excessive doping densities ($> 10^{17}$ cm^{-3}) [33]-[36]. An ac planar magnetic current sheet M_y, with a cell size thickness is considered in the top air section for the excitation. The magnetic current is oriented along $+y$ direction and is placed far enough away from the device, so that its evanescent modes do not reach the device. In this manner, only a plane wave hits the dielectric surface. The current source variations in time follow a sinusoidal shape with a single frequency f = 1 THz. Although the reported results are only for the single frequency of the incident sinusoidal wave, a wide band simulation can also be achieved using a Gaussian excitation pulse. Moreover, standard Perfect Match Layers (PML) developed by Berenger [37] are applied to the rest of the boundaries as depicted in Fig. 1. To reduce the numerical artifacts due to a finite spatial sampling of Maxwell equations, the PML losses along the direction normal to the boundary increase slowly from zero. To this end, PML layers with graded conductivities of a third order polynomial profile and with the reflection error of 10^{-8} are employed [37]. It is assumed that the size of the device along y-axis is very large in comparison to the wavelength of the 2D plasmons. Therefore, a 2D FDTD simulation is adequate. The mesh size along x axis (Δx) is mainly controlled by the Debye length criteria $\left(\Delta x < \sqrt{\varepsilon k_B T / n_v} \right)$ inside the semiconductor

82

simulator and the wavelength criteria (λ_p / 10 where λ_p is the 2D plasmon wavelength) within the EM solver [25]. This condition leads to $\Delta x \approx 10$ nm which ought to be applied inside both simulators. Within the FDTD code, the 2DEG is represented as an electric current source with one cell size thickness. This sets the minimum mesh size along z axis ($\Delta z_{min} = d$). In order to reduce the computational burden enforced by the small 2DEG thickness, a non-uniform mesh is employed along z direction. The maximum allowable mesh size along z (Δz_{max}) is defined by the wavelength of the incident field λ inside the dielectric. The maximum allowable simulation time step Δt is primarily defined by the Courant-Friedrichs-Lewy stability condition [37]. Taking this constraint into account, Δt becomes in the order of 10^{-17} (s). Here, a 1D solution of the transport equation is performed. This does not affect the accuracy of our analysis since electron movement in the z direction is restricted by the quantum confinement that exists inside the hetero-structure.

Appropriate boundary conditions are required to solve continuity and Poisson equations. To this end, charge densities of the 2DEG end nodes are fixed to their equilibrium value. This means that the Ohmic contacts do not allow any charge density variations at their adjacent points. Inside the biased structure, the node placed at the source contact is grounded while the one at the drain is connected to the external bias voltage V_{ds}.
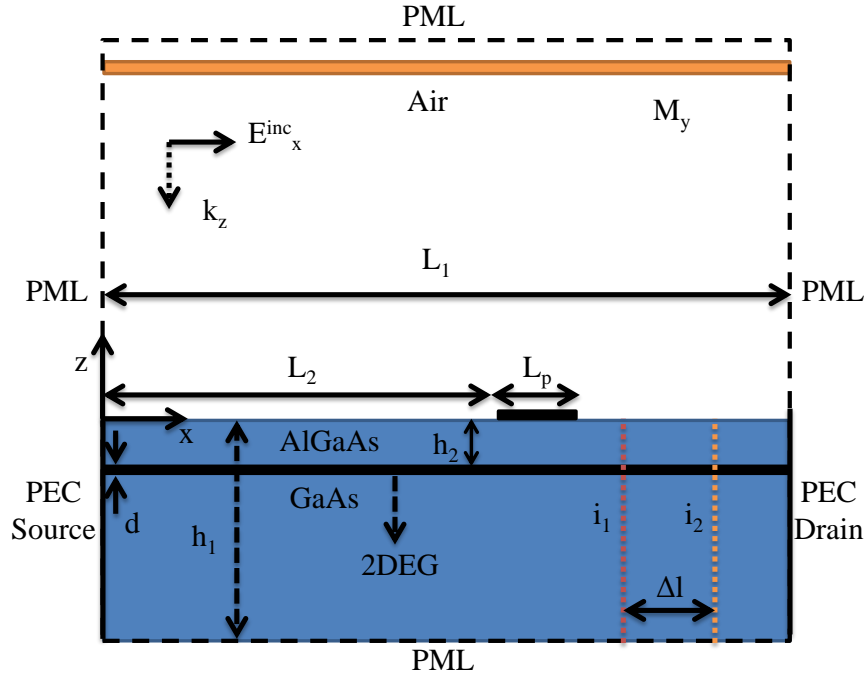
Fig. 1. The 2-D structure simulated by the global modeling technique (figure not to scale).
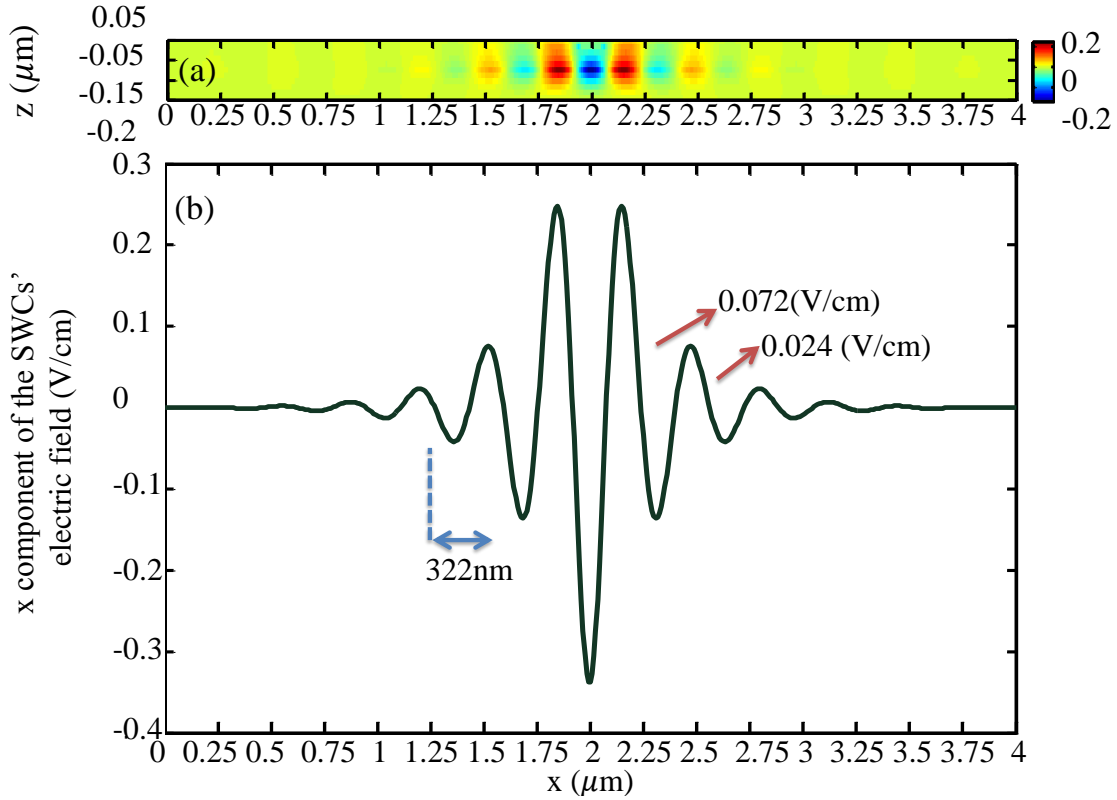

Fig. 2. The SWCs' x component of the electric field: (a) distribution close to the 2DEG layer and (b) variations at $z = -h_2$ are illustrated. The SWCs' attenuation constant is approximated ± 29.5 (dB/μm). The SWCs' phase constants are
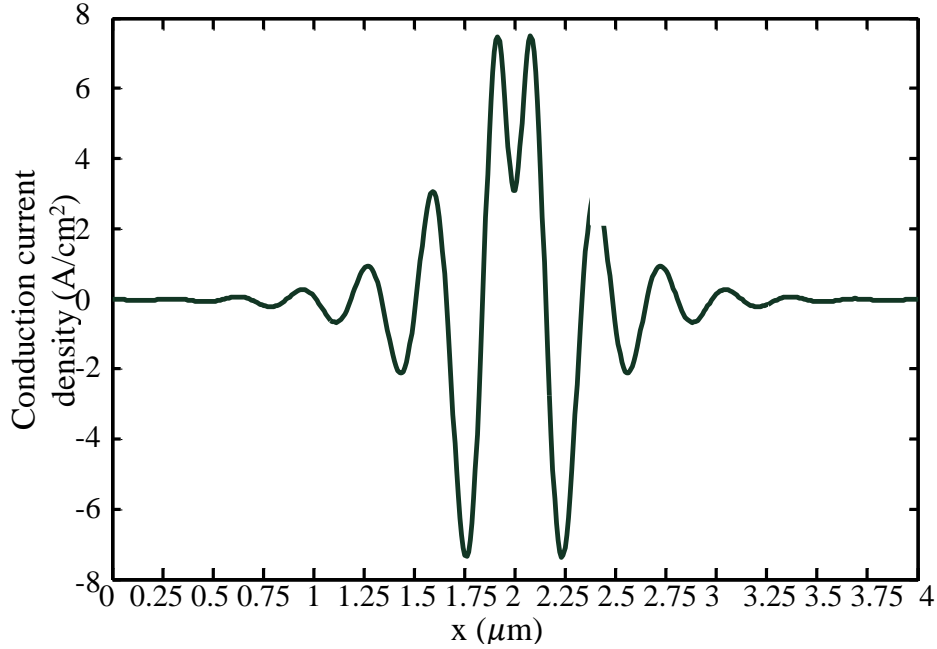
estimated as ± 19.6 (Rad/μm).

Fig. 3. The conduction current density variations due to the SWCs originated from the plasmon launcher at $z = -h_2$ are shown.

In order to excite the 2D plasmons inside the 2DEG, a PEC section with one cell size thickness is placed on the top surface of the device ($z = 0$) at $x = L_2$. Its length has been chosen to be very small compared to the wavelength of the radiating mode in the air. This PEC section represents thin metallic gratings that are mostly placed adjacent to the 2DEG layer. The gratings are frequently employed to excite 2D plasmons by the incident wave diffraction. Hereafter, this thin metal is called plasmon launcher. The distance between the 2DEG and the plasmon launcher should be chosen appropriately so that a substantial amount of the diffracted wave couples to the 2DEG layer.

Results and discussion

In this section, the described full wave simulator is employed to characterize the 2D plasmon propagation along the detailed hetero-structure under different bias voltages at a single frequency f = 1THz. This frequency is chosen arbitrarily and the analysis is applicable at different

frequencies. Herein, the surface charge density of the 2DEG layer is assumed $n_0 = 10^{11} cm^{-2}$.

Moreover, the length of the simulated device is $L_1 = 4$ μm (see Fig. 1). In this paper, the low field mobility of the hetero-structure is considered by the transport parameters $\tau_m = 1$ ps and m^* $= 0.063 m_0$, where m_0 is the electron rest mass. The corresponding electron mobility is accessible even at 200K [38]. In order to excite the SWCs, a plasmon launcher with length $L_p = 100$ nm is placed in the middle of the structure ($L_2 = 1.95$ μm) in the close proximity of the 2DEG layer at the top surface of the semiconductor.

In order to separate the SWCs excited at the plasmon launcher from the other field values such as the transmitted time varying field, two different simulations have been performed. First, the plasmon launcher is placed on the surface of the structure and the simulation is performed until a specific time step t_1. Next, a similar simulation is executed as the plasmon launcher is removed. Afterwards, the respective field values computed in the simulations are subtracted from each other.

1. 2D plasmon propagation inside an unbiased hetero-structure

As previously presented in [7] and [30], 2D plasmons propagate along unbiased conductors with propagation constants:

$$\gamma = \pm \frac{j}{2a} \sqrt{ \omega^4 - \frac{\omega^2}{\tau_m^2} - \frac{2 j \omega^3}{\tau_m} + \frac{4 a^2 \omega^2 \varepsilon_r}{c^2} }, \quad a = \frac{n_0 q^2}{4 \varepsilon m^*} \tag{9}$$

where, $\omega = 2\pi f$ and c are angular frequency and the speed of light in the vacuum, respectively. In the calculation of the dispersion relation (9), wave function (refer to [39] for the definition) of the plasmonic mode is considered as:

$$\psi = \begin{cases} \phi_1 \exp(j\omega t - \gamma x - \delta z) & z \geq 0 \\ \phi_2 \exp(j\omega t - \gamma x + \delta z) & z < 0 \end{cases} \tag{10}$$

86

where, γ is the complex propagation constant. Real (α) and imaginary (β) parts of γ are called attenuation and phase constants, respectively.

Inserting the 2DEG layer charge density and the transport parameters (including the momentum relaxation time) into (9), it is calculated that $\alpha_{1,2} = \pm 26.9$ (dB/µm), $\beta_{1,2} = \pm 19.5$ (Rad/µm) and the 2D plasmons wavelength ($\lambda_p = 2 \times \pi / |\beta_{1,2}|$) is 322nm.

In Fig. 2.(a), the electric field distribution of the 2D plasmons in the proximity of the 2DEG layer calculated by the numerical solver, in the time step t_1 is depicted. As shown, SWCs are excited as a result of the incident wave diffraction at the plasmon launcher. It is also observed that the SWCs are facing large attenuations due to the electron scatterings as moving in $\pm x$ directions. In Fig. 2.(b), the x component of the electric field (at $z = -h_2$) of the SWCs inside the unbiased hetero-structure is depicted. As illustrated, the numerical technique has calculated the 2D plasmon propagation constant nearly equal to the values estimated by the analytical model (9). The small deviation of the attenuation constant from the value predicted in (9) can be partly due to the presence of the Ohmic contacts that are not considered by the analytical model. Here, the accuracy of the attenuation constant calculation has been improved using the technique detailed in Appendix I.

In Fig. 3, the conduction current variations (J_v) at $z = -h_2$ are depicted. This physical property can be useful in the design of plasmonic detectors with a specific responsivity. By choosing appropriate device length, channel properties and plasmon launcher size, the design of an efficient THz non-resonant plasmonic detector is possible. As shown in Fig. 3, the electrons are accelerated and decelerated at specific locations that correspond to the maximum magnitudes of the electric field.

2. 2D plasmon propagation inside a biased hetero-structure

As previously proved analytically [30], the symmetrical 2D plasmons inside the un-biased 2DEG with the dispersion relation defined in (9) split into four asymmetrical modes. The propagation constant of these modes are:

$$A_1\gamma^4 + A_2\gamma^3 + A_3\gamma^2 + A_4\gamma + A_5 = 0 \tag{11}$$

where,

$$
\begin{aligned}
&A_1 = v^4{}_0, \quad A_2 = -\frac{2v^3{}_0}{\tau_m} - 4j\omega v^3{}_0, \ A_3 = -6\omega^2 v^2{}_0 + \\
&\frac{v^2{}_0}{\tau_m{}^2} + \frac{6j\omega v^2{}_0}{\tau_m} + 4a^2, \ A_4 = 4jv_0\omega^3 + \frac{6v_0\omega^2}{\tau_m} - \frac{2jv_0\omega}{\tau_m{}^2} \\
&A_5 = \omega^4 - \frac{\omega^2}{\tau_m{}^2} - \frac{2j\omega^3}{\tau_m} + \frac{4a^2\omega^2\varepsilon_r}{c^2}.
\end{aligned}
\tag{12}
$$

In (12), v_0 is the electron average drift velocity inside the biased hetero-structure.

Here, the bias voltage V_{ds} = 143 (mV) is applied onto the Ohmic contacts. This voltage establishes the electric field E_0 = 360 (V/cm) inside the device. Considering the linear relation between the electron average velocity and the electric field ($v_0 = \frac{q\tau_m}{m^*} \times E_0$), the electron velocity becomes $v_0 \approx 10^7$ (cm/s). Using (11)-(12), it is concluded that the plasmonic modes propagating opposite to the electron drift stream suffer from very high attenuations compared to ones moving parallel to it. From (11), it is calculated that the $+x$ going plasmonic mode inside the biased structure propagates with α'_1 = 14.7 (dB / μm), β'_1 = 12 (Rad/μm) and the wavelength 524 nm. On the other hand, the mode propagating in the opposite direction ($-x$) yields the attenuation constant α_2' = 39.9 (dB / μm). Due to the large attenuation constant of the $-x$ going SWC, this specific mode is not excited as will be reported in the following.

In Fig. 4.(a), the SWC electric field distribution in the proximity of the 2DEG layer inside the biased hetero-structure at time t_1 is depicted. In contrast to the unbiased device (Fig. 2.a), the 2D

plasmons are propagating only in one direction (+*x*). In Fig. 4.(b), the x component of the SWC electric field at z = -h$_2$ is depicted. As illustrated, there exist a slight difference between the phase constant of the plasmonic mode computed by the analytical method (12 Rad/μm) and the one obtained from the numerical techniques (11.6 Rad/μm). This alteration is by virtue of the wideband-gap semiconductor thickness consideration inside the full wave simulator. As expected, the bias field has caused large changes in the phase constant of the plasmonic mode. Besides, the *-x* going plasmonic mode has not been excited due to the large attenuations. Considering these results, it seems that the steering of the 2D plasmons can effectively become possible by applying bias voltage along the plasmonic waveguide. In Fig. 5, the variations of the 2D plasmon conduction current at z = -h$_2$ are shown.
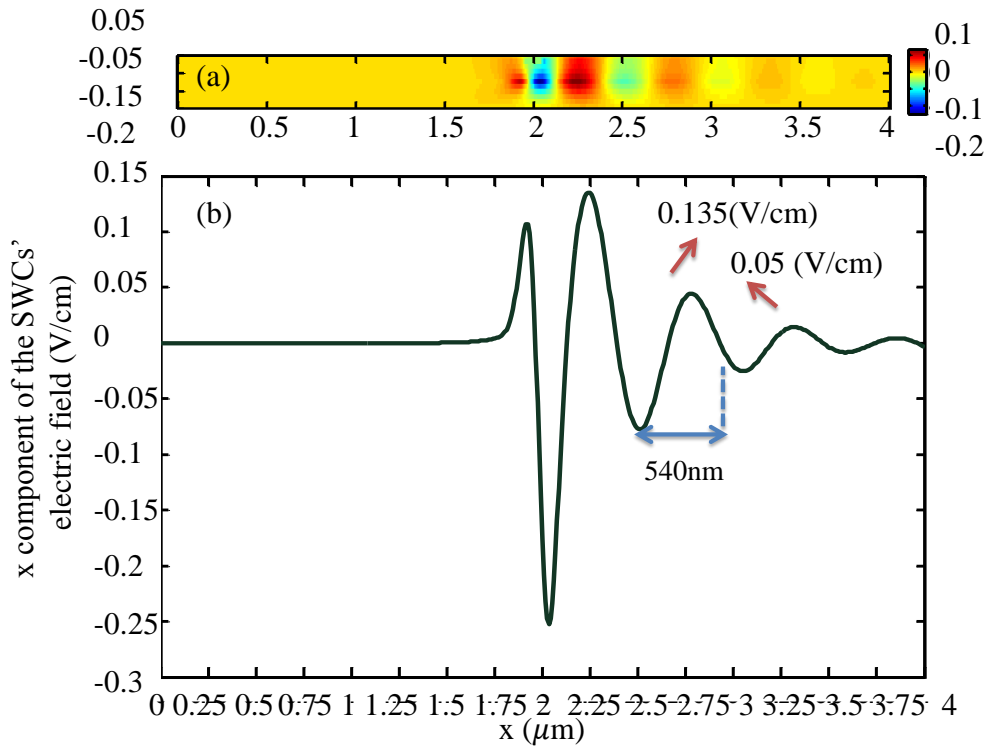

Fig. 4. The SWCs' x component of the electric field: (a) distribution next to the 2DEG layer and (b) variations at z = -h$_2$ are depicted. The SWCs' attenuation and phase constants are approximated as 15.9 (dB/μm) and 11.6 (Rad/μm), respectively.
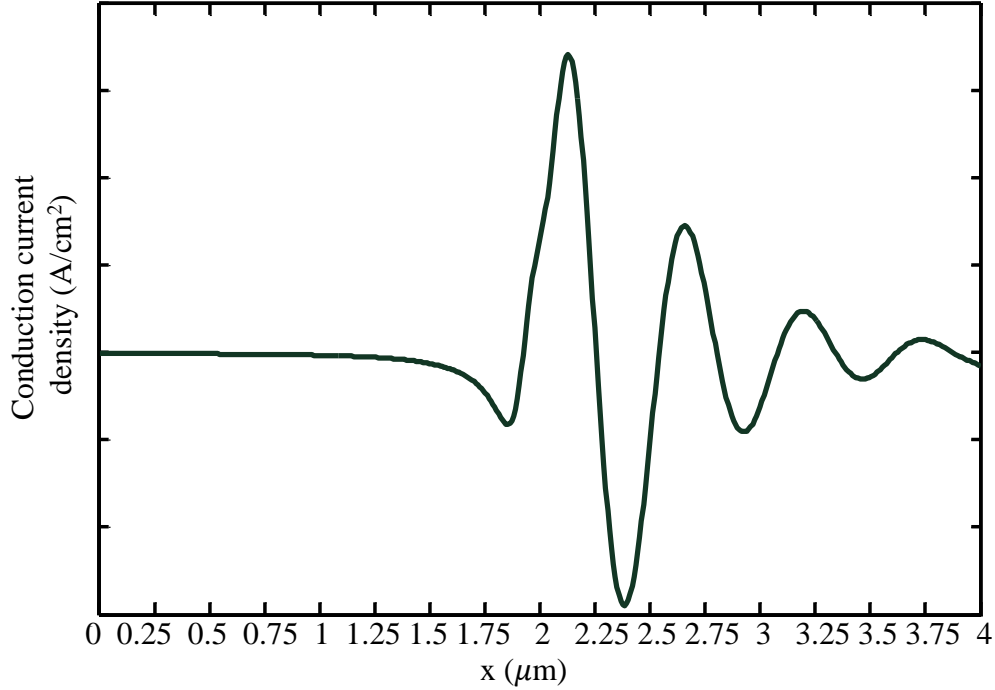
Fig. 5. The SWCs' conduction current density variations at $z = -h_2$ is illustrated.

3. 2D Plasmon reflection from Ohmic contacts inside a biased hetero-structure

To present the capabilities of the developed numerical technique compared to the analytical model, the 2D plasmon reflections from Ohmic contacts of the biased structure is analyzed. To this end, the plasmon launcher is considered closer to the drain contact ($L_2 = 3$ μm) compared to the previous case of study. This enables the excited surface waves to reach the contact before its amplitude becomes almost equal to zero. Fig. 6 depicts the variations of the x component of the electric field inside the biased hetero-structure. As expected, the $+x$ moving surface waves are originated from the launcher while high attenuations prevent any plasmon generation with the opposite direction of propagation. As illustrated in Fig. 6, the phase constant of the dominant mode along the electron gas layer has not been changed. Considering the magnitude of the electric field component at the proximity of the drain contact, interesting changes in the field distribution are observed. As depicted in Fig. 7., the surface wave does not follow the wave function of the +x going mode strictly next to the contact. This is due to the excitation of higher

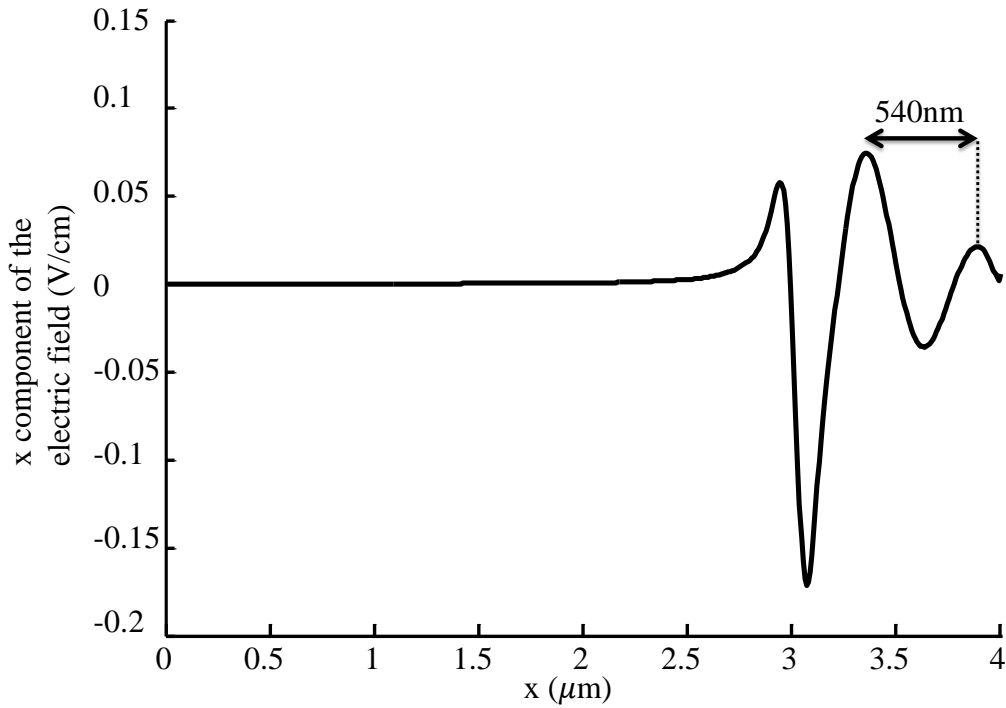order evanescent modes or possibly the –x moving plasmonic modes.

Fig. 6. The variations of the x component of the electric field (V/cm) at z = -h_2 is depicted. The location of the plasmon launcher is chosen intentionally to observe the wave reflections from the drain. The inset portrays the field value changes next to the drain contact at x = 4 μm.
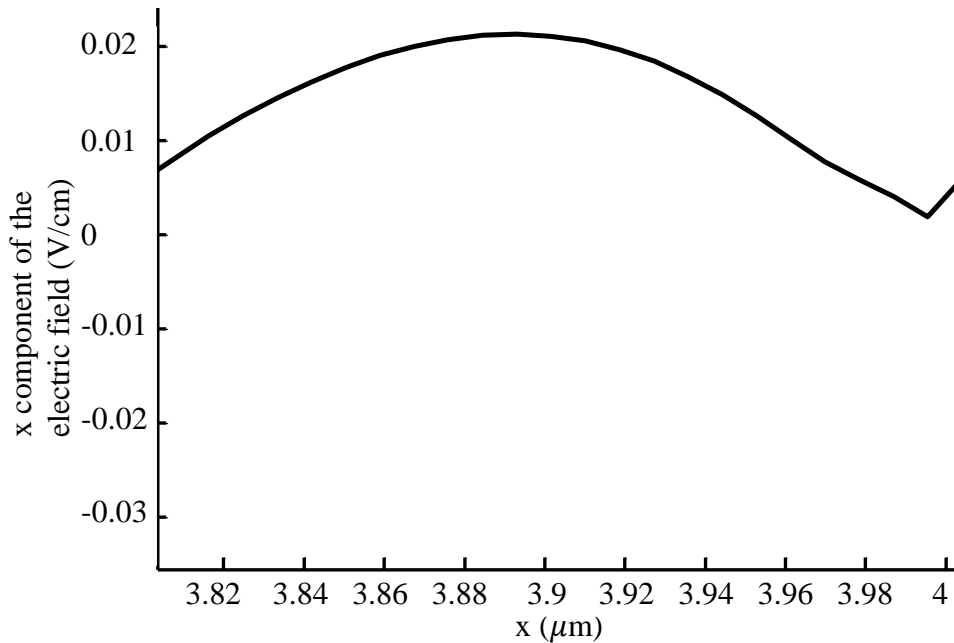

Fig. 7. The field value changes next to the drain contact at x = 4 μm.

Controlling the Wave Properties of the 2D Plasmons by Changing the Bias Voltage:

Commonly, the charge densities of the 2DEG layers of hetero-structures are controlled by implementing a gate above the wideband gap semiconductor (top-gate) or beneath the substrate (back-gate). In this manner, the designer can simultaneously optimize the plasmonic circuit by changing the gate and the drain-source voltages. Here, the dependency of the plasmon properties on the 2DEG layer charge density is considered. To this end, the numerical simulator is employed to simulate the described structure as the electron density of the 2DEG layers has been increased to a new value $n'_0 = 2 \times 10^{11}$ (cm^{-2}).

Using (9), it is expected that the unbiased hetero-structure can guide plasmons with $\alpha_{1,2} = \pm 13$ (dB / μm) and $\beta_{1,2} = \pm 10$ (Rad / μm). However, the plamonic modes will divide into asymmetrical modes as the electrons are accelerated by an external bias field with an average electron velocity $v_0 \approx 10^7$ (cm / s). The mode that propagates in $+x$ direction attains $\alpha'_1 = 9.5$ (dB / μm) and $\beta'_1 = 7.6$ (Rad / μm) as the other mode which travels against the electron drift stream has $\alpha'_2 = -26.9$ (dB / μm) and $\beta'_2 = -15$ (Rad / μm).

In the full wave simulation, the device length and the surface charge density of the 2DEG have been increased to $L_1 = 6$μm and $n'_0 = 2 \times 10^{11}$ (cm^{-2}) as other specification are kept similar to the previous structure. In order to accelerate the electrons with the average velocity $v_0 = 10^7$ (cm / s), the applied voltage has been augmented to $V_{ds} = 215$(mV).

1. Surface wave excitation using a single plasmon launcher:

Here, a metallic layer is considered in the middle of the simulated structure surface ($L_2 = 2.95$μm) to excite the plasmons. Fig. 7. (a),(b) display the ac electric field distribution of the 2D plasmons calculated by the global modeling technique. As depicted in Fig. 7.(a), the 2D plasmons are propagating in the $\pm x$ directions symmetrically. As the bias voltage is applied onto

the contacts, asymmetric 2D plasmons are excited in the $+x$ and $-x$ directions (see Fig. 7.(b)). The x component of the ac electric field at $z = -h_2$ is presented in Fig. 7. (c) as $V_{ds} = 0$ and 215 (mV). As depicted, the numerical solver has calculated the propagation constants of the plasmonic modes equal to ±9 (Rad / μm) as $V_{ds} = 0$, and 6.3, -13.1 (Rad / μm) as $V_{ds} = 215$ (mV). Comparing the results attained from the analytical and the numerical techniques, it is understood that there exists a difference (about ten percent) between the outcomes which is due to the consideration of the wideband-gap semiconductor thickness inside the full wave simulator. As illustrated in Fig. 7. (c), the wavelength of the $+x$ moving 2D plasmons has been increased about 30 percent after applying the bias field. As demonstrated, the 2D plasmonic mode that is allowed to propagate in the $-x$ direction has also been excited in contrast to the previous example. Therefore, the gate control voltage has helped to excite new plasmonic modes inside the device by doubling the electron gas charge density.
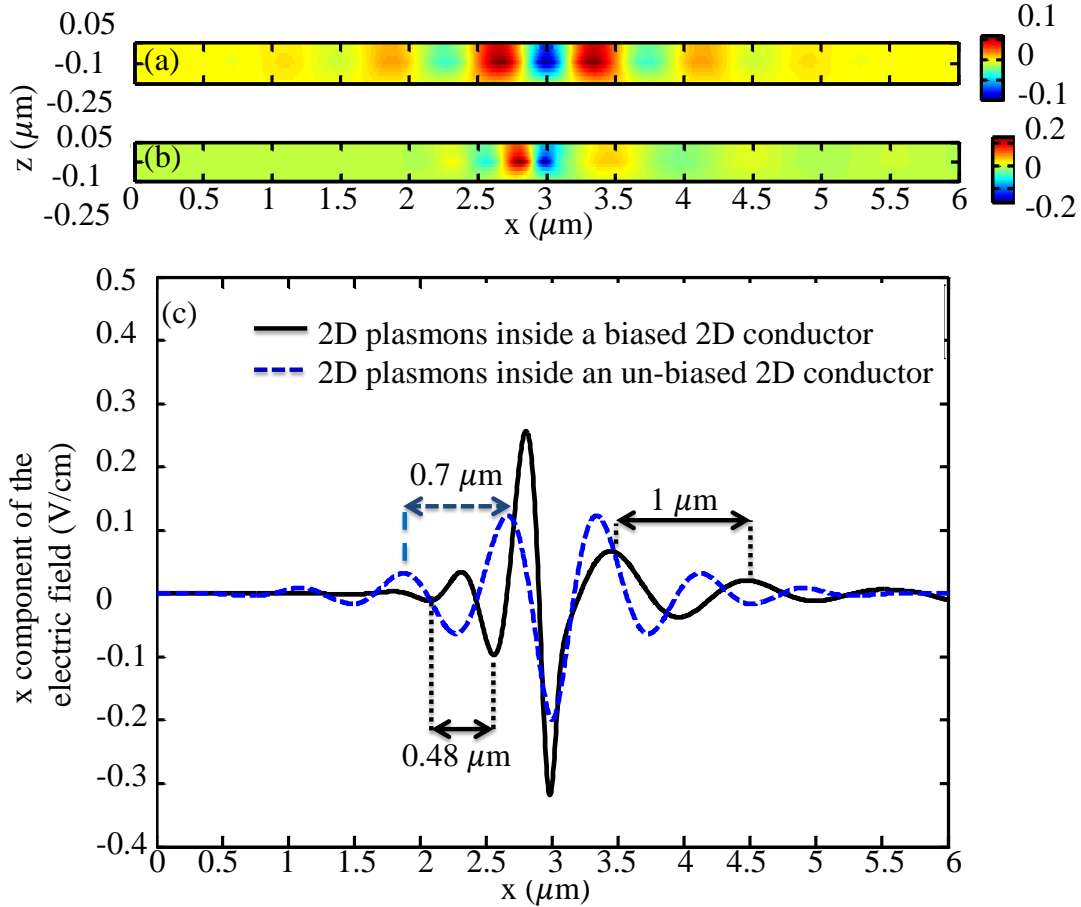
Fig. 7. (a), (b) The distribution of the "x" component of the electric field next to the 2DEG layer of the unbiased and the biased hetero-structure are shown, respectively. (c) The x component of the electric field variations at z = -h_2 inside the device under different bias conditions is shown. The approximated attenuation constant inside the unbiased structure is 14.7 (dB/μm). The +x and –x mode attenuation constants of the plasmons inside the biased device are 9.5 and 30.4 (dB/μm), respectively.

2. Plasmon excitation using a metallic grating:

Here, the wave propagation along the 2DEG in the presence of a periodic grating is investigated. To this end, five periods of the PEC layer with length 0.2 μm employed. The arrangement of the grating on the device top surface is detailed in Fig. 8. The period of the grating (0.7 μm) is chosen equal to the wavelength of the plasmons inside the unbiased structure.

Fig. 9.(a), (b) depict the ac electric field distributions along the electron gas layer as $V_{ds} = 0$ and 215 (mV), respectively. As presented in Fig. 9.(a), (b), the surface waves are launched along

94

the hetero-structure in both conditions. In Fig. 9.(c), the variations of the electric field component are illustrated. As described in Fig. 9.(c), the plasmonic mode with wavelength 0.7 μm is uniformly launched along the electron gas inside the unbiased structure. However, the 2D plasmons are weakly excited as the bias voltage is applied between the contacts. As presented, the $+x$ and $-x$ moving surface waves are excited inside the biased structure due to the diffraction of the incident wave at the periodic metallic grating. Due to the mismatch between the grating period and the plasmonic mode wavelengths, the plasmon launcher is performing inefficiently. Non-sinusoidal distribution of the electric field at locations between the periodic gratings is because of the summation of the different modes excited at the edges of neighboring metals. The field deviations from the $+x$ moving mode wave function discussed in section III, part C, are also depicted in Fig. 9.(c) at the vicinity of the drain contact ($x = 6$ μm).
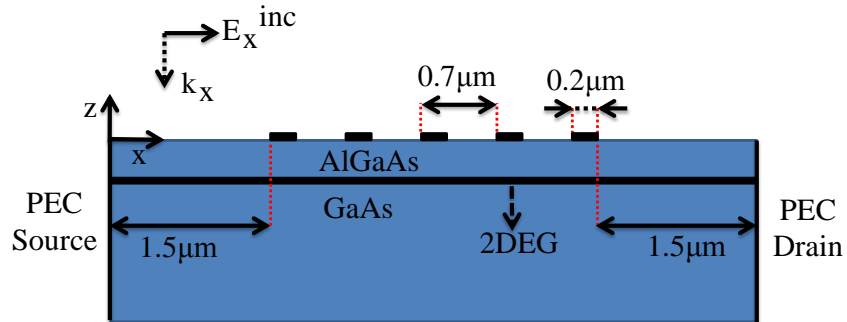

Fig. 8. A schematic of the simulated hetero-structure as the periodic grating is presented on the device surface.
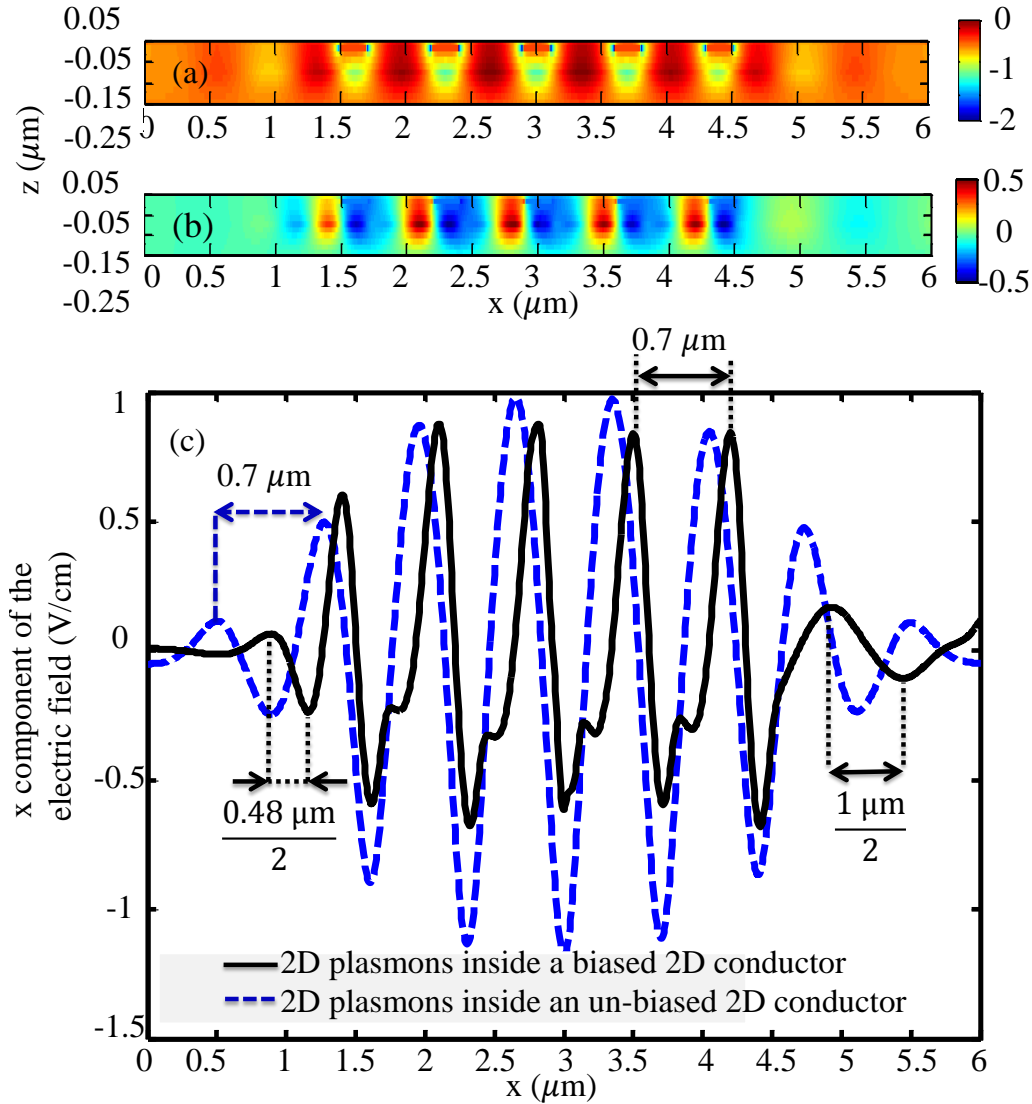
Fig. 9. (a), (b) The distribution of the "x" component of the electric field next to the 2DEG layer with the periodic grating under different bias conditions are shown. (c) The x components of the electric field variations at z = -h_2 inside the device as $V_{ds} = 0$ and 215 (mV) are shown.

Conclusion

A full wave simulation technique is employed to analyze novel active plasmonic devices. The simulator solves Maxwell and the moments of Boltzmann equations numerically in a self-consistent manner. The effectiveness of this method is presented by characterizing 2D plasmon propagation along the two dimensional electron gas layer of a hetero-structure under different bias conditions. Using this technique, vast variations in the plasmon properties originating from

the biasing of the hetero-structure are reported. It is observed that the 2D plasmons propagating against the electron drift motion face larger attenuations compared to the ones moving in the same direction. The analysis has been performed inside 2DEG layers with different charge densities to investigate the gating effects on the 2D plasmon characteristics. It is concluded that new plasmonic modes can be excited by applying various bias voltages onto the device. This idea can help the designers to fabricate novel plasmonic devices such as switches and modulators. This numerical technique can also be useful in the modeling of available THz plasmonic detectors and sources.

References:

[1]   L. Ju, B. Geng, J. Horng, C. Girit, M. Martin, Z. Hao, H. A. Bechtel, X. Liang, A. Zettl, Y. R. Shen and F. Wang "Graphene plasmonics for tunable terahertz metamaterials" *Nature Nanotech.*, vol. 6, pp. 630-634, Sep. 2011.

[2]   L. Ji, and V. V. Varadan, "Fishnet metastructure for efficiency enhancement of a thin film solar cell", *J.* Appl. Phys., vol. 110, p. 043114, Aug. 2011.

[3]   M. Lee and M C. Wanke, "Searching for a solid state technology", Science, vol. 316, pp. 64-65, Apr. 2007.

[4]   S. A. Maier, "Plasmonics: Fundamentals and applications", Springer, 2007.

[5]   Z. Fu, Q. Gan, Y. J. Ding and F. J. Bartoli, "From waveguiding to spatial localization of THz waves within a plasmonic metallic grating", *IEEE J. Sel. Topics Quantum Electron.*, vol. 14, no. 2, pp. 486-490, Apr. 2008.

[6]   W. Zhu, A. Agrawal, A. Cui, G. Kumar and A. Nahata, "Engineering the propagation properties of planar plasmonic terahertz waveguides", *IEEE J. Sel. Topics Quantum Electron.,* vol. 17, no. 1, pp. 146-153, Jan. 2011.

[7]   F. Stern, "Polarizabilty of a two-dimensional electron gas", *Phys. Rev. Lett.*, vol. 18, no. 14, pp. 546-548, Apr. 1967.

[8]   M. Dyakonov and M. Shur, "Detection, mixing, and frequency multiplication of Terahertz radation by two-dimensional electron fluid", *IEEE Trans. Electron Dev.,* vol. 43, no. 3, pp. 380-387, March 1996.

[9]   P. J. Burke, I. B. Spielman, J. P. Eisenstein, L. N. Pfeiffer, "High frequency conductivity of the high-mobility two-dimensional electron gas", *App. Phys. Lett.,* vol. 76, no. 6, pp. 745-747, Feb. 2000.

[10]   M. A. Khorrami, and S. El-Ghazaly, "2D plasmon propagation inside a two-dimensional electron gas layer with a low loss metallic gate", *IEEE Photonics Conference (IPC),* pp. 895-896, Sept. 2012.

[12]   A. K. Geim, and K. S. Novoselov, "The rise of graphene", *Nature*, vol. 6**,** pp. 183-191, March 2007.

[13]   R. Alaee, M. Farhat, C. Rockstuhl, and F. Lederer, "A perfect absorber made of a graphene micro-ribbon metamaterial"*Opt. Express,*vol. 20, no. 27, p. 28017, Dec. 2012.

[14]   W. F. Andress, H. Yoon, K. Y. M. Yeung, L. Qin, K. West, L. Pfeiffer and D. Ham, "Ultra-subwavelength two-dimensional plasmonic circuits", *Nano Lett.,* vol. 12, pp. 2272-2277, Apr. 2012.

[15]   M. Nakayama, "Theory of surface waves coupled to surface cariers", J. *Phys. Soc. Jpn.* vol. 36, no. 2, pp. 393–398, Sept. 1974.

[16]   B. Sensale-Rodrigues, L. Liu, P. Fay, D. Jena, and H. Grace, "Power amplification at THz via plasma wave exciation in RTD-Gated HEMTs", *IEEE Trans. THz Sci. Technol.,* vol. 3, no. 2, March 2013.

[17]   W. Knap, J. Lusakowski, T. Parenty, S. Bollaert, A. Cappy, V. V. Popov and M. S. Shur, **"**Terahertz emission by plasma waves in 60 nm gate high electron mobility transistors", *Appl. Phys. Lett.*, vol. 84, pp. 2331-2333, Mar. 2004.

[18]   T. Otsuji, T. Watanabe, S. A. B. Tombet, A. Satou, W. M. Knap, V. V. Popov, M. Ryzhii, and V. Ryhzhii, "Emission and detection of terahertz radiation using two-dimensional electrons in III-V semiconductors and graphene", *IEEE Trans. THz Sci. Technol.,* vol. 3., no. 1, Jan. 2013.

[19]   H. Saxena, R. E. Peale and W. R. Buchwald, "Tunable two-dimensional plasmon resonances in an InGaAs/InP high electron mobility transistor", *J. Appl. Phys.,* vol. 105, pp. 113101-113106, Jun. 2009.

[20]   V. V. Popov, D. M. Ermolaev, K. V. Maremyanin, N. A. Maleev and V. E. Zemlyakov, "High-responsivity terahertz detection by on-chip InGaAs/GaAs field-effect-transistor array", *Appl. Phys. Let*t., vol. 98, pp. 153504(1)-153504(3), Apr. 2011.

[21]   M. A. Khorrami, S. El-Ghazaly, S. Q. Yu, H. Naseem, "Compact terahertz surface plasmon switch inside a two dimensional electron gas layer" *Int. IEEE Microw. Symp.,* Montreal, Canada*,* Jun. 2012.

[22]   A. R. Davoyan, V. V. Popov, and S. A. Nikitov, "Tailoring terahertz near-field enhancement via two-dimensional plasmons", *Phys. Rev. Lett.*, vol. 108, p. 127401, Mar. 2012.

[23]   G. R. Aizin, and G. C. Dyer, "Transmission line theory of collective plasma excitation in periodic two-dimensional electron systems: Finite plasmonic crystals and Tamm states", *Phys. Rev. B.,* vol. 86, p. 235316, Dec. 2012.

[24]   H. Marinchio, J. F. Millithaler, C. Palermo, L. Varani, L. Reggiani, P. Shiktorov, E. Starikov, and V. Gruzinskis, "Plasma resonances in a gated semiconductor slab of arbitrary thickness", *Appl. Phys. Lett.,* vol. 98, p. 203504, May 2011.

[25]   J. Mateos, and T. Gonzalez, "Plasmsa enhanced terahertz rectification and noise in InGaAs HEMTs", *IEEE Trans. THz Sci. Technol.,* vol. 2, no. 5, pp. 562-569, Sep. 2012.

[26]   M. A. Alsunaidi, S. M. S. Imtiaz and S. El-Ghazaly, "Electromagnetic wave effects on microwave transistors using a full-wave high-frequency time-domain model", *IEEE Trans. Microw. Theory,* vol. 44, no. 6, pp. 779-808, Jun. 1996.

[27]   R. O. Grondin, S. El-Ghazaly and S. Goodnick, "A review of global modeling of charge transport in semiconductors and full-wave electromagnetics", *IEEE Trans. Microw. Theory & Tech.,* vol. 47, no. 6, pp. 817-829, Jun. 1999.

[28]   K. J. Willis, S. C. Hagness and I. Knezevic, "Terahertz conductivity of doped silicon calculated using the ensemble Monte Carlo/finite-difference time-domain simulation technique", *Appl. Phys. Lett.*, vol. 96, p. 062106, Feb. 2010.

[29]   N. Sule, K. J. Willis, S. C. Hagness and, I. Knezevic, "Simulation of carrier dynamics in graphene on a substrate at terahertz and mid-infrared frequencies" *12th International Conference on Numerical Simulation of Optoelectronic Devices* (NUSOD), pp. 79-80, Shanghai, China, Aug. 2012.

[30]   M. A. Khorrami, S. El-Ghazaly, S. Q. Yu, H. Naseem, "Analytical modeling of THz wave propagation inside ungated two dimensional electron gas layers", *Int. IEEE Microw. Symp.*, Baltimore, Jun. 2011.

[31]   M. A. Khorrami, S. El-Ghazaly, S. Q. Yu, H. Naseem, "THz plasmon amplification using two-dimensional electron-gas layers", *J. Appl. Phys.*, vol. 111, p. 094501, May 2012.

[32]   S. M. Sze, and K. K. Ng, "Physics of Semiconductor Devices", *John Wiley & Sons*, New Jersey, 2007.

[33]   K. S Yee, "Numerical solution of initial boundary value problems involving Maxwell's equation in isotropic media", *IEEE Trans. Antennas Propagat.,* vol. AP-14, pp. 302-307, May 1966.

[34]   V. Palankovski, R. Quay, *Analysis and Simulation of Heterostructure Devices,* Springer-Verlag, Austria, 2004.

[35]   C. M. Snowden, "Semiconductor device modeling", *Reports on Progress in Physics,* vol. 48, no. 2, p. 223, Feb. 1985.

[36]   F. J. Crowne, "Contact boundary conditions and the Dyakonov–Shur instability in high electron mobility transistors", *J. Appl. Phys.,* vol. 82, no. 3, p. 1242, Aug. 1997.

[37]   W. R. Calderón-Muñoz, D. Jena, and M. Sen, "Hydrodynamic instability of confined two-dimensional electron flow in semiconductors" *J. Appl. Phys.*, vol. 106, p. 014506, July 2009.

[38]   A. Taflove and S. C. Hagness, "Computational Electrodynamics: The Finite-Difference Time-Domain Method", 3rd edition, *Artech House Inc.,* Norwood, MA, 2005.

[39]   L. Pfeiffer, K. W. West, H. L Stormer and K. W. Baldwin, "Electron motilies exceeding 10^7 cm^2/V.s in modulation-doped GaAs", *Appl. Phys. Lett*., vol. 55, pp. 1888-1890, Aug. 1989.

[39]   C. A. Balanis, *Advanced Engineering Electromagnetics.* John Wiley & Sons, Inc., USA, 1989.

APPENDIX I:

In order to calculate the plasmon attenuation constant α accurately, the following method is pursued. First, the *x* components of the Poynting vector at each grid point of two integration lines at an arbitrary time step t_1 are calculated ($E_y \times H_z$). The locations of the integration lines should be chosen appropriately to represent a unique mode. This has been considered while choosing the integration lines i_1 and i_2 (see Fig. 1). Afterward, numerical integrations along the lines i_1 and i_2 on the computed power fluxes are performed. Thus, the transmitted power P(t) handled by the specific plasmonic mode at time t_1 is obtained. This process is similarly repeated in the following time steps until a period of the incident field (T = 1 / f). Next, the time average transmitted power at each integration line is estimated as:

$$P^{i_1,i_2}_{avg} = \frac{1}{T} \sum_{t=t_1}^{t=t_1+T} \left[\Delta t \times P^{i_1,i_2}(t) \right]. \tag{13}$$

In this manner, the plasmon attenuation constant of each specific mode is calculated as:

$$\alpha = \frac{1}{2\Delta l} \ln\left(\frac{P_{avg}^{i_1}}{P_{avg}^{i_2}} \right), \tag{14}$$

where, Δl is the distance between i_1 and i_2.

APPENDIX II:

A.   NUMERICAL SOLUTION OF CONTINUITY EQUATION:

To appropriately solve continuity equation, a first up-winding semi-implicit technique is employed. To this end, the continuity equation in one dimension (*x*) is repeated as:

$$\frac{\partial n}{\partial t} + \frac{\partial (n\vec{v})}{\partial x} = 0 \tag{1}$$

where, n and v are volume charge density and velocity respectively. Using the up-winding scheme, (1) can be discretized as:

$$\frac{n^{k+1}_{i} - n^{k}_{i}}{\Delta t} = -0.5 \times$$

$$\begin{cases} \dfrac{(nv)^{k+1}_{i+1} - (nv)^{k+1}_{i}}{\Delta x} + \dfrac{(nv)^{k}_{i+1} - (nv)^{k}_{i}}{\Delta x} & v < 0 \\[4mm] \dfrac{(nv)^{k+1}_{i} - (nv)^{k+1}_{i-1}}{\Delta x} + \dfrac{(nv)^{k}_{i} - (nv)^{k}_{i-1}}{\Delta x} & v \geq 0 \end{cases} \qquad (2)$$

In (2), time and location instances are displayed as subscripts and superscripts, respectively. As example, electron density at time step k and location i × Δx is displayed as n^{k}_{i}. Using (2), the charge density at i × Δx and in time step (k+1) is calculated as:

$$n^{k+1}_{i} = \begin{cases} \dfrac{An^{k}_{i} - Bn^{k}_{i+1}}{C} & v < 0 \\[4mm] \dfrac{A'n^{k}_{i} - B'n^{k}_{i+1}}{C'} & v \geq 0 \end{cases}, \qquad (3)$$

where, $A = 1 + \dfrac{\Delta t}{2\Delta x} v^{k}_{i}, \ B = \dfrac{\Delta t}{\Delta x} v^{k}_{i+1}, \ C = 1 - \dfrac{\Delta t}{2\Delta x} v^{k}_{i}, \ A' = 1 - \dfrac{\Delta t}{2\Delta x} v^{k}_{i}, \ B' = \dfrac{\Delta t}{\Delta x} v^{k}_{i-1}$ and

$C' = 1 + \dfrac{\Delta t}{2\Delta x} v^{k}_{i}$.

B.   NUMERICAL SOLUTION OF MOMENTUM CONSERVATION EQUATION:

Momentum conservation equation along *x* axis can be described as:

$$\frac{\partial (m^{*}v_{x})}{\partial t} = -v_{x}\frac{\partial (m^{*}v_{x})}{\partial x} - qE - \frac{mv_{x}}{\tau_{m}} - \frac{1}{n} \times \frac{\partial}{\partial x}(n_{v}k_{B}T). \qquad (4)$$

where, m^{*}, τ_{m}, k_{B},q and T are electron: effective mass, momentum relaxation time, unit charge, and temperature, respectively. Equation (4) can be discretized using various finite difference schemes. Here, each part of (4) is discretized as:

$$\frac{\partial\left(m^{*}v_{x}\right)}{\partial t}=\frac{\left(m^{*}v_{x}\right)_{i+0.5}^{k+1}-\left(m^{*}v_{x}\right)_{i+0.5}^{k}}{\Delta t}$$

$$v_{x}\frac{\partial\left(m^{*}v_{x}\right)}{\partial x}=\frac{\left(v_{x}\right)_{i+0.5}^{k+1}+\left(v_{x}\right)_{i+0.5}^{k}}{2}\times$$

$$\begin{cases}\dfrac{\left(m^{*}v_{x}\right)_{i+0.5}^{k}-\left(m^{*}v_{x}\right)_{i-0.5}^{k}}{\Delta t} & \left(v_{x}\right)_{i+0.5}^{k}\geq 0\\[2mm]\dfrac{\left(m^{*}v_{x}\right)_{i+1.5}^{k}-\left(m^{*}v_{x}\right)_{i+0.5}^{k}}{\Delta t} & \left(v_{x}\right)_{i+0.5}^{k}<0\end{cases} \qquad (5)$$

$$\frac{m^{*}v_{x}}{\tau_{m}}=\frac{m^{*}}{\tau_{m}}\times\frac{\left(v_{x}\right)_{i+0.5}^{k+1}+\left(v_{x}\right)_{i+0.5}^{k}}{2}$$

$$\frac{1}{n}\times\frac{\partial}{\partial x}\left(nk_{B}T\right)=\frac{k_{B}T}{n_{i+0.5}^{k}}\times\frac{n_{i+1}^{k}-n_{i}^{k}}{\Delta x} \qquad (6)$$

Simplifying (5) to calculate the electron velocity at the next time step and location (i+0.5) × Δx

leads to:

$$v_{i+0.5}^{k+1}=\frac{C_{1}-\Delta t\times\left(C_{2}+0.5\times C_{3}\times v_{i+0.5}^{k}+C_{4}+0.5\times C_{5}\right)}{m^{*}+m^{*}\times\Delta t\times\dfrac{1}{2\tau_{m}}+\dfrac{\Delta t}{2}\times C_{3}} \qquad (7)$$

where,

$$C_{1}=m^{*}v_{i+0.5}^{k},\ C_{2}=qE_{i+0.5}^{k},\ C_{3}=\begin{cases}\dfrac{\left(m^{*}v_{x}\right)_{i+0.5}^{k}-\left(m^{*}v_{x}\right)_{i-0.5}^{k}}{\Delta t} & \left(v_{x}\right)_{i+0.5}^{k}\geq 0\\[2mm]\dfrac{\left(m^{*}v_{x}\right)_{i+1.5}^{k}-\left(m^{*}v_{x}\right)_{i+0.5}^{k}}{\Delta t} & \left(v_{x}\right)_{i+0.5}^{k}<0\end{cases},\ C_{4}=\frac{k_{B}T}{n_{i+0.5}^{k}}\times\frac{n_{i+1}^{k}-n_{i}^{k}}{\Delta x},$$

and $C_{5}=\dfrac{m^{*}}{\tau_{m}}\times v_{i+0.5}^{k}$.

APPENDIX III:

UNIVERSITY OF ARKANSAS.

College of Engineering
Department of Electrical Engineering

May 17, 2014

To whom it may be concerned,

I certify that Mr. Mohammadali Khorrami is the first author of the paper titled "Global modeling of plasmonic terahertz devices," published in *IEEE Transaction on THz Science and Technology*, in Jan. 2014. Mr. Khorrami completed the majority (more than 51 percent) of this research and writings of this paper.

Dr. Samir El-Ghazaly
Distinguished Professor
Electrical Engineering
Office: 3169 Bell Engineering Center
Phone: (479) 575-6048
Email: elghazal@uark.edu

3217 Bell Engineering Center • Fayetteville, AR 72701 • 479-575-3005 • Fax: 479-575-7967 • www.uark.edu
The University of Arkansas is an equal opportunity/affirmative action institution.

103

APPENDIX IV:

Thesis / Dissertation Reuse

The IEEE does not require individuals working on a thesis to obtain a formal reuse license, however, you may print out this statement to be used as a permission grant:

Requirements to be followed when using any portion (e.g., figure, graph, table, or textual material) of an IEEE copyrighted paper in a thesis:

1) In the case of textual material (e.g., using short quotes or referring to the work within these papers) users must give full credit to the original source (author, paper, publication) followed by the IEEE copyright line © 2011 IEEE.
2) In the case of illustrations or tabular material, we require that the copyright line © [Year of original publication] IEEE appear prominently with each reprinted figure and/or table.
3) If a substantial portion of the original paper is to be used, and if you are not the senior author, also obtain the senior author's approval.

Requirements to be followed when using an entire IEEE copyrighted paper in a thesis:

1) The following IEEE copyright/ credit notice should be placed prominently in the references: © [year of original publication] IEEE. Reprinted, with permission, from [author names, paper title, IEEE publication title, and month/year of publication]
2) Only the accepted version of an IEEE copyrighted paper can be used when posting the paper or your thesis on-line.
3) In placing the thesis on the author's university website, please display the following message in a prominent place on the website: In reference to IEEE copyrighted material which is used with permission in this thesis, the IEEE does not endorse any of [university/educational entity's name goes here]'s products or services. Internal or personal use of this material is permitted. If interested in reprinting/republishing IEEE copyrighted material for advertising or promotional purposes or for creating new collective works for resale or redistribution, please go to http://www.ieee.org/publications_standards/publications/rights/rights_link.html to learn how to obtain a License from RightsLink.

If applicable, University Microfilms and/or ProQuest Library, or the Archives of Canada may supply single copies of the dissertation.

B.   COMPACT TERAHERTZ SURFACE PLASMON SWITCH INSIDE A TWO DIMENSIONAL ELECTRON GAS LAYER

Abstract:

   The possibility of realizing a terahertz (THz) switch by employing Surface Plasmons (SPs) along a Two Dimensional Electron Gas (2DEG) layer of a hetero-structure is presented. It is shown that SP's properties may be easily controlled by changing the motion of the electrons inside the 2DEG. The electron drift velocity is controlled by applying an external bias voltage at the 2DEG's ends. A compact and efficient THz switch with high On/OFF signal ratio is reported using this concept. The control voltage of the switch is considerably low. A multi-physic simulator, based on numerical solution of Maxwell's and Boltzmann's equations, is developed to analyze the switch appropriately. This micro-meter size plasmonic switch demonstrates a very promising method for navigating the sub-wavelength THz signals inside future plasmonic circuits.

Introduction:

Recently, many researches are aimed at THz frequency range, the less explored section of electromagnetic spectrum located between microwave and optical ranges. Operation of microwave devices in THz range is limited by the maximum achievable electron velocity inside semiconductors. On the other side, lower frequency edge of photonics is about 20 THz [1]. Besides, photonic devices are very bulky and their integration into modern nano-meter size packages is troublesome. In order to address these issues, application of Surface Plasmons (SPs) or propagating bound oscillations of electrons and EM field at a metal surface [2], is proposed [1]-[3]. The SPs offer wavelengths that are several orders of magnitude smaller than the radiative mode counterpart, and phase velocities which are at least one order of absolute value larger than the electron velocity maximum.

Mostly, researches in the plasmonic area are focused in optical ranges where noble metals such as gold and silver are being used. However, SPs are not bound to the surface of the metals in THz frequency ranges and hence; those desired properties are not observed anymore. In THz frequencies, application of highly doped semiconductor [4] or noble metals with engineered surfaces [5] are proposed. Propagation of SPs along doped semiconductors suffers from large losses therefore; utilization of Two Dimensional Electron Gas (2DEG) layers of hetero-structures with low SP losses is more popular [6]-[8]. Implementing THz plasmonic sources and detectors, inside 2DEG layers of solid state devices such as High Electron Mobility Transistor (HEMT), is very appealing. Novel plasmonic detectors inside 2DEG layers have shown comparable performances with respect to the other state of the art THz detection techniques [7]. However, active steering of SPs is required before the promise of a complete THz plasmonic circuit becomes achievable.

In this paper, we present a novel method to obtain a THz plasmonic switch inside the 2DEG

106

layer of a hetero-structure. Lately, it has been reported that SPs' wave properties such as propagation constants and phase velocities can be controlled by changing the bias voltage applied at the 2DEG's ends [6]. The electric field induced by the bias voltage accelerates the electrons of the 2DEG. This motion alters how effectively electrons and wave interact with each other and consequently; SPs' wave properties will change vastly. In particular, two normal SP modes along an unbiased hetero-structure will divide into four new modes as the electrons' drift motion is included [6]. It can be shown that the SP mode that propagates against the electron stream is very lossy. Here, the modification of SPs' properties, caused by the biasing, is employed to introduce a new concept for switching SPs. In order to simulate the proposed device, a full wave analysis method first proposed in the study of high frequency transistors, so called global modeling [9] is employed.

In the following, a brief overview of the analytic method [6] and global modeling [9] is presented. Also, details of the simulated structure and designed plasmonic switch are reported.

Overview of the modeling techniques and details of the simulated devices:

Consider a 2DEG sheet with surface charge density n_0 confined inside a hetero-structure (Fig 1). The 2DEG's length is L_1 while it is infinitely wide (along *y* axis). The hetero-structure is represented by two lossless semiconductors with similar dielectric constants $\varepsilon = \varepsilon_0\varepsilon_r$, $\varepsilon_0 = 8.85 \times 10^{-12}$ (F/m). Here, ground state spread of the 2DEG along *z* axis is assumed to be negligible compared to SP decay length in this direction and therefore; only electron motion along *x* axis is taken into account.

In [6], an analytical solution of Maxwell's and Boltzmann's equations is presented as several assumptions are considered to make the analysis achievable. This method provides a detailed characterization of TM^x mode with time and position variations of $e^{j\omega t - \gamma x}$, where $\gamma = \alpha + j\beta$.

Noting that γ, α, β and ω are propagation, attenuation, phase constants and angular frequency, respectively. As shown in [6], two normal SP modes along the unbiased 2DEG with dispersion relations:

$$\gamma_{1,2} = \pm \frac{j\omega^2}{2a} \tag{1}$$

divides into four new modes inside the biased 2DEG with dispersion relations:

$$A_1\gamma'^4 + A_2\gamma'^3 + A_3\gamma'^2 + A_4\gamma' + A_5 = 0 \tag{2}$$

where $A_1 = v_0^4$, $A_2 = -2v_0^3/\tau_m - 4j\omega v_0^3$, $A_3 = -6\omega^2 v_0^2 + v_0^2/\tau_m^2 + 6\omega v_0^2/\tau_m + 4a^2$, $A_4 = 4jv_0\omega^3 + 6v_0\omega^2/\tau_m - 2jv_0\omega/\tau_m^2$, $A_5 = \omega^4 - \omega^2/\tau_m^2 - 2j\omega^3/\tau_m$, $q = 1.6 \times 10^{-19}$(C) and $a = n_0 q^2/4\varepsilon m^*$. Also, τ_m and m^* are electron momentum relaxation time and electron effective mass, respectively.

Global modeling [9] provides a numerical solution of the moments of Boltzmann's equation (momentum and charge conservation) and Maxwell's equations. In this manner, interactions between EM fields and moving electrons are characterized. This numerical method eliminates several assumptions taken in the analytical model and makes the simulation more realistic.

In order to model the plasmonic switch inside the global modeling simulator [9], the structure in Fig. 1 is employed. A 2-D Finite Difference Time Domain (FDTD) code is developed that calculates field values inside a portion of the semiconductor and air. For excitation, a magnetic current sheet is placed above the structure so that evanescent modes do not reach the device and hence; only planar waves hit the device surface. Also, perfect match layers are applied to all boundaries except the ones at source and drain. In these two ends, a perfect electric conductor represents Ohmic contacts. A multi-grid mesh is applied along z axis to handle the negligible thickness of the 2DEG. The 2DEG is represented by one unit cell thick electric current source inside the FDTD simulator. Mesh sizes along x axis and time step dt are defined to satisfy the stability criteria of both EM and transport solvers. A 2DEG thickness d and surface charge

108

density n_0 is considered here. The 2DEG is located h_2 below the surface of an AlGaAs/GaAs hetero-structure that is represented by a dielectric ε_r with thickness h_1. It is assumed that the 2DEG is terminated by two Ohmic contacts with fixed equilibrium charge density $N_c = n_0/d$. The source contact is grounded while the drain contact is connected to a control voltage. The control voltage switches between 0 in ON state and 40(mV) in OFF state of the plasmonic switch. Transport parameters are: $m^* = 0.063 \times m_0$ ($m_0 = 9.1 \times 10^{-31}$kg) and $\tau_m = 2$ps.

Due to the intrinsic phase difference between the incident wave and the SPs, a special technique is required to launch the SPs. In this work, a zero thickness perfect electric conductor layer, called SP launcher, is placed on the top surface of the device next to the drain. The length of the SP launcher L_p is chosen very small compared to the wavelength of the incident field and therefore; considerable amount of the incident wave diffracts from the edges of the SP launcher. The diffracted wave experiences different phase constants which at least one of them will match the allowed SP mode's phase constant. In this manner, this specific SP propagates toward –*x*. The SP launcher is placed next to the PEC modeling drain so that it only excites –*x* moving SPs.

Results and discussion:

Inserting the 2DEG's properties and the transport parameters into (1), propagation constants of SPs inside the unbiased 2DEG are concluded: $\gamma_{1,2} = \pm 10^7 \times (0.16 + j1.95)$. These modes will divide into four new modes (2) inside the biased 2DEG with propagation constants: $\gamma_1' = 10^8 \times (0.03 + j1.65)$, $\gamma_2' = 10^8 \times (0.44 - j0.05)$, $\gamma_3' = 10^8 \times (-0.4 - j0.02)$ and $\gamma_4' = 10^8 \times (0.07 + j0.11)$. Considering the SPs' phases constants along the biased 2DEG, it is concluded that the 1st and the 4th modes are propagating toward +*x* while the other two modes are moving in the opposite direction. Noticing the propagation constants of the –*x* moving SPs', it is realized that the 2nd mode is a growing mode while the 3rd one faces losses as it propagates. By positioning the SP

launcher next to drain, it is expected that both –*x* moving SPs become excited. However, only the 3rd mode is launched inside our structure and will be employed as follows. Comparing the magnitude of the attenuation constants in the un-biased device and the 3rd mode of the biased 2DEG, it is clear that the 3rd mode propagates with several orders of magnitude larger losses. Therefore, one can switch off SPs' propagation by controlling the bias voltage. The signal attenuation of the switch in the ON state is approximately 13dB/µm while it is about 340dB/ µm in the OFF state.
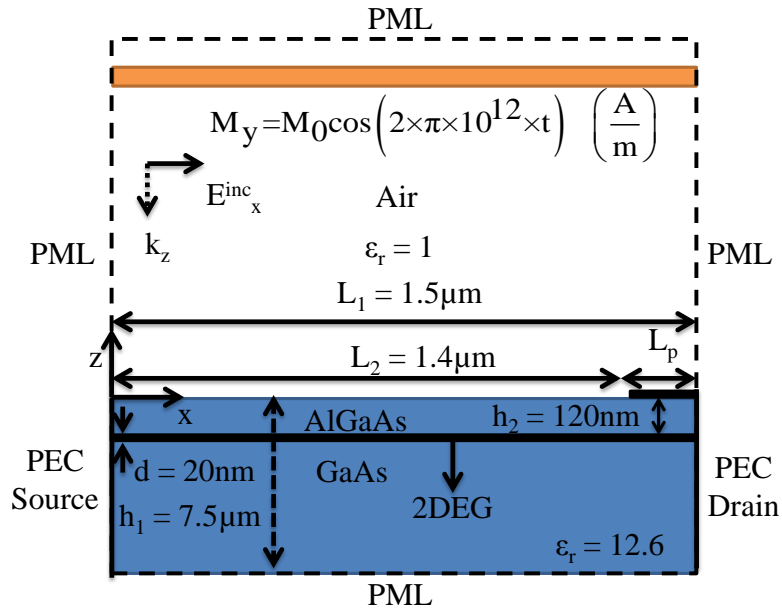

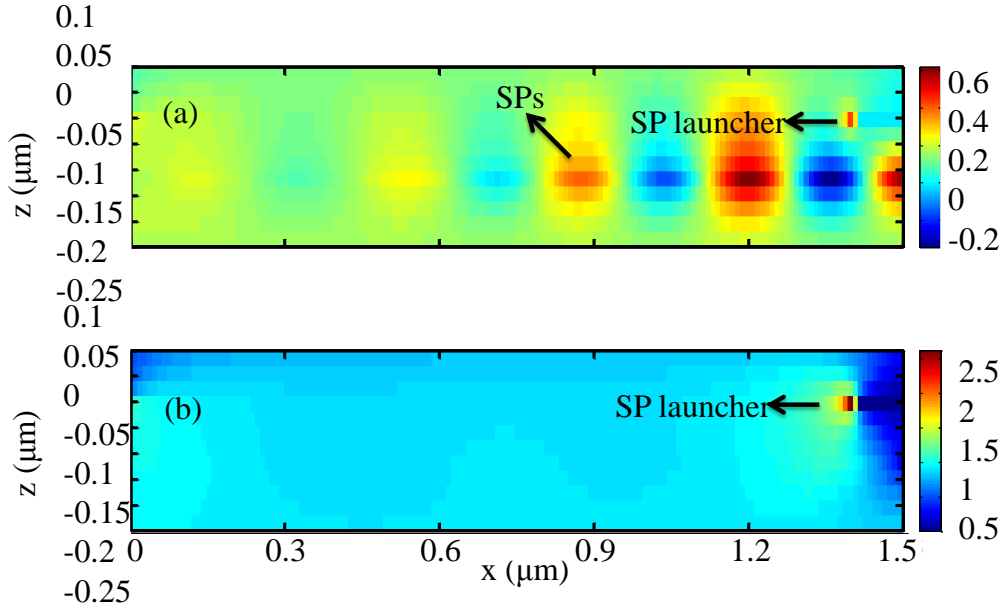Fig. 1. 2-D schematic of the simulated structure (figure not scale).

Fig. 2 Normalized x component of electric fields inside parts of the device and air at *xz*-plane a) SPs are propagating along the 2DEG as bias voltage is zero (ON state). b) SPs are attenuated as bias is set to 40(mV) (OFF state).
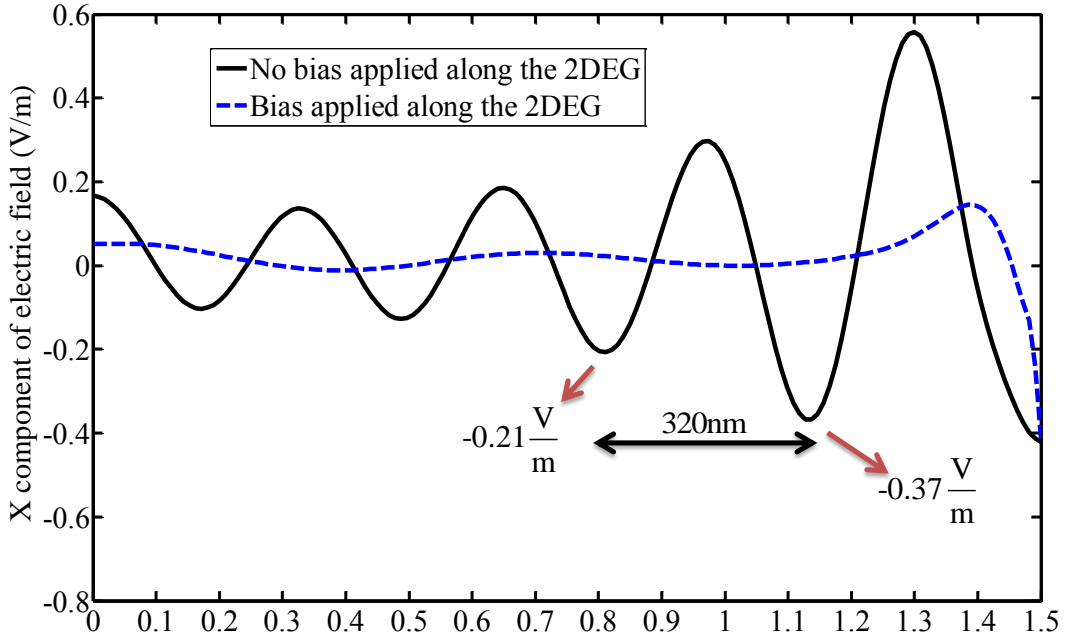

Fig. 3 Calculated x component of electric field at z = 120nm. Phase and attenuation constants of SPs in the ON state are estimated as: $\beta= 1.96\times10^7$ (Rad/m) and exp($-\alpha\times$320nm) = -0.21/-0.37 or $\alpha = 0.17\times10^7$ (np/m).

Fig. 2.a shows ac electric field distribution inside the un-biased device (V_{ds} = 0) at a specific time instant of simulation t_0. As calculated, SPs are propagating along the un-biased 2DEG

toward –*x*. As the bias voltage changes to $V_{ds} = 40$(mV), electrons are accelerated by the bias field and hence; the 3rd mode is launched. In Fig. 2.b, electric field distribution of SPs at time t_0 inside the biased device is presented. Comparing these field distributions, it is shown how effectively this switching technique is able to disconnect the flow of SPs. In Fig. 3, the electric field distributions along the 2DEG of both biased and unbiased structures are compared. SPs' properties along the unbiased 2DEG clearly follow the analytical model.

Conclusion:

In this paper, an active method for controlling SP signal at THz frequencies is demonstrated. It is shown that by changing the bias voltage across the device ends, a SP switch is viable in a very compact dimension. However, further investigations are required before implementing the idea proposed here. First, large attenuation in the ON state should be addressed by employing a hetero-structure with better quality and lower electron scatterings. Also, a high efficiency plasmon launcher should be designed. Beside, a sophisticated matching network placed at input and output is required before employing the switch inside a plasmonic circuit. It seems that the switching speed is mainly controlled by the time response of the circuit that drives the bias. Therefore, the switching speed is expected to be in the order of nano second. In spite of these challenges, the basic method reported here provides promising potentials for the design of active THz devices with micro-meter dimensions.

References:

[1]   Lee and M C. Wanke, "Searching for solid-state terahertz technology", *Science,* vol. 316, pp. 64-65, 2007.

[2]   K. F. MacDonald, Z. L. Samson, M. I. Stockman and N. I. Zheludev, "Ultrafst active plasmonics", *Nature Photonics*, vol. 3, pp. 55-58, Jan. 2009

[3]   E. Ozbay, "Plasmonics: Merging photonics and electronics at nanoscale dimensions", *Science,* vol. 311, pp. 189-193, Jan. 2006.

[4]   S. A. Maier, *Plasmonics: Fundamentals and applications.*   Springer, 2007, ch. 6.

[5]   Z. Fu, Q. Gan, Y. J. Ding and F. J. Bartoli, "From waveguiding to spatial localization of THz waves within a plasmonic metallic grating", *IEEE J. Sel. Topics Quantum Electron.,* vol. 14, no. 2, pp. 486-490, Apr. 2008.

[6]   M. A. Khorrami, S. El-Ghazaly, S. Q. Yu, H. Naseem, "Analytical modeling of THz wave propagation inside ungated two dimensional electron gas layers", *Int. IEEE Microw. Symp.*, Baltimore, Jun. 2011.

[7]   G. C. Dyer, G. R. Aizin, J. L. Reno, E. A. Shaner and S. J. Allen, "Novel tunable millimeter-wave grating-gated plasmonic detectors", *IEEE J. Sel. Topics Quantum Electron.,* vol, 17, no. 1, pp. 85-91, Feb. 2011.

[8]   T. A. Elkhatib, V. Y. Kachorovskii, W. J. Stillman, D. B. Veksler, K. N. Salama, X. Zhang and M. Shur, "Enhanced plasma wave detection of terahertz radiation using multiple high electron-mobility transistors connected in series," *IEEE Trans. Microw. Theory & Tech.,* vol. 58, no. 2, pp. 331-339, 2010.

[9]   R. O. Grondin, S. El-Ghazaly and S. Goodnick, "A review of global modeling of charge transport in semiconductors and full-wave electromagnetics", *IEEE Trans. Microw. Theory & Tech.,* vol. 47, no. 6, pp. 817-829, Jun. 1999.

APPENDIX I:

UNIVERSITY OF ARKANSAS.

College of Engineering
Department of Electrical Engineering

May 17, 2014

To whom it may be concerned,

I certify that Mr. Mohammadali Khorrami is the first author of the paper titled "Compact terahertz surface plasmon switch inside a two dimensional electron gas layer," published in *IEEE International Microwave Symposium* in Canada. Mr. Khorrami completed the majority (more than 51 percent) of this research and writings of this paper.

Dr. Samir El-Ghazaly
Distinguished Professor
Electrical Engineering
Office: 3169 Bell Engineering Center
Phone: (479) 575-6048
Email: elghazal@uark.edu

APPENDIX II:

Copyright Clearance Center

RightsLink®

Home   Create Account   Help

IEEE
Requesting permission to reuse content from an IEEE publication

Title: Compact terahertz Surface Plasmon switch inside a Two Dimensional Electron Gas layer

Conference Proceedings: Microwave Symposium Digest (MTT), 2012 IEEE MTT-S International

Author: Ali Khorrami, Mohammad; El-Ghazaly, S.; Shui-Qing Yu; Naseem, Hammed

Publisher: IEEE

Date: 17-22 June 2012

Copyright © 2012, IEEE

Thesis / Dissertation Reuse

The IEEE does not require individuals working on a thesis to obtain a formal reuse license, however, you may print out this statement to be used as a permission grant:

Requirements to be followed when using any portion (e.g., figure, graph, table, or textual material) of an IEEE copyrighted paper in a thesis:

1) In the case of textual material (e.g., using short quotes or referring to the work within these papers) users must give full credit to the original source (author, paper, publication) followed by the IEEE copyright line © 2011 IEEE.
2) In the case of illustrations or tabular material, we require that the copyright line © [Year of original publication] IEEE appear prominently with each reprinted figure and/or table.
3) If a substantial portion of the original paper is to be used, and if you are not the senior author, also obtain the senior author's approval.

Requirements to be followed when using an entire IEEE copyrighted paper in a thesis:

1) The following IEEE copyright/ credit notice should be placed prominently in the references: © [year of original publication] IEEE. Reprinted, with permission, from [author names, paper title, IEEE publication title, and month/year of publication]
2) Only the accepted version of an IEEE copyrighted paper can be used when posting the paper or your thesis on-line.
3) In placing the thesis on the author's university website, please display the following message in a prominent place on the website: In reference to IEEE copyrighted material which is used with permission in this thesis, the IEEE does not endorse any of [university/educational entity's name goes here]'s products or services. Internal or personal use of this material is permitted. If interested in reprinting/republishing IEEE copyrighted material for advertising or promotional purposes or for creating new collective works for resale or redistribution, please go to http://www.ieee.org/publications_standards/publications/rights/rights_link.html to learn how to obtain a License from RightsLink.

If applicable, University Microfilms and/or ProQuest Library, or the Archives of Canada may supply single copies of the dissertation.

115

IV.   DESIGN AND ANALYSIS OF A SILICON-BASED TERAHERTZ PLASMONIC SWITCH

A.   DESIGN AND ANALYSIS OF A SILICON-BASED TERAHERTZ PLASMONIC SWITCH

Abstract:

In this paper, a novel terahertz (THz) plasmonic switch is designed and simulated. The device consists of a periodically corrugated n-type doped silicon wafer covered with a metallic layer. Surface plasmon propagation along the structure is controlled by applying a control voltage onto the metal. As will be presented, the applied voltage can effectively alter the width of the depletion layer appeared between the deposited metal and the semiconductor. In this manner, the conductivity of the silicon substrate can be successfully controlled due to the absence of free electrons at the depleted sections. Afterwards, the effectiveness of the proposed plasmonic switch is enhanced by implementing a p^{++}-type doped well beneath the metallic indentation edges. Consequently, a P-Intrinsic-N diode is formed which can manipulate the plasmon propagation by modifying the electron and hole densities inside the intrinsic area. The simulation results are explained very concisely by the help of scattering matrix formalism. Such a representation is essential as employing the switches in the design of complex plasmonic systems with many interacting parts.

Introduction:

The terahertz frequency band, located between microwave and optical ranges is considered to be a promising section of the electromagnetic (EM) spectrum. THz radiation with uniquely attractive characteristics has been employed in laboratory demonstrations to identify explosives, find hidden weapons, and detect cancer cells and tooth decays [1]. In spite of these laboratory level researches, the real world application of THz radiation has proven to be challenging. One of the major pitfalls in the commercial application of THz radiation is the lack of room temperature active devices as modulators, switches, sources and detectors. In recent years, there have been considerable efforts to employ novel devices based on the collective oscillations of electrons mostly called plasmons, in the THz frequency range [2]-[8]. Specifically, plasmonic materials formed by the periodical texturing of metal or highly doped semiconductor surfaces have been extensively studied and applied in microwave and THz frequency ranges [9]-[20]. These structures can support surface waves which are mostly called Spoofed Surface Plasmon Polaritons (SSPPs), since they mimic the properties of surface plasmon polaritons at visible frequencies. Recently, there has been an increasing interest in exploiting SSPPs because of their unique properties as high field confinement and comparatively low propagation losses [9]-[12].

SSPPs are particularly important in the development of THz Quantum Cascade (QC) lasers to efficiently out-couple the output power from a cavity with sub-wavelength dimensions [13]-[14]. Furthermore, the application of SSPPs inside cylindrical two-dimensional periodic surfaces has been recommended for the design of future Cherenkov THz amplifiers [15]. Moreover, there has been a significant interest in the design of modern active plasmonic switches and modulators with different upcoming applications [16]-[20].

The idea of changing the wave properties of a plasmonic waveguide by heating to modulate

117

plasmons was first coined in [21] and applied in the visible frequency range. Subsequently, reversible variations in the waveguide characteristics caused by femto-second optical excitation have been employed to develop faster and more efficient plasmonic switches and modulators [22]. In terahertz frequency range, the optical and thermal control of the SSPP propagation along the surfaces of indented doped semiconductors has been investigated in [16]-[17]. Recently, a terahertz plasmonic switch implemented inside a metallic surface with a periodic array of grooves filled with an electro-optical material is proposed in [19]-[20]. It is shown that the incorporation of the electro-optical material such as nematic Liquid Crystal (LC), with controllable refractive index into the plasmonic gap provides a compact and efficient THz switch. However, the switching speed of the logic blocks developed based on the LC based gates or the ones with the thermally controlled plasmonic waveguides are undesirably low. Besides, the device implementation and wiring of such a gate is difficult [20]. In spite of short response times, the modulators with optical manipulation of SSPPs require a separate high power source for an efficient operation.

To avoid the above mentioned fabrication difficulties and to increase the switching speed of future terahertz plasmonic active devices, the application of doped semiconductors instead of the LCs is proposed here. As widely known, the conductivity of a semiconductor is dependent upon the number of the free charges which can be controlled by different mechanism as light illumination and electrical doping [23]. While photo-doping is a fast and effective approach for many applications, the significant amount of the conductivity modulation required in active plasmonic devices necessitates large incident optical powers which are impractical in many applications. Alternatively, the doping level within a semiconductor can be varied via the application of a voltage across an appropriately designed metal-semiconductor (Schottky)

junction [23]. This is due to the variations of the depletion region width that exists along the metal-semiconductor interface. In this manner, the conductivity of the semiconductor can be manipulated by changing the bias voltage. The semiconductor conductivity can be regulated more effectively by implanting different doping levels and types (p or n) in various locations within the structure. For instance, depositing a thin layer of highly p[++]-type doped silicon inside an intrinsic silicon wafer with an n[++]-type doped back gate can establish a PIN (P-Intrinsic-N) diode. The existence of the PIN diode makes the manipulation of the silicon conductivity possible with the aid of electron and holes, simultaneously.

   In this paper, we propose a THz plasmonic modulator implemented inside a corrugated silicon substrate covered with a platinum layer. By applying the bias voltage on the doped silicon-platinum junction, the wave propagation along the waveguide is controlled. The design starts with a finite element solution of the well-known drift-diffusion and Poisson equations to calculate the charge distribution inside the device. Next, Drude model is employed to estimate the doped silicon conductivity from the calculated charge densities. Afterwards, a full wave commercial simulator [24] is used to characterize the surface wave propagation along the structure. This simulation is repeated as the silicon conductivity is varied by applying various bias voltages across the junction. This characterization is performed in a wide frequency range located at terahertz regime (200 GHz- 320 GHz). However, the device is aimed to operate efficiently at a specific frequency range (250 GHz – 320 GHz).To concisely present the results; the scattering matrix formulation of the non-TEM plasmonic mode is developed. Finally, a more sophisticated design is introduced that employs a PIN diode to electrically modify the doping density of the silicon substrate.
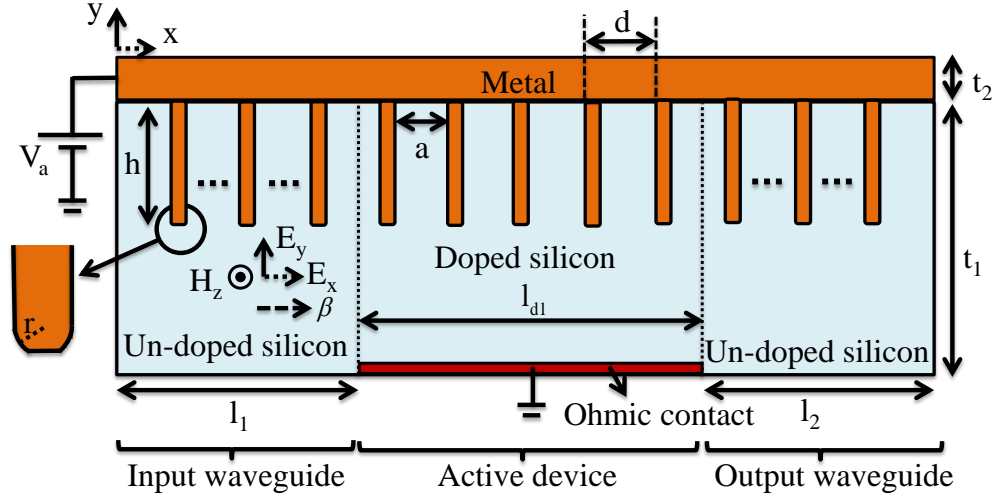
Fig. 1. A front view of the proposed plasmonic THz switch and input and output plasmonic waveguides. The switch and the waveguides are respectively designed inside the doped and un-doped sections of a silicon wafer with thickness $t_1 = 160$ μm indented with periodic holes with repetition d = 30 μm, in distances a = 24 μm and height h = 60 μm.

The structure of the proposed THz plasmonic switch:

As demonstrated in [9]-[12], a periodically corrugated metallic layer is able to carry EM surface waves with TM^x mode characteristics at terahertz frequency ranges. An example of this structure is depicted in Fig. 1. It includes a silicon wafer (deliberately doped at a specific section) with relative permittivity ε_r, tailored with linearly spaced grooves which are filled with a metal. The electric and magnetic field components and the wave vector of the TM^x mode are also depicted in Fig. 1. Generally, the field variations of the TM^x mode at frequency "f", follows the exponential function exp (jωt – jβx – δ (y–h–t$_2$)); where, ω = 2πf, β and δ, h and t$_2$ are angular frequency, phase and attenuation constants along x and y directions, indentation height and metallic layer thickness, respectively. As proved in [10] for the case of periodically grooved metal surface with sharp edge indentations, the dispersion relation of the fundamental plasmonic mode is:

$$\frac{\sqrt{\beta^2 - k^2_{si}}}{k_{si}} = S^2_0 \tan\left(k_{si}h\right), \; k = \frac{\omega\sqrt{\varepsilon_r}}{c} \tag{1}$$

as $\lambda_{si} \gg$ a, d and where:

$$S_0 = \sqrt{\frac{a}{d}} \, \text{sinc}\left(\frac{\beta \times a}{2}\right), \tag{2}$$

$\delta = \pm\sqrt{\beta^2 - k^2_{si}}$ and $\lambda_{si} = 2\pi / k_{si}$. In Eq. (1) and Eq. (2), c and, k_{si} and λ_{si} are the speed of light in vacuum (m/s) and the phase constant and wavelength of the radiating mode inside the silicon wafer, respectively. Additionally, the TM^x mode wave impedance along x is defined as $Z^x = \beta /$ ($\omega \times \varepsilon$) [25], where the silicon permittivity is $\varepsilon = \varepsilon_r \times \varepsilon_0$ ($\varepsilon_0 \approx 8.85 \times 10^{-12}$ F/m). Using Eq. 1, it can be concluded that SSPPs (with $\beta \geq k_{si}$) are only allowed to propagate along the grooved metal as $\tan(k_{si} \times h) > 1$. Therefore, SSPPs are not bounded to the metal-semiconductor interface at $z = (-h - t_2)$ as $f > f_r = c / \left(4h\sqrt{\varepsilon_r}\right)$, where f_r is called the resonant frequency herein. Thus, f_r sets the upper limit for the operating frequency bandwidth of the plasmonic structure. As taking Ohmic and dielectric losses into account, the phase constant (j β) within the wave function is substitute with $\gamma = \alpha + j \beta$ where, α is the fundamental mode attenuation constants along x. Moreover, the TM^x wave impedance along x is re-defined as: $Z^x = \gamma / (j \omega \varepsilon)$ [25]. Considering the well-known Helmholtz equation [25]:

$$\gamma^2 + \delta^2 + \frac{\omega^2}{c^2} \times \varepsilon_r = 0, \tag{3}$$

it is understood that the fundamental mode is mainly confined in the proximity of the metal edges as $\lambda_{si} \gg \lambda = 2 \times \pi / \beta$. In addition to the fundamental mode, higher order modes excited due to the wave diffraction at the edges also exist in the proximity of the indented surface.

Here, the active plasmonic device depicted in Fig. 1 is proposed to navigate the SPPSs using the concept of semiconductor electrical doping by the means of a Schottky contact. The Schottky

contact is established between the deposited metal and the n-type doped (with donor density N_{D1} = 5×10^{14} cm^{-3}) section of the silicon wafer. In order to couple EM wave to the active device, two plasmonic waveguides are considered inside the un-doped sections of the silicon wafer. The waveguides transfer EM wave to the plasmonic switch at the input ($x = l_1$) and the output ($x = l_1 + l_{d1}$) ports (see Fig. 1). The suggested silicon wafer (with thickness t_1 = 160 μm) is periodically corrugated with cubic holes. The period, the height and the distances of the holes are d = 30 μm, h = 60 μm and a = 24 μm, respectively. The indentations are completely filled with platinum. Besides, the wafer top surface is covered with a t_2 = 20 μm thick platinum layer. Platinum can be deliberately substituted with any other popular metal in the semiconductor industry if it offers high electrical conductivity in the interested frequency range. However, this can change the expected threshold voltage of the Schottky junction and the wave attenuations due to the variations of the metal-semiconductor barrier height and the electrical conductivity of the metal, respectively. The length of the plasmonic switch considered in the first design is l_{d1} = $5 \times$ d (see Fig. 1). To establish an Ohmic contact beneath the structure, very high level of n^{++}-type doping up to N_{D_Ohmic} = 2×10^{17} cm^{-3} with a Gaussian profile is maintained at y = - ($t_1 + t_2$) throughout the active device length (from x = l_1 to $l_1 + l_{d1}$). The thickness of the wafer is chosen such that it stays larger than the fundamental mode decay length in the *y* direction (1 / δ), throughout the interested frequency range (260 GHz-320 GHz). In this manner, the Ohmic contact may not disturb the SSPP field distribution.

As shown in Fig. 1, the edges of the holes located inside the wafer are considered to be rounded with radius "r". The width of the structures along z axis is considered to be at least an order of magnitude larger than the desired plasmonic mode wavelength. Therefore, a 2D solution of the electromagnetic and charge transport equations can obtain accurate results. In order to

122

control the width of the Schottky contact depletion region, an external control voltage V_a is applied between the Schottky and Ohmic contacts. In this manner, the conductivity of the doped silicon substrate is externally controlled. As the Schottky diode is under forward bias condition (switch is in the OFF mode), SSPPs suffer from large attenuations as propagating along the device. On the other hand, plasmons face less attenuation as the diode is reversely biased (switch is in the ON mode). To reduce the insertion losses of the switch in the ON mode, it is favorable to increase the width of the depleted area. However, the width is restricted to a maximum allowable reverse voltage. This limit corresponds to the silicon breakdown condition that happens as the total magnitude of electric field is larger than the 3×10^5 V/cm. The consideration of the rounded edges in the simulation allows us to apply higher reverse bias voltages onto the Schottky junction compared to the right angle ones, without reaching the breakdown limit of the silicon substrate.

<u>The simulation details:</u>

In order to completely capture the electron-wave interactions inside the proposed plasmonic switch, a set of electronic transport and wave equations ought to be solved. The simulation of the charge transport inside the semiconductor device is accomplished by solving the well-known steady-state Drift-Diffusion equations. Moreover, Maxwell equations can completely describe the wave propagation inside the plasmonic device. In this section, the details of the electronic transport and the full simulations are described.

1. The charge transport model:

Mostly, the analysis of semiconductor devices starts with a solution of the Poisson equation using the boundary condition (external voltage) to estimate the electrostatic potential φ inside the device. This solution is next coupled to the steady-state Drift-Diffusion equations to accurately

123

compute electron, n (cm^{-3}), and hole, p (cm^{-3}), densities inside the solution domain. Details of this type of simulation can be found elsewhere [23]. Here, a commercial solver with semiconductor simulation capabilities is used [26] to solve these equations.

In the developed model, Shockley-Read-Hall formulation with the electron-hole recombination rate:

$$R = \frac{n \times p - n^2_i}{\tau_p \left(n + n_i\right) + \tau_n \left(p + n_i\right)}.$$ (4)

is employed. In Eq. (4), $n_i = 1.45 \times 10^{10}$ cm^{-3}, τ_n and $\tau_p = 10^{-7}$ (s) are silicon intrinsic carrier concentration, electron and hole lifetimes, respectively. The set of three differential equations (two drift-diffusion equations for electron and hole densities and the Poisson equation) are solved numerically as considering specific boundary conditions over the computational domain. Here, constant values of electron "n" and hole "p" densities are considered at the location of the Ohmic contact. This is correct as presuming infinite carrier recombination velocities at the contact. Furthermore, the electrostatic potential of the boundaries adjacent to the Ohmic and Schottky contacts are:

$$\varphi_{Schottky} = V_a + \frac{kT}{q} \ln\left(\frac{n}{n_i}\right) - \varphi_B \text{ and } \varphi_{Ohmic} = \frac{kT}{q} \ln\left(\frac{n}{n_i}\right),$$ (5)

respectively. In Eq. (5), T = 300 (K), q = 1.602 × 10^{-19} (C), φ_B = 0.83 (eV) and $k = 1.38 \times 10^{-23}$ (J / K) are the room temperature, unit charge, Pt/Si barrier height [23] and Boltzmann constant, respectively. The carrier densities beneath the Schottky contacts formed between the deposited Pt layer and the wafer in Fig. 1 are n = N_c × exp(q φ_B / kT) and p = n_i^2 / n where, N_c = 2.82 × 10^{19} (cm^{-3}) is effective density of states at the silicon conduction band. In the other boundaries, vanishing normal components of electron and hole current densities, and electric field are enforced.

2. Details of the full wave simulation:

In this paper, a commercial EM solver [24] is utilized to numerically solve Maxwell equations inside the computational domain. To this end, Drude model is exploited to represent the metal frequency dependent permittivity:

$$\varepsilon_M = 1 - \frac{\omega_p^{\,2}}{\omega^2 - j\omega\gamma} \tag{6}$$

inside the simulator. In Eq. (6), $\omega_p = 1.4 \times 10^{16}$ (Rad/s), and $\gamma = 4 \times 10^{16}$ (s^{-1}) are plasma and scattering frequencies, respectively. In this manner, Ohmic losses of the propagating surface wave are taken into account. Similarly, the high frequency characteristics of the silicon wafer are included into the full wave solver. As presented in [27-28], Drude model can accurately estimate the permittivity $\varepsilon(\omega)$ and the conductivity σ_{si} of the silicon substrate at frequency ranges below 400 GHz as:

$$\sigma_{si} = \frac{\sigma_{dc}}{1 + (\omega\tau)^2}, \ \varepsilon(\omega) = \varepsilon_r - \frac{\tau\sigma_{dc}}{1 + (\omega\tau)^2}, \tag{7}$$

In Eq. (7), τ and m, and σ_{dc} are electron scattering time and effective mass, and dc conductivity, respectively. The dc conductivity $\sigma_{dc} = q \times (\mu_n \, n + \mu_p \, p)$ where, μ_n and μ_p (cm^2 / V s) are electron and hole mobilities, respectively. In the following, $\tau = 0.2$ ps, m $= 1.08 \times m_0$ ($m_0 = 9.1 \times 10^{-31}$ kg is electron unit mass) and $\varepsilon_r = 11.9$. Furthermore, the electron and hole mobilities at the room temperature are approximated as [29]:

$$\mu_n = \frac{0.1318}{\left(1 + \dfrac{N_D + N_A}{10^{17}}\right)^{0.85}} + 0.0092 \tag{8}$$

and,

$$\mu_p = \frac{0.042}{\left(1 + \frac{N_D + N_A}{1.6 \times 10^{17}}\right)^{0.7}} + 0.005 , \qquad (9)$$

respectively. In Eq. (8) and Eq. (9), N_A is ionized acceptor density. In order to link the charge transport and the EM solvers, the calculated electron and hole densities are first inserted into Eq. (7) to update the silicon conductivity and relative permittivity. Next, the updated silicon properties are included into the full wave simulator. This process is repeated as the applied voltage is changing.

3. The definition of the scattering parameters for the plasmonic device

Recently, there has been a trend to employ scattering parameters as reporting the properties of novel plasmonic devices [30]-[32]. Here, the definition of the characteristic impedance of a non-TEM transmission line, as a plasmonic waveguide is reviewed. Next, the employed method for the S-parameter calculation is detailed. As described in [33], there are many ways to determine the voltage, current, and the characteristic impedance of a non-TEM transmission line. However, the voltage and current waves are mostly defined for the transverse electric and magnetic fields of a specific mode, respectively. Besides, an arbitrary characteristic impedance may be chosen to relate $\pm x$ going voltage and current [33]. As mentioned, there exist infinite numbers of plasmonic modes inside the designed device, along the interface of the indented metal and the dielectric. However, the fundamental mode extends furthest into the dielectric. Therefore, the characteristic impedance Z_0 is selected equal to the real part of the fundamental TM^x mode wave impedance Z^x_r where $Z^x = Z^x_r + j\, Z^x_i$.

In this paper, the simulated plasmonic switches are represented as a two port network. Such a representation of the active device is depicted in Fig. 2(a). In the developed EM model, two plasmonic waveguides with length l_1 and l_2, are included at the input and output ports of the

126

network to transfer the waves into and out of the switch (see Fig. 2(a)). Moreover, the presence of the waveguides allows that the excitation enforced at $x = 0$ (planar wave with electric field component E^{inc}_y and propagation constant k_{si}) completely follows the fundamental mode variations as it reaches the switch. In order to avoid wave attenuations inside the waveguides, the corresponding silicon wafers and the deposited metallic layers are assumed to be loss-free. In this manner, the waveguides can handle the TM^x mode with real wave impedance Z^x_r. Here, the reference planes of the reported S-parameter are located at the boundaries of the active device as depicted in Fig. 2(a).
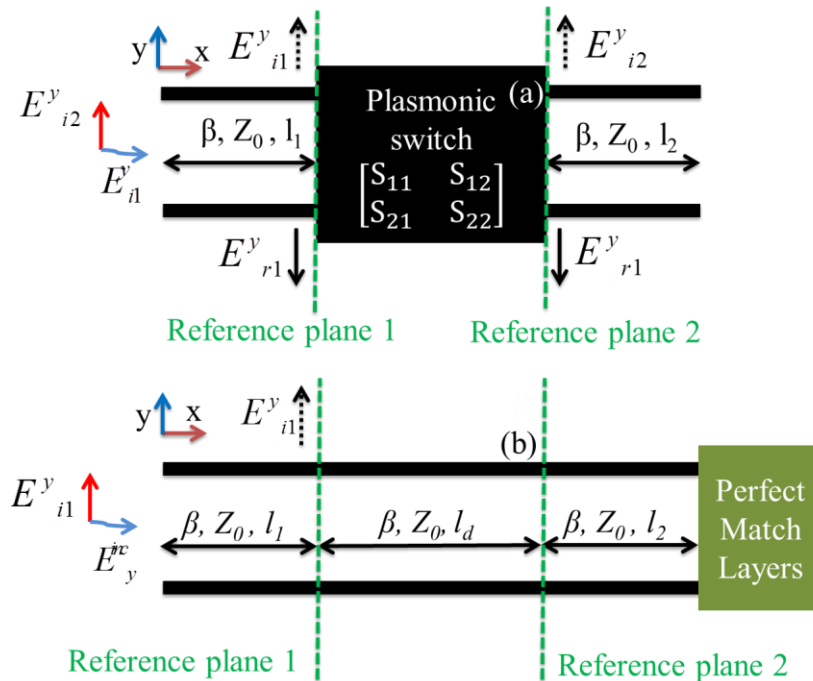

Fig. 2. (a) 2-port demonstration of the plasmonic device terminated with plasmonic waveguides. (b) A schematic showing the details of the initial simulation performed for the calibration.

In the following, the scattering matrix is formulated in terms of the fundamental TM^x mode electric field y component E^y. Considering the two-port network in Fig. 2(a), the scattering parameters are defined as:

$$\begin{pmatrix} E_{r_1}{}^y \\ E_{r_2}{}^y \end{pmatrix} = \begin{pmatrix} S_{11} & S_{12} \\ S_{21} & S_{22} \end{pmatrix} \begin{pmatrix} E_{i_1}{}^y \\ E_{i_2}{}^y \end{pmatrix}. \qquad (10)$$

In Eq. (10), $E^y{}_{i_1, i_2}$ and $E^y{}_{r_1, r_2}$ are incident and reflected field components (at ports 1 and 2),

respectively. Using Eq. (10), scattering parameters can be obtained as:

$$S_{11} = \left. \frac{E_{r_1}{}^y}{E_{i_1}{}^y} \right|_{E_{i_2}{}^y = 0}, S_{21} = \left. \frac{E_{r_2}{}^y}{E_{i_1}{}^y} \right|_{E_{i_2}{}^y = 0}. \qquad (11)$$

Here, the 2-port network is assumed to be reciprocal and symmetric ($S_{12} = S_{21}$ and $S_{22} = S_{11}$). To

calculate the scattering matrix, the following procedure is adopted. First, an initial simulation is

performed using the commercial EM solver for the calibration purposes. To this end, the output

waveguide is terminated with a perfectly matched layer and the incident planar wave is applied

onto the input transmission line (see Fig. 2(b)). In this manner, the incident wave at port 2 is set

to zero ($E^y{}_{i_2} = 0$). In order to only compute the incident field $E^y{}_{i_1}$ at $x = l_1$, the discontinuity

(plasmonic switch) is eliminated. To achieve this goal, the doped silicon section with the back

gate is substituted with an un-doped one. Moreover, the platinum layer is substituted with a

Perfect Electric Conductor (PEC). In this manner, the middle section becomes equivalent to the

plasmonic waveguide shown in Fig. 2(b), with characteristic impedance Z_0, phase constant β and

length $l_d = l_{d1}$. This setup is employed to estimate the incident field $E_{i1}{}^y$ at an observation point

along the reference plane 1 and the wave impedance of the dominant mode. The observation

point is chosen sufficiently far from the metal edges so that the evanescent fields that exist in the

proximity of the edges do not affect the estimated field with the dominant mode variations. Now

that the required information is available, the S-parameter calculation of the active devices is

continued. To this end, the discontinuity with the unknown scattering matrix is introduced

between the waveguides as the output transmission line is terminated with the perfect match

layers. Afterward, the electric field component is computed at the similar observation point along reference plane 1. The calculated total field is equal to $E^y_{total1} = E_{i1}{}^y - E^y_{r1}$. Knowing $E_{i1}{}^y$ from the previous simulation, S_{11} can be computed: $S_{11} = E^y_{r1} / E_{i1}{}^y$. After estimating the transmitted field E^y_{r2} at the reference plane 2, S_{21} is similarly calculated as $S_{21} = E^y_{r2} / E_{i1}{}^y$.

Plasmonic switch with the Schottky contact

In order to present a guideline for designing the plasmonic switch in different frequency ranges, the dispersion relation of the described structure (in Fig. 1) with different indentation depths "h", calculated by the analytical mode (Eq. (1) and Eq. (2)) are shown in Fig. 3. As depicted, the resonance frequency of the plasmonic structure "f_r" decreases as the depths of the holes "h" increases. In this manner, the indentation heights "h" can be determined for a specific design with a required maximum working frequency limit. In Fig. 3, the dispersion relation of the radiating mode is also illustrated. Comparing the phase constants of the radiating mode and the TM^x modes along the plasmonic structure with different "h" in Fig. 3, it is understood that the SSPPs are not bounded to the metal edges at $z = (-h - t_2)$ plane as $f < 200\,\text{GHz}$. This places a minimum operating frequency limit on the plasmonic device since the SSPPs are not restricted inside the silicon wafer as $\beta \simeq k_{si}$.

Figure 4 represents the fundamental mode wave impedance Z^x_r and dispersion relation of the input and output waveguides calculated by the full wave simulator as $h = 60\,\mu\text{m}$. To this end, the calibration simulation (detailed in Fig. 2(b)) is performed. In this manner, the phase constant β is first computed for a section of the waveguide with length l_d as $\beta = \varphi / l_d$ where, φ is the phase of the waveguide port 1 to 2 transmission coefficient S^{WG}_{21} ($= |S^{WG}_{21}| \times e^{(j \times \varphi)}$). Next, the wave impedance of the fundamental mode is computed as $Z^x_r = \beta/ \omega \times \varepsilon$. As mentioned, the characteristic impedances of the waveguides are chosen equal to their fundamental mode wave

impedance $Z_0 = Z^x_r$. As depicted in Fig. 4, the resonant frequency is located at 320 GHz. The differences between the SSPP characteristics (resonant frequency and maximum achievable phase constant) calculated by the analytical model in Eq. (1) and Eq. (2), and the full wave simulator are due to the consideration of the exact shape of the indentations edges inside the numerical solver. The dispersion relation variations of a corrugated metal with curved-shape edges compared to the one with sharp corners have been also discussed in [12].
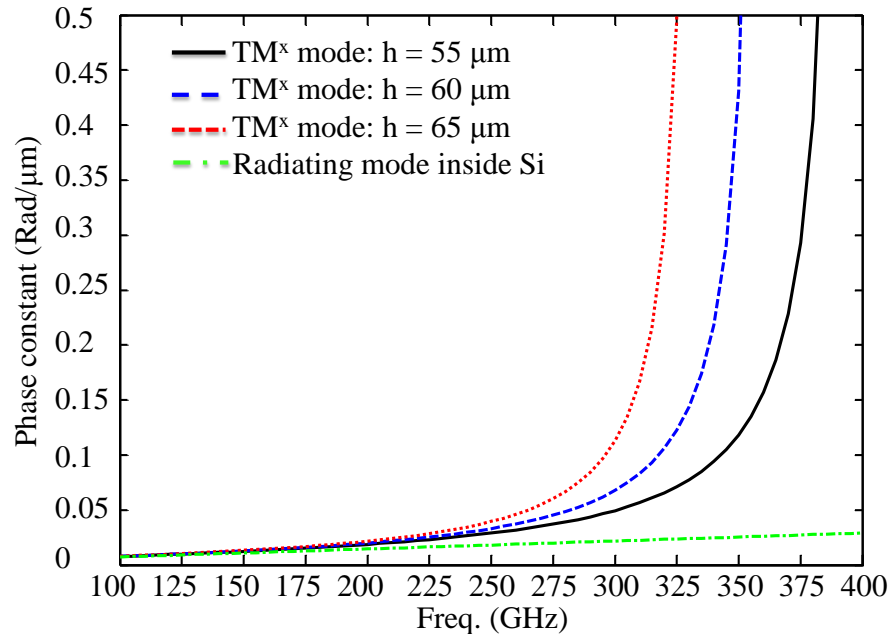
Fig. 3. The TM fundamental mode phase constants calculated by the analytical model (1) and (2) versus frequency as the indentation height h is changing.
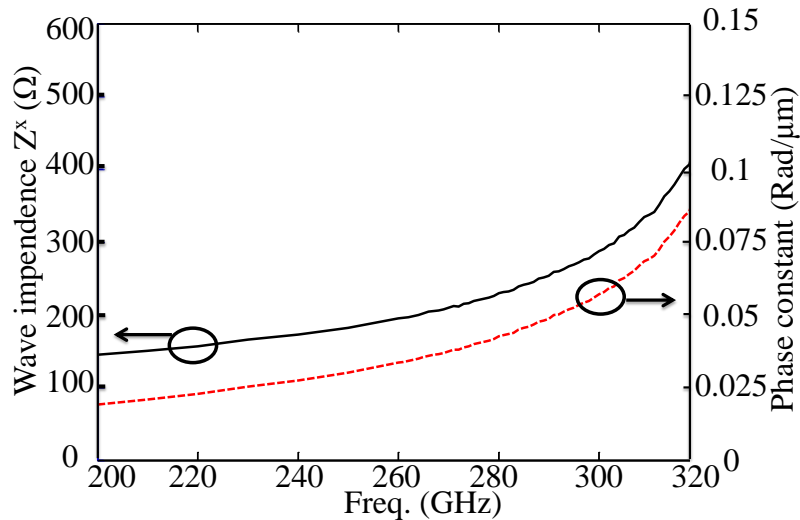

130

Fig. 4. Variations of the waveguide's fundamental mode wave impedances Z^x_r and phase constant, calculated by the full wave solver versus frequency.

To show the effectiveness of the designed switch, the simulation is performed with different applied voltages. Figure 5(a)-5(b) and Fig. 5(c)-5(d) depict the distribution of the electron density logarithm ($\log_{10} n$) inside the doped silicon wafer and the magnitude of the electric field $|E| = (|E_x|^2 + |E_y|^2)^{0.5}$ at f = 300 GHz, throughout the active device as the applied voltages are 1 V and -80 V, respectively. As presented in Fig. 5(a), the depletion layer width is almost negligible as the Schottky diode is forward-biased ($V_a = 1$). In this condition, the plasmons are attenuated as they propagate along the device (see Figure 5(b)). However, the depletion layer width increases up to 14 μm as the diode is reverse-biased (see Fig. 5(c)). In this case, the switch is operating in the ON mode and SSPPs suffers from small attenuations (see Fig. 5.(d)), if they are concentrated inside the depleted region, with small electrical conductivity. Comparing the distribution of the electric field magnitude shown in Fig. 5(b) and 5(d), it is concluded that the wave concentration along the edges of the metallic indentation are kept similar at a single frequency, as the device is operating in the ON and the OFF mode. Applying high reverse voltages in a structure, grooved with sharp angle edges is not possible due to charge accumulation on the corners. This high charge density results into high electric field values which can end up to the silicon breakdown. Employing rounded metal edges allow the designer to apply very high reverse voltages up to -80 V before reaching the breakdown condition. In the design with curved edges, the breakdown limit will not reach unless V_a becomes less than -90 V.

Figure 6 presents the transmission coefficient S_{21} of the plasmonic THz switch implemented inside the doped silicon as different bias voltages are applied onto the Schottky contact. As illustrated, the insertion loss of the proposed device is less than 1dB in a wide frequency range.

131

Moreover, the switch offers signal isolations $(S_{21}^{ON} - S_{21}^{OFF})$ up to 13 dB at 320GHz. On the other hand, the isolation reduces down to 1.5 dB in the first portion of the simulated frequency range. The signal isolation offered by the plasmonic switch can impose another criterion on the minimum operating frequency of the switch. Here, at least 3 dB signal isolation is expected from a single Schottky-diode-based switch. Therefore, it is concluded that the operating bandwidth of the first design is 60 GHz from 260 GHz to 320 GHz.
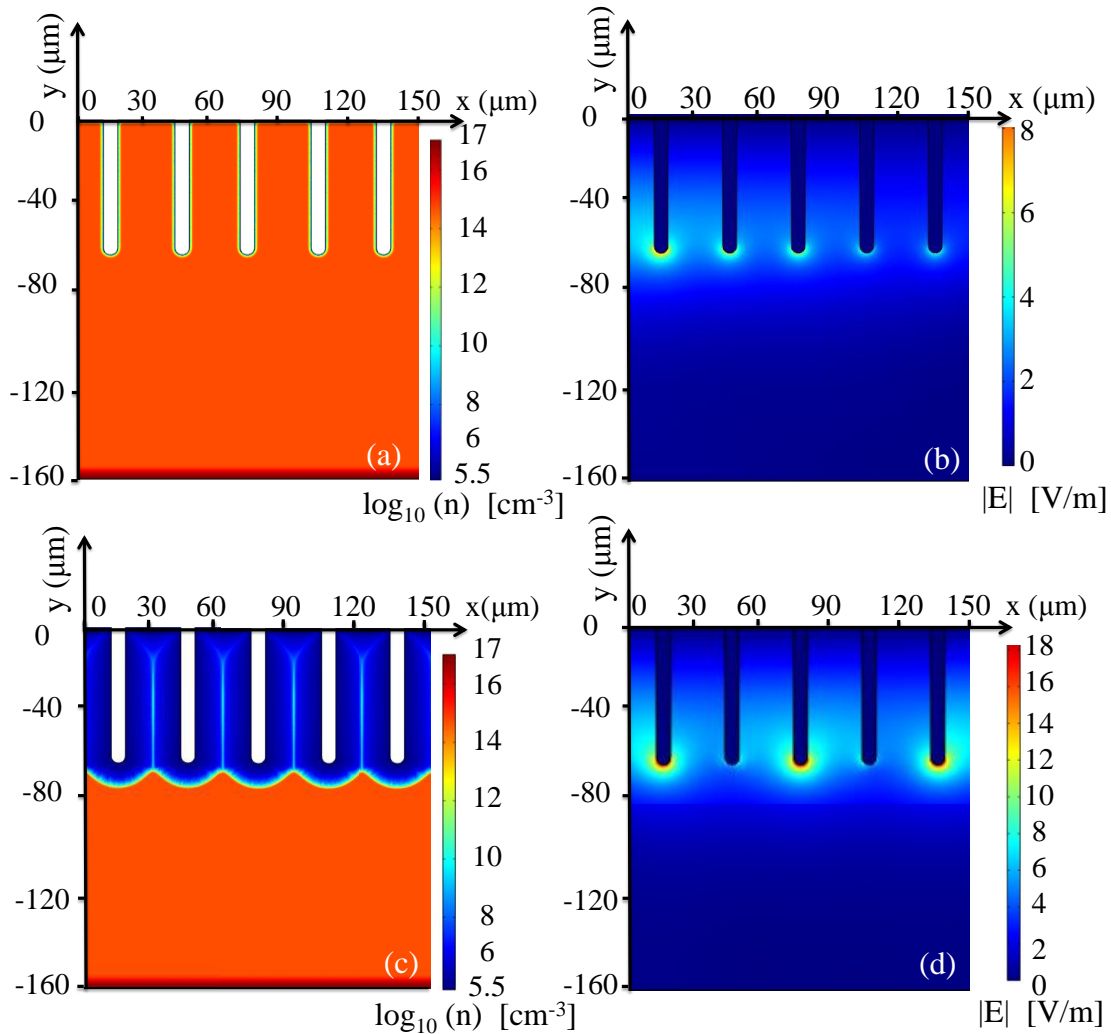

Figure 5 (a) and (b) show the distribution of the electron density inside the doped silicon wafer, and the magnitude of the electric field at $f = 300$ GHz as $V_a = 1$ V, respectively. (c), (d) similarly present the variations of the charge density and the electric field magnitude at the same frequency as the applied voltage is -80 V.
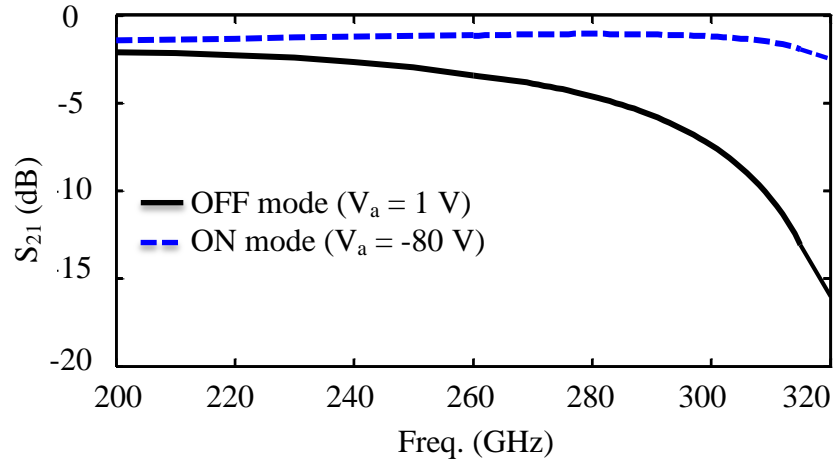
Fig. 6. S_{21} of the plasmonic switch versus frequency as the device is operating in different modes at THz frequency range.
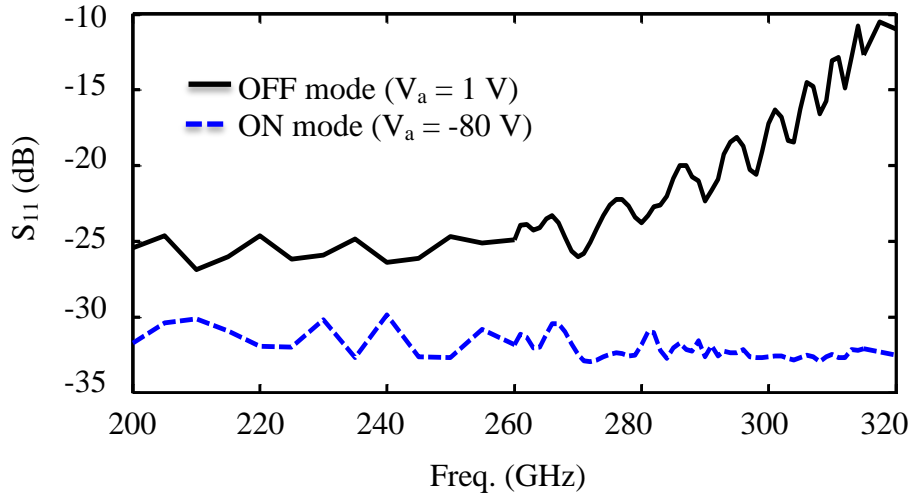

Fig. 7. S_{11} of the plasmonic switch versus frequency as the device is operating in different modes at THz frequency range.
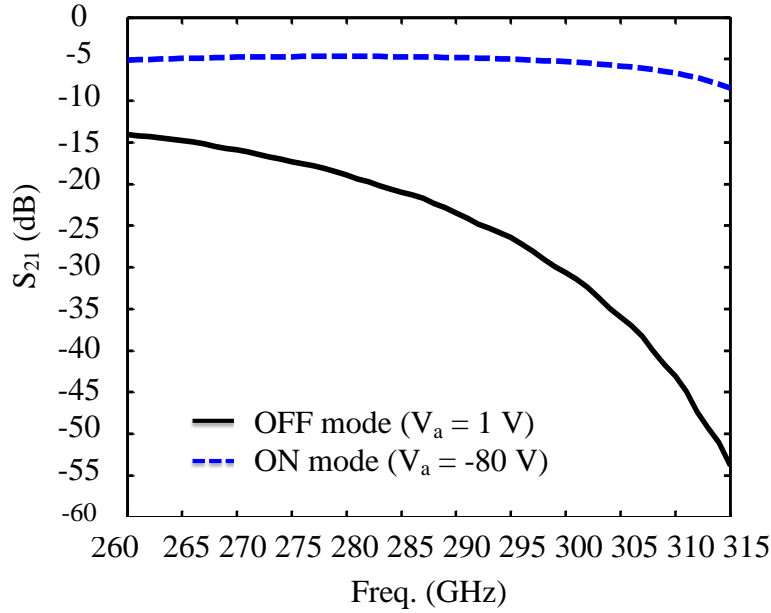
Fig. 8. S_{21} of the plasmonic switch with the Schottky contact as its length is $l_{d1} = 20 \times d$.

In Fig. 7, the return loss of the plasmonic THz switch is depicted. As presented, the return loss of the device is better than -30 dB as operating in the ON mode. The small amount of the input signal reflection is very attractive especially as connecting several components in a complex photonic system.

In order to achieve a more appropriate plasmonic switch, it is critical to improve the signal isolation between the ON and the OFF modes. For this purpose, several switches can be cascaded next to each other. This can increase the wave attenuation as the switch is in the OFF mode. However, it can also hurt the device insertion losses. To show the effectiveness of this method, four series of the designed switches are cascaded to establish a structure with $20 \times d$ length. Figure 8 depicts the simulated transmission coefficients of the series of the switches with an acceptable level of signal isolation (>10 dB) in the frequency range of interest (260GHz - 320GHz). As expected, this configuration suffers from at least 5 dB attenuations throughout the frequency range as operating in the ON mode.

134

As shown, it is possible to achieve high levels of signal isolation by extending the length of the active device. However, the large reverse voltages required to achieve an acceptable level of insertion losses make the device application in modern compact photonic systems unfeasible. To address this problem, an optimized plasmonic switch is proposed in the following section.

Optimization: plasmonic switch using a PIN diode:

Figure. 9 depicts a schematic of the optimized structure. In this design, a highly p^{++}-type doped well with the acceptor ion density $N_{A\_Ohmic} = 10^{17} cm^{-3}$ and Gaussian profile is considered beneath a section of the metallic layer (see Fig. 9). Moreover, the silicon wafer employed in this design is almost intrinsic with n-type doping density $N_{D2} = 5 \times 10^{13}$ (cm^{-3}). As will be presented, the p^{++}-type doped well and the n^{++}-type doped Ohmic contact (with doping density $N_{D-Ohmic} = 10^{17} cm^{-3}$ located at $y = - t_1 - t_2$) establish a PIN diode with promising properties. It is famous that the PIN diode operates in high-level-injection mode. This means that the spilled carriers from the p^{++} and n^{++} areas fill the diode intrinsic region as it is forward-biased. The long intrinsic layer with length ($t_1 - h = 100$ μm) is beneficial in several aspects. First, it enables fast switching of the diode compared to conventional PN diodes. Additionally, it establishes a low loss plasmonic waveguide for the SSPP as the switch is operating in the ON mode and the diode is reverse-biased. Furthermore, high SSPP attenuations are expected as the diode is forward-biased and the switch is operating in the OFF mode. In accordance with the previous design, the control voltage V_a is applied between the metal and the Ohmic contact located beneath the device at $y = - t_1 - t_2$.
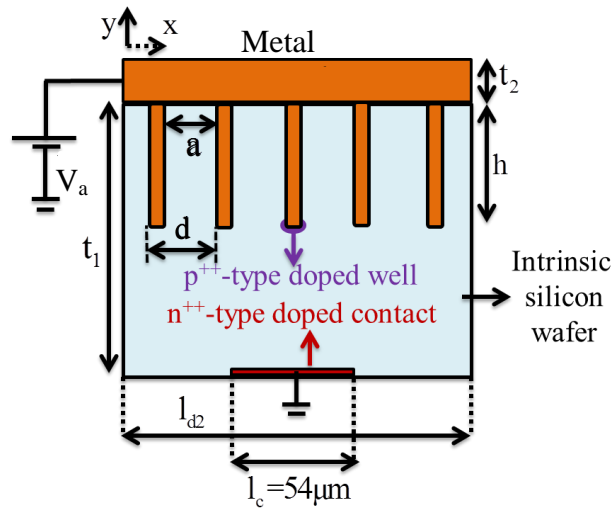
Fig. 9. A front view of the optimized plasmonic THz switch consists an un-doped silicon wafer indented with periodic holes (d = 30 μm, a = 24 μm, h = 60 μm and t_1 = 160 μm) and highly p and n type doped at specific locations.
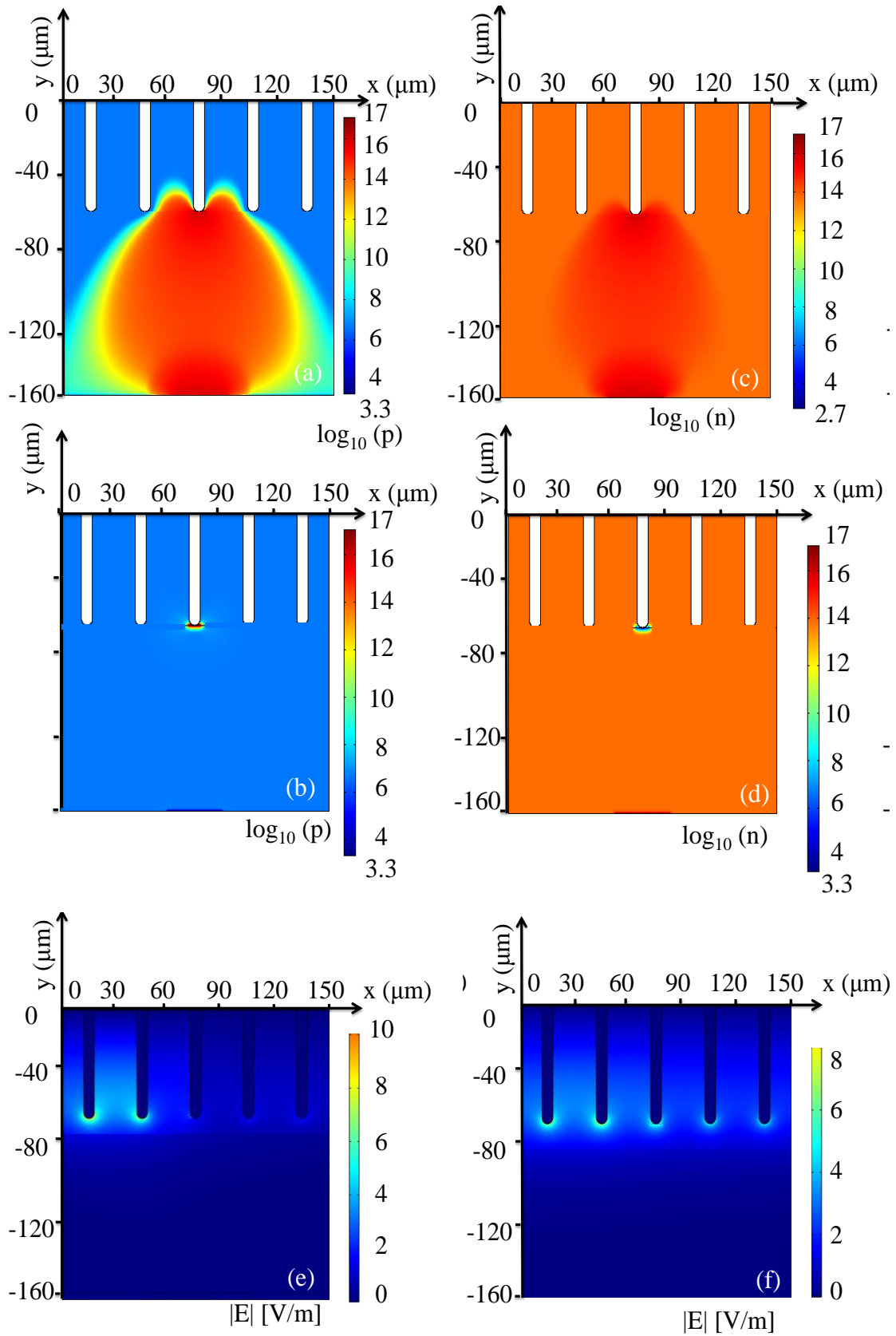
Fig. 10. The hole and electron density distributions, and the magnitude of the

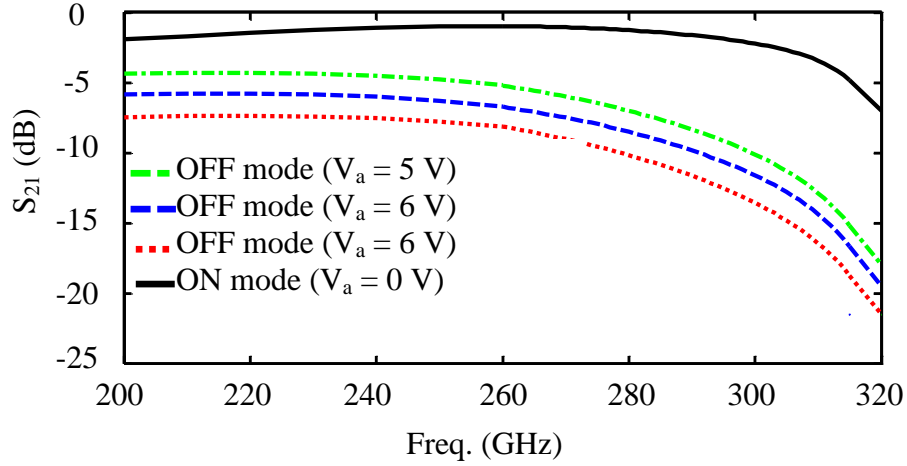electric field at f = 300 GHz as: (a), (b), (c) $V_a = 5$ V and (d), (e), (f) $V_a = 0$ V, respectively.

Fig. 11. Insertion losses of the optimized plasmonic switch versus frequency under different bias conditions

Here, the simulation results of the optiized device with the length $l_{d2} = 5 \times d$ are reported. Figure 10(a) and 10(b) respectively depict the distributions of the hole and electron density logarithm ($\log_{10} p$ and $\log_{10} n$) inside the intrinsic silicon wafer as the applied voltage is 5V. As shown in Fig. 10(a)-10(b), the PIN diode operates in the high-level-injection mode with very high level of electron and hole densies as $V_a = 5$ V. Figure 10(c) depicts the magnitude of the ac electric field inside the plasmonic switch as the PIN diode is forward-biased. As expected, the presence of the high electron and hole densies in the forward bias condition causes large wave attenuations as the SPPs are passing through the device. In Fig. 10(d)-10(e), the distributions of the electron and hole density logarithm inside the device with $V_a = 0$ V are presented, respectively. As the diode is reverse-biased, the electron and hole densies are respectively less than or equal to 5×10^{13} (cm^{-3}) and 10^7 (cm^{-3}). This is true throughout the silicon wafer except at the locations of the Ohmic contacts. The small numbers of free carriers in the reverse-biased diode guarantee negligible insertion losses as the switch is operating in the ON mode. This is confirmed by the magnitude of the ac electric field inside the active device presented in Fig.

10(f). Comparing the field distribution inside the plasmonic switch in the ON and OFF mode (Fig. 10(c) and 10(f)) at a single frequency, it is concluded that the field profile is largest at the proximity of the indentation edges and it decreases exponentially as moving to the perpendicular direction (y axis).

Figure 11 presents the transmission coefficient S_{21} of the optimized plasmonic switch as different voltages are applied between the p^{++} and n^{++}-type doped Ohmic contacts. The PIN diode is forward-biased as V_a rises above the threshold voltage $V_{th} = 5$ V. As illustrated in Fig. 11, the signal isolations can be further improved by increasing the applied voltage above V_{th}. This is due the increase of the carrier densities compared to the ones depicted in Fig. 10(a)-10(b). As illustrated in Fig. 11, the difference between the power of the transmitted signal in the ON ($V_{a\text{-}ON} = 0$ V) and the OFF ($V_{a\text{-}OFF} = 7$ V) modes can reach up to 14 dB at 320GHz, and the minimum expected isolation in the frequency range is about 7 dB. The insertion loss of the proposed device is less than 2dB in a wide frequency range.

In Fig. 12, the return losses of the THz plasmonic switch with the PIN diode under different bias voltages are shown. As illustrated, the return loss of the switch operating in the ON mode ($V_a = 0$ V) is better than -20 dB.
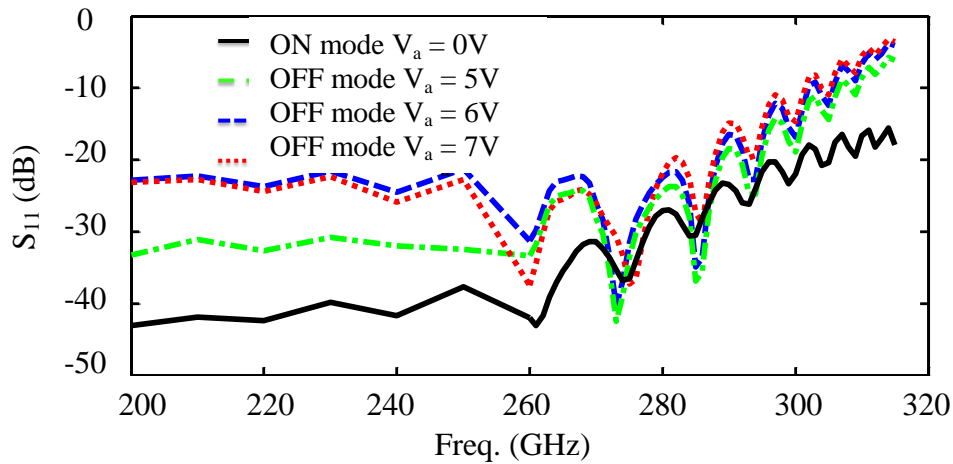

Fig. 12. Return losses of the optimized plasmonic switch (with the PIN diode) versus frequency as the device is operating in THz frequency range.

Conclusion:

In this paper, a THz plasmonic switch inside a silicon wafer is proposed and simulated. The results are presented using the scattering parameters of the active device. Due to the maturity of the semiconductor device fabrication techniques, it is anticipated that the proposed design can be implemented easily compared to the previously proposed plasmonic switches. However, the developed device suffers from high required control voltages. To address this challenge, an optimized design with an integrated PIN diode is suggested. As illustrated, the optimized switch provides comparatively high signal isolations and acceptable level of insertion losses. Moreover, it is shown that the device can operate in a wide THz frequency range. Additionally, it is expected that this design can be further improved by incorporating a variety of doped areas inside the device. For instance, this may be possible by increasing the number of the p^{++}-doped wells. Small input reflection coefficients of the designed switches suggest that they can be cascaded to achieve high signal isolations. We envision that the proposed switches may be useful in future all-integrated silicon-based THz plasmonic devices and communication systems.

References:

[1]   C. M. Armstrong, "The truth about terahertz," *IEEE Spectrum,* vol. 49, pp. 36-41, 2011.

[2]   C. W. Berry, N. Wang, M.R. Hashemi, M. Unlu, and M. Jarrahi, "Significant performance enhancement in photoconductive terahertz optoelectronics by incorporating plasmonic contact electrodes," *Nat. Commun.,* vol. 4, p. 1622, March 2013.

[3]   W. F. Andress, H. Yoon, K. Y. M. Yeung, L. Qin, K. West, L. Pfeiffer, and D. Ham, "Ultra-subwavelength two-dimensional plasmonic circuits," *Nano Lett.,* vol. 12, pp. 2272-2277, Apr. 2012.

[4]   T. Otsuji, T. Watanabe, S. A. B. Tombet, A. Satou, W. M. Kanp, V. V. Popov, M. Ryzhii, and V. Ryzhii, "Emission and detaction of terahertz radiation using two-dimensional electrons in III-V semiconductors and graphene," *IEEE Trans. Terahertz Sci. & Technol.,* vol. 3, pp. 63-71, Jan. 2013.

[5]   G. C. Dyer, S. Preu, G. R. Aizin, J. Mikalopas, A. D. Grine, J. L. Reno, J. M. Hensley, N. Q. Vinh, A. C. Gossard, M. S. Sherwin, S. J. Allen, and E. A. Shaner, "Enhanced performance of resonant sub-terahertz detection in a plasmonic cavity," *Appl. Phys. Lett.,* vol. 100, p. 083506, Feb. 2012.

[6]   M. A. Khorrami, S. El-Ghazaly, S. Q. Yu, and H. Naseem, "Compact terahertz surface plasmon switch inside a two dimensional electron gas layer," *IEEE MTT-S Int. Microwave Symp. Dig.,* Montreal, Canada, Jun. 2012.

[7]   M. A. Khorrami, S. El-Ghazaly, S. Q. Yu, and H. Naseem, "Terahertz plasmon amplification using two dimensional electron-gas layers," *J. App. Phys.,* vol. 111, p. 094501, May 2012.

[8]   M. A. Khorrami, S. El-Ghazaly, S. Q. Yu, and H. Naseem, "Analytical modeling of THz wave propagation inside ungated two dimensional electron gas layers," *IEEE MTT-S Int. Microwave Symp. Dig.,* Baltimore, Jun. 2011.

[9]   J. B. Pendry, L. Martin-Moreno, and F. J. Garcia-Vidal, "Mimicking plasmons with structured surfaces," *Science,* vol. 35, pp. 847-848, Jul. 2004.

[10]   Stefan A. Maier, *Plasmonics fundamentals and applications,* Springer, pp. 93-100, 2007.

[11]   L. Shen, X. Chen, and T. Yang, "Terahertz surface plasmon polaritons on periodically corrugated metal surfaces," *Optic Express,* vol. 16, p. 3326, Feb. 2008.

[12]   B. Wang, L. Liu, and S. He, "Propagation loss of terahertz surface plasmon polaritons on a periodically structured Ag surface," *J. Appl. Phys.,* vol. 104, p. 103531, Nov. 2008.

[13]   N. Yu, Q. J. Wang, M. A. Kats, J. A. Fan, S. P. Khanna, L. Li, A. Giles Davis, E. H. Linfield, and F. Capasso, "Designer spoof surface plasmon structures collimate terahertz laser beams," *nature materials,* vol. 9, pp. 730-735, Aug. 2010.

[14]   G. Liang, H. Liang, Y. Zhang, S. P. Khanna, L. Li, A. G. Davies, E. Linfield, D. F. Lim, C. S. Tan, S. F. Yu, H. C. Liu, and Q. J. Wang, "Single-mode surface-emitting concentric-circular-grating terahertz quantum cascade lasers," *App. Phys. Lett.,* vol. 102, p. 031119, Jan. 2013.

[15]   V. Konoplev, A. R. Phipps, A. D. R. Pheps, C. W. Robertson, K. Ronald, and A. W. Cross, "Surface field excitation by an obliquely incident wave," *App. Phys. Lett.,* vol. 102, p. 141106, Apr. 2013.

[16]   J. Gomez Rivas, J. A. Sanchez-Gil, M. Kuttge, P. H. Bolivar, and H. Kurz, "Optically switchable mirrors for surface plasmon polaritons propagating on semiconductor surfaces," *Phys. Rev. B,* vol. 74, p. 245324, Dec. 2006.

[17]   J. A. Sanchez-Gil, and J. G. Rivas, "Thermal switching of the scattering coefficients of terahertz surface plasmon polaritons impinging on a finite array of subwavelength grooves on semiconductor surfaces," *Phys. Rev. B.,* vol. 73, p. 205410, May 2006.

[18]   E. Hendry, M. J. Lockyear, J. Gomez Rivas, L. Kuipers, and M. Bonn, "Ultrafast optical switching of the THz transmission through metallic subwavelength hole arrays," *Phys Rev. B,* vol. 75, p. 235305, Jun. 2007.

[19]   K. Song, and P. Mazmuder, "Active terahertz spoof surface plasmon polariton switch comprising the perfect conductor metamaterial," *IEEE Trans. on Elect. Devices,* vol. 56, p. 2792, Nov. 2009.

[20]   Z. Xu, K. Song, and P. Mazumder, "Dynamic terahertz spoof surface plasmon-polariton switch based on resonance and absorption," *IEEE Trans. on Elect. Dev.,* vol. 58, pp. 2172-2176, Jul. 2011.

[21]   A. V, Krasavin, and N. Zheludev, "Active plasmonics: Controlling signals in Au/Ga waveguide using nanoscale structural transformations," *Appl. Phys. Lett.,* vol. 84, pp. 1416-1418, Nov. 2004.

[22]   K. F. MacDoland, Z. L. Samson, M. I. Stockman, and N. I. Zheludev, "Ultrafast active plasmonics," *Nature Photonics,* vol. 3, pp. 55-58, Dec. 2009.

[23]   Y. Urzhumov, J. S. Lee, T. Tyler, S. Dhar, V. Nguyen, N. M. Jokerst, P. Schmalenberg, and D. R. Smith, "Electronically reconfigurable metal-on-silicon metamaterial," *Phys. Rev. B.,* vol. 86, p. 075112, Aug. 2012.

[24]   Ansoft HFSS, Ansys Inc., Pittsburg, PA.

[25]   C. A. Balanis, *Advanced Engineering Electromagnetics,* 1rd edition, John Wiley & Sons, New Jeresey, 1989.

[26]   Atlas User's Manual, Silvaco, Santa Clara, CA, Jul. 2010.

[27]   M. van Exter, and D. Grischkowsky, "Optical and electronic properties of doped silicon from 0.1 to 2 THz," *Appl. Phys. Lett.,* vol. 56, pp. 1694-1696, Feb. 1990.

[28]   T. Jeon, and D. Grischkowsky, "Nature of conduction in doped silicon," *Phys. Rev. Lett.,* vol. 78, p. 1106, 1997.

[29]   C. C. Hu, *Modern Semiconductor Devices for Integrated Circuits*, Prentice Hall, Upper Saddle River, NJ, 2010.

[30]   S. E. Kocabas, G. Veronis, D. A. B. Miller, and S. Fan, "Transmission line and equivalent circuit models for plasmonic waveguide components," *IEEE J. Sel. Topics Quantum Electron.,* vol. 14, pp. 1462-1472, 2008.

[31]   J. S. Gomez-Diaz, and J. Perruisseau-Carrier, "Graphene-based plasmonic switches at near infrared frequencies," *Optics Exp.,* vol. 21, pp. 15490-15504, Jun. 2013.

[32]   P. Chen, C. Argyropoulos, and A. Alu, "Terahertz antenna phase shifters using integrally-gated graphene transmission-lines," *IEEE Trans. on Antenna Propag.,* vol. 61, pp. 1528-1537, Sep. 2013.

[33]   D. M. Pozar, *Microwave Engineering,* 3rd edition, John Wiley & Sons, New Jeresey 2005.

APPENDIX I:

UNIVERSITY OF ARKANSAS.

College of Engineering
Department of Electrical Engineering

May 17, 2014

To whom it may be concerned,

 I certify that Mr. Mohammadali Khorrami is the first author of the paper titled "Design and analysis of a silicon-based terahertz plasmonic switch," published in *Optics Express* in 2013. Mr. Khorrami completed the majority (more than 51 percent) of this research and writings of this paper.

Dr. Samir El-Ghazaly
Distinguished Professor
Electrical Engineering
Office: 3169 Bell Engineering Center
Phone: (479) 575-6048
Email: elghazal@uark.edu

3217 Bell Engineering Center • Fayetteville, AR 72701 • 479-575-3005 • Fax: 479-575-7967 • www.uark.edu
The University of Arkansas is an equal opportunity/affirmative action institution.

143

APPENDIX II:

Optics Express

Copyright and Permissions

Copyright Transfer

OSA asks all authors of articles for its journals, magazines, and books to sign a Transfer of Copyright. In doing so, an author transfers ownership of his or her article or book to OSA. Ownership of copyright gives OSA the right to publish the article and to defend against improper use (or even theft) of the article. It also permits OSA to mount the article online or to use the article in other forms, such as when a journal article becomes a chapter in an OSA-published book.

OSA needs copyright for an article because, as publisher, the society is in the best position to defend the article legally. In addition, transfer of copyright assures OSA that the work in question is entirely the author's own. Once again, the purpose of transfer of copyright is not to prevent the author from free publication of his or her own work, as long as this doesn't involve republication in a competing journal.

If you are planning to send a manuscript to one of OSA's peer-reviewed journals, you will be given the opportunity during submission to agree to our electronic transfer of copyright. **You should print and send a hard copy of the below Transfer of Copyright form only if you are unwilling or unable to use the online option.**

- OSA Copyright Transfer Agreement (PDF)
- Photonics Research Copyright Transfer Agreement (PDF)

Author Posting Policy

Transfer of copyright does not prevent an author from subsequently reproducing his or her article. OSA's Copyright Transfer Agreement gives authors the right to publish the article or chapter in a compilation of the author's own works or reproduce the article for teaching purposes on a short-term basis. **The author may also publish the article on his or her own noncommercial web page ("noncommercial" pages are defined here as those not charging for admission to the site or for downloading of material while on the site).** In addition, we allow authors to post their manuscripts on the Cornell University Library's arXiv site prior to submission to OSA's journals.

If the author chooses to publish the article on his or her own noncommercial websiteor on the arXiv site , the following message must be displayed at some prominent place near the article and must include a working hyperlink to OSA's journals website:

This paper was published in [Journal Name] and is made available as an electronic reprint with the permission of OSA. The paper can be found at the following URL on the OSA website: [article URL]. Systematic or multiple reproduction or distribution to multiple locations via electronic or other means is prohibited and is subject to penalties under law.

NIH Public Access Policy

The NIH Public Access Policy (http://publicaccess.nih.gov/) states that peer-reviewed manuscripts that received NIH funding and are accepted for publication in a journal on or after April 7, 2008, should be deposited with PubMed Central within 12 months of publication. OSA acknowledges the NIH policy and the author's right to place eligible OSA journal articles in PubMed Central. Biomedical Optics Express authors: Please note that OSA automatically submits all published articles to PMC. Optics Express authors: Please note that OSA automatically submits all NIH-funded articles to PMC.

- **How do I comply?** Authors who are required to do so may submit the accepted version of their manuscript to PubMed Central through the NIH Manuscript Submission System. Authors should select method "C" as explained on the NIH Public Access information page.
- **What about copyright transfer?** OSA's current Copyright Transfer Agreement in no way precludes deposit of OSA journal articles to PubMed Central (see http://www.opticsinfobase.org/submit/forms/copyxfer.pdf). Note that copyright to all material deposited in PubMed Central remains with the publisher or individual authors, whichever is applicable.

URLs for Early Posting and Final Articles

The following syntax can be used to create URLs to OSA articles. The URL is also displayed on the abstract page of any published article.

- **Final Version:** Append journal code, volume, issue, and final page number to the following base URL:

  ```
  http://www.opticsinfobase.org/abstract.cfm?URI=JOSAA-19-1-24
  ```

  See InfoBase Help for details.

- **Early Posting Version:** Append the ADS manuscript ID number (which appears on every Early Posting article) to the following base URL:

  ```
  http://www.opticsinfobase.org/abstract.cfm?msid=73530
  ```

  See the Early Posting FAQ for details.

One print or electronic copy may be made for personal use only. Systematic or multiple reproduction, distribution to multiple locations via electronic or other means, duplication of any material in this paper for a fee or for commercial purposes, or modification of the content of the paper are prohibited.

Permissions

For OSA to consider a copyright permission request we require in writing by fax, mail, or e-mail:

- a complete citation of the item to be reproduced, including figure numbers, etc.,
- a clear explanation of the intended use of the item, and
- the requestor's complete contact information.

Please direct further questions regarding copyright to copyright@osa.org.

V. BROADBAND EXCITATION AND ACTIVE CONTROL OF TERAHERTZ PLASMONS IN GRAPHENE

A. BROADBAND EXCITATION AND ACTIVE CONTROL OF TERAHERTZ PLASMONS IN GRAPHENE

Int. IEEE Microw. Symp., Tampa, FL, Jun. 2014.

Abstract:

A novel broadband technique to effectively launch plasmons along a single graphene layer at terahertz (THz) frequencies is proposed. To this end, the coupling of the electromagnetic wave from a readily available plasmonic waveguide established by a periodically corrugated metallic surface to the graphene sheet is proposed. As will be shown, this technique can significantly surmount the need for efficient excitation of plasmons in graphene. For this purpose, an analytical technique based on transmission line theory is employed to calculate the scattering parameters of the connection of the plasmonic waveguides. In this manner, the gating effects of the graphene waveguide on the input reflection and transmission of the junction are also

investigated. For comparison, a full wave numerical simulator is employed.

Introduction:

Graphene is a carbon-based, two-dimensional (2D) nanomaterial revealed less than a decade ago [1]. Afterwards, graphene has been extensively examined as a platform for future photonic and electronic devices. This is due to its extremely high carrier mobility at room and cryogenic temperatures (up to 230,000 cm^2 / Vs for suspended exfoliated graphene at T = 5 K [2]), as well as exceptional thermal and mechanical properties [3]. Additionally, the charge density and the surface conductivity of a graphene sheet can be effectively controlled by applying a perpendicular electric field. Moreover, surface waves coupled to carriers, mostly called plasmons can propagate distances up to 100 wavelengths along graphene layers with negligible attenuations in upper section of terahertz (THz) frequency range [4]. All these unique properties have made graphene a promising platform for future compact active plasmonic devices and systems [4]. Plasmonic structures implemented inside two-dimensional electron gas layers of hetero-structures [5]-[8] and graphene [9]-[10] have been vastly explored to develop compact terahertz sources and detectors. In addition, the emergence of plasmon-based logic gates [11] has introduced another beyond CMOS technology alternative that once combined with some of today's best logic design paradigms and practices [12]-[13] may revolutionize the future of computing. In spite of the numerous prospective applications of graphene-based structures, the key remaining challenge is how to efficiently excite the plasmons in graphene using an incident radiating mode electromagnetic wave. This problem is originated from the large phase mismatch between the incident and the plasmonic waves.

Recently, a near field scattering setup with an atomic force microscopy tip and infrared excitation light has been employed to launch plasmons along a graphene layer [14]. However,

this is very inefficient technique with very negligible percentage of incident field coupled to the surface wave [15]. Moreover, surface acoustic waves [16] and modulated graphene conductivity [17] have been suggested to launch graphene plasmons. Subsequently, plasmon excitation along a graphene sheet laid over a fabricated silicon diffractive grating and illuminated by an incident radiating mode EM field has been achieved in [15]. Unfortunately, the suggested technique is successful only in a single wave number which is related to the silicon grating period. Therefore, the urgent need to effectively launch the propagating plasmonic mode along graphene layers in a wide frequency range still exists.

In this paper, the possibility of launching the plasmons along a suspended graphene sheet using another plasmonic waveguide is investigated. As will be shown, the surface wave on the interface of a corrugated metal and a dielectric can appropriately launch plasmons along a suspended graphene layer at terahertz frequencies. These specific surface waves traveling on the exterior of a metal with engineered cuts and grooves are mostly called Spoof Surface Plasmon Polaritons (SSPPs) [18]. The SSPPs can be effectively launched using a network analyzer source or a quantum cascade laser. Here, the transmission and the input reflection of the plasmonic wave traveling from the indented metallic structure to a suspended graphene sheet are considered in a wide frequency range. To report and compare the results, conventional microwave theory scattering parameter notation is used.

<u>Simulation details:</u>

Fig. 1.(a) depicts a metallic surface corrugated with linearly spaced grooves with period D, distance (D - A), height H, filled with a dielectric (air) with permittivity $\varepsilon_{\text{r-SSPP}} = 1$. On the last edge of the indented metal, a graphene layer is located (see Fig. 1.(a)). Here, the details of the analytical and full wave simulation of the structure in Fig. 1. (a) are described.

1. 2D plasmons along graphene

The surface conductivity of the graphene layer σ_g is mostly calculated by Kubo formalism [4]. Using the computed conductivity, it can be proved that a TM^x mode electromagnetic wave (known as 2D plasmons) may propagate along a graphene sheet as $|E_F| > \bar{h} \times \omega$ [4], where E_F, $\bar{h}$ and $\omega = 2\pi \times f$ are graphene Fermi energy, reduced Planck constant and radial frequency, respectively. The condition is easily satisfied in terahertz and infrared frequency range. Furthermore, the Fermi energy can be altered by applying perpendicular electric fields E_0 (see Fig. 1 (a)). The surface wave field variations follow $\exp\left(j\omega t - \gamma_G x - \delta_{G1,2} y\right)$, where $\delta_{G1} = \delta_G$ as $y \geq 0$ and $\delta_{G2} = -\delta_G$ if $y < 0$. Besides, $\gamma_G = \alpha_G + j \times \beta_G$, α_G and β_G are the 2D plasmon propagation, attenuation and phase constants, respectively. After solving Maxwell equations and applying boundary conditions, the dispersion relation of the 2D plasmons is obtained:

$$\gamma_G = \pm \sqrt{\frac{4\omega^2 \varepsilon_G^2}{\sigma_G^2} - \frac{\omega^2 \varepsilon_{r-G}}{c^2}} \tag{1}$$

where, $\varepsilon_G = \varepsilon_0 \times \varepsilon_{r-G}$ ($\varepsilon_0 = 8.85 \times 10^{-12}$ F / m) and $c = 3 \times 10^8$ (m/s) [15]. Moreover, the graphene characteristic impedance is chosen similar to the TM^x mode wave impedance $Z_G = \gamma_G / (j\omega \times \varepsilon_G)$. Here, the measured transport parameters of the suspended graphene layer (in air $\varepsilon_{r-G} = 1$) with extremely high electron mobility $\mu = 230,000$ cm^2 V^{-1} s^{-1} at T = 5K is considered [2].
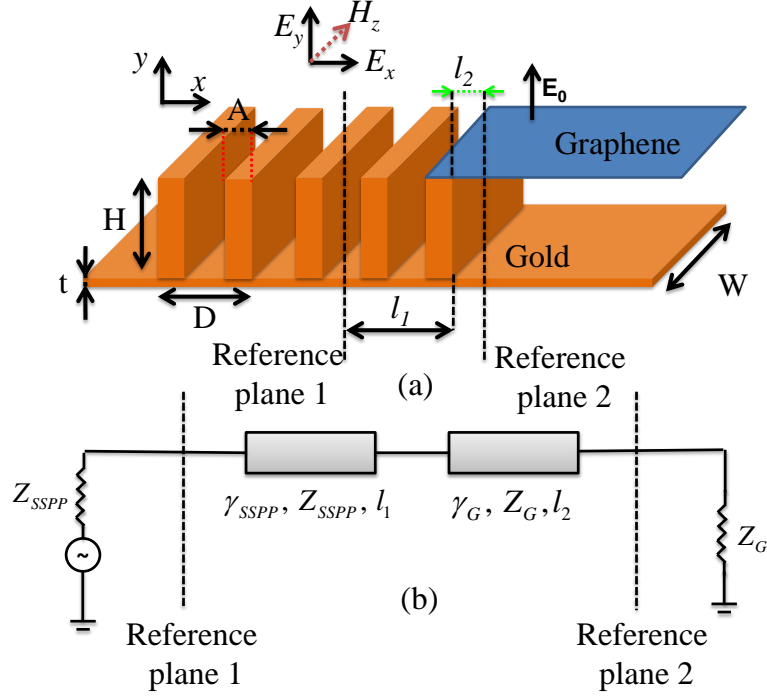
Fig. 1. (a) Proposed mechanism to excite 2D plasmons of a graphene sheet using SSPPs along a periodically indented metallic surface.

2. Spoof surface plasmon polaritons along a corrugated metal:

As proved in [19], the dispersion relation of the fundamental plasmonic mode (with components E_x, E_y and H_z) that can propagate along an indented perfect electric conductor filled with a dielectric (with relative permittivity $\varepsilon_{r\text{-SSPP}}$) is:

$$\frac{\sqrt{\beta_{SSPP}^2 - k^2_0}}{k_0} = S^2_0 \tan\left(k_0 h\right), \tag{2}$$

where, $S_0 = [(D-A)/D]^{0.5} \times \text{sinc}\,(\beta_{SSPP} \times (D - A)/2)$ and $k_0 = \omega\sqrt{\varepsilon_{r\text{-SSPP}}}/c$. In (2), β_{SSPP} is the phase constant of the SSPPs and $k_0 = \omega/c$. As the perfect electric conductor is substituted with a metal (gold here), the SSPP Ohmic attenuations are considered using the formulation in [19]. In this manner, SSPP propagation constant $\gamma_{SSPP} = \alpha_{SSPP} + j \times \beta_{SSPP}$ can be obtained, where α_{SSPP} is the attenuation constant. Similarly, the characteristic impedance of this transmission line is

150

selected equal to the SSPP fundamental mode wave impedance: $Z_{SSPP} = \gamma_{SSPP} \big/ \left(j\omega \times \varepsilon_{SSPP} \right)$

where $\varepsilon_{SSPP} = \varepsilon_0 \times \varepsilon_{r\text{-}SSPP}$. Here, A = 20 μm, H = 70 μm, D= 60 μm have been considered in the design. The thickness of the metallic surface "t" is assumed to be larger compared to the skin depth in the interested frequency range.

3. Details of the full-wave simulation and the analytical model:

The electromagnetic modeling of the proposed structure is performed using two different approaches, namely a transmission line (TL) formalism and a full wave simulator [20].

The transition of the electromagnetic wave from the SSPP on the grooved metallic surface to the 2D plasmons on the graphene layer can be characterized by cascading two TLs depicted in Fig. 1 (b). To this end, a section of the indented metallic surface with length l_1, characteristic impedance Z_{SSPP} and propagation constant γ_{SSPP} is considered as the first TL. The other sections of the SSPP waveguide and the exciting field are represented as a voltage source with internal resistance Z_{SSPP}. Furthermore, a small portion of the suspended graphene sheet adjacent to the metallic edge, with length l_2 is represented as the second TL with characteristic impedance Z_G and propagation constant γ_G. The remaining part of the graphene layer is recognized as a load with impedance Z_G. In this manner, the scattering parameters of the equivalent circuit in Fig. 1 (a), calculated at reference planes 1 and 2, may be obtained using TL theory. This method provides a fast solution of the mentioned problem. However, it cannot include the effects of higher order modes which exist in the vicinity of the junction of the waveguides. These evanescent higher order modes exist near the discontinuity because of different characteristic impedances and propagation constants of the TLs. The evanescent modes specifically cause higher than expected attenuations, due to impedance mismatch.

For comparison and to provide more accurate results, a complete solution of Maxwell equation

is performed using the numerical solver [20]. The simulation domain is excited by applying a wave port at x = 0 plane. In order to calculate scattering parameters, the methodology proposed in [16] is followed.

Results and Discussion:

In Fig. 2, the phase constants of the SSPPs and the 2D plasmons of the graphene sheet with various applied electric fields E_0 are depicted. As depicted in Fig. 2, the plasmons along both structures obtain higher momentums compared to the radiating mode counterpart (k_0), especially as f > 500 GHz. Moreover, slight changes in the chemical potential of the graphene lead to considerable variations in the 2D plasmon phase constants. It is also observed that there exists a single frequency for each Fermi energy, which the properties of the 2D plasmons are exactly similar to the ones of the SSPPs. It is expected that the transition of EM field from the SSPP to the plasmons on graphene can be ideally occurred at this frequency. Moreover, the differences between the phase constants of the 2D plasmons with E_F = 0.18 and 0.16 eV, and the properties of the SSPPs are not very not very deep. Therefore, it is anticipated that an acceptable level of impedance matching between these waveguides may exist for these specific chemical potentials of the graphene.

Fig. 3 and Fig. 4 depict the calculated transmission (S_{21}) and input reflection (S_{11}) of the plasmonic waves. As shown in Fig. 3, the EM energy is transferred from the SSPPs to 2D plasmons with acceptable level of attenuation. Additionally, this technique is effective in a wide frequency range. Considering the input reflection coefficient in Fig. 4, it is understood that the matching between the transmission lines may be optimized in a certain frequency by changing the graphene chemical potential. The frequency of the minimum reflection coefficient in Fig. 4 is identical to the crossing point of the dispersion relations of the 2D plamsons and SSPPs.
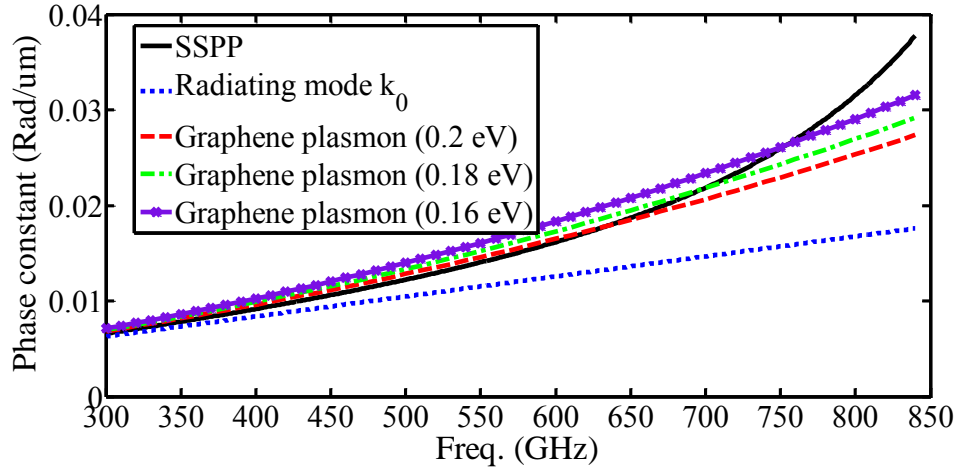
Fig. 2. Dispersion relation of the plasmons along the periodically corrugated metal and a suspended graphene with different Fermi energy levels obtained by the analytical model.
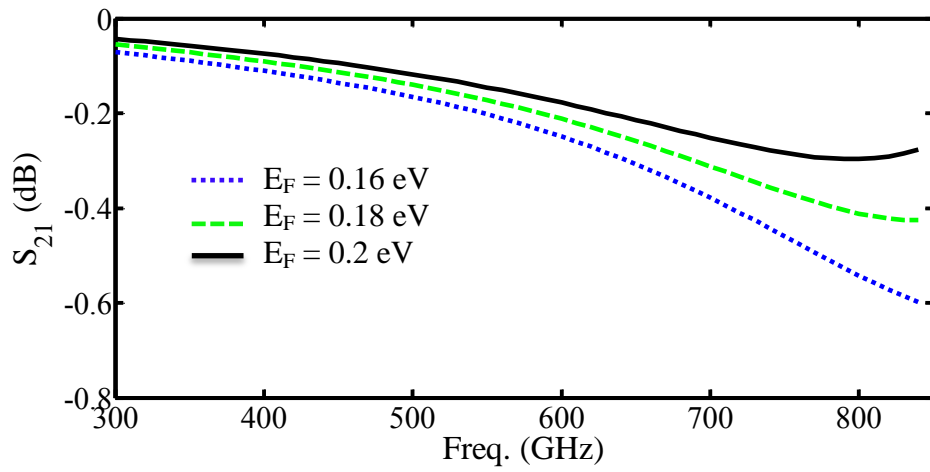

Fig. 3. Wave transmission from the corrogated metal to the suspended graphene with different Fermi energy levels.
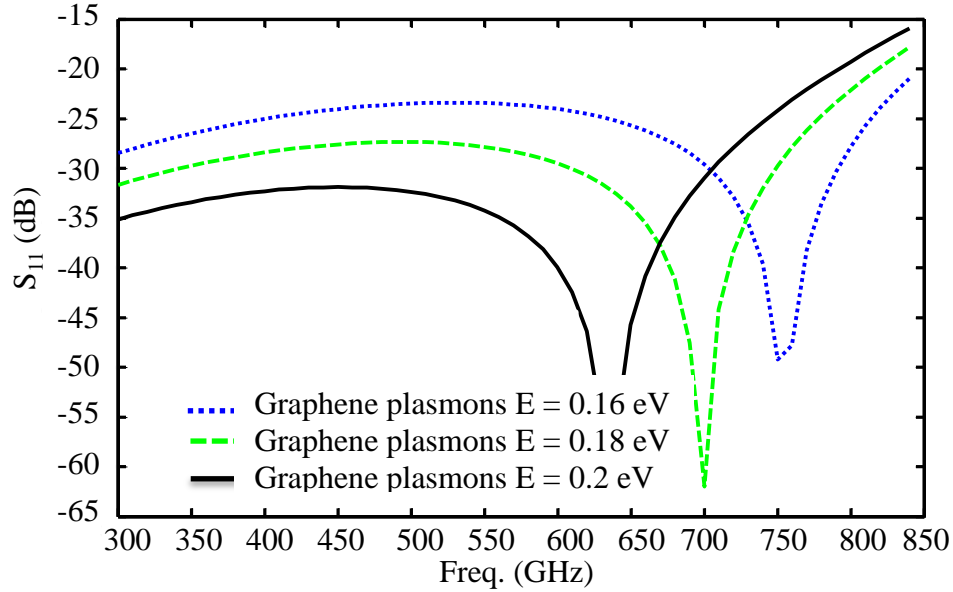
Fig. 4. Input wave reflection as transiting from the metallic surface to the graphene sheet with different Fermi energy levels.

Fig. 5, 6 presents a comparison between S_{11} and S_{21} of the structure in Fig. 1. (a) (as $E_F = 0.16$ eV) obtained by the analytical and numerical models. As depicted, there is a good similarity between estimated transmission using different approaches. However, HFSS predict slightly higher attenuations throughout the simulated frequency range which is due to the consideration of higher order modes which are not included into the analytical model. Favorably low S_{11} reported by both methods verify the usefulness of the proposed technique to launch 2D plasmons in a wide frequency range.
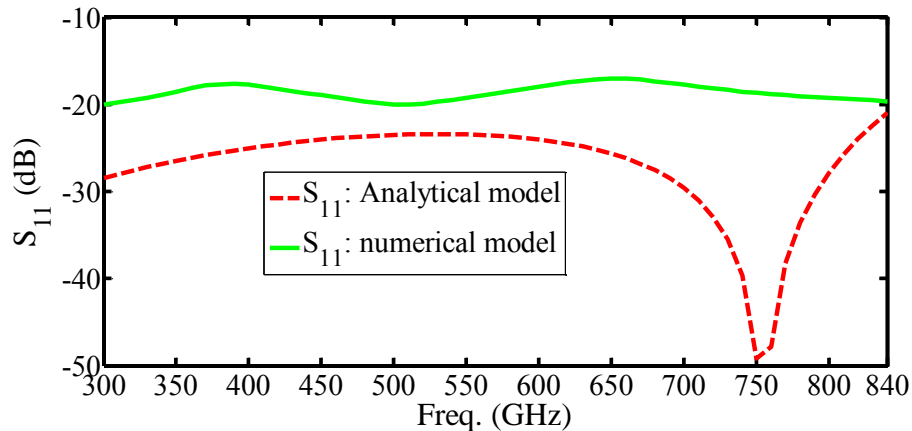

154

Fig. 5. A comparison between the reflection coefficients (as $E_F = 0.16$ eV) calculated by the TL model and numerical solver.
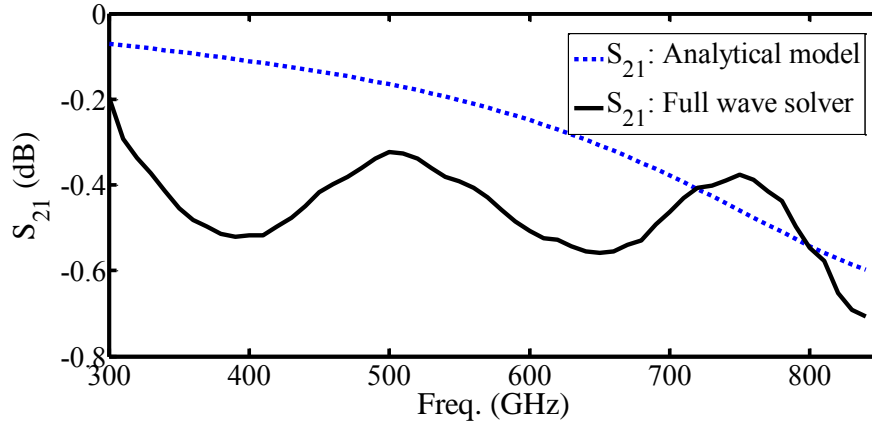

Fig. 6. A comparison between the transmission coefficients (as $E_F = 0.16$ eV) calculated by the TL model and numerical solver.

Conclusion:

In this paper, a promising technique to effectively launch 2D plasmons in a suspended graphene layer using spoof surface plasmons polaritons along a periodically indented metal is proposed. To show the effectiveness of the suggested method, an analytical technique based on transmission line theory is proposed. To verify the results, a full-wave commercial solver is employed.

References:

[1]   K. S. Novoselov, A. K. Geim, S. V. Morozov, D. Jiang, M. I. Katsnelson, I. V. Grigorieva, S. V. Dubonos, and A. A. Firsov, "Two-dimesnional gas of massless Dirac fermions in graphene," *Nat.,* vol. 438, pp. 197-200, Nov. 2005.

[2]   K.I. Bolotin, K.J. Sikes, Z. Jiang, M. Klima, G. Fudenberg, J. Hone, P. Kim and H.L. Stormer, "Ultrahigh electron mobility in suspended graphene," *Solid State Comm.,* vol. 146, pp. 351-355, Mar. 2008.

[3]   A. K. Geim, and K. S. Novoselov, "The rise of graphene," *Nat. Mater.,* vol. 6, pp. 183-191, 2007.

[4]   W. Gao, J. Shu, C. Qiu, and Q. Xu, "Excitation of plasmonic waves in graphene by guided-mode resonances," *ACS Nano,* vol. 6, no. 9, pp. 7806-7813, Aug. 2012.

[5]   M. A. Khorrami, S. El-Ghazaly, S. Q. Yu, H. Naseem, "THz plasmon amplification using two-dimensional electron-gas layers," *J. of Appl. Phys.*, vol. 111, p. 09450, May 2012.

[6] M. A. Khorrami, S. El-Ghazaly, S. Q. Yu, H. Naseem, "Analytical modeling of THz wave propagation inside ungated two dimensional electron gas layers," *2011 IEEE Int. Microwave Symp. Dig.*, Baltimore, MD, Jun. 2011.

[7] M. A. Khorrami, S. El-Ghazaly, H. Naseem, and S. Q. Yu, "Global modeling of active terahertz plasmonic devices," *IEEE Trans. on THz Sci. & Technol.*, vol. 4, no. 1, pp. 101-109, Jan. 2014.

[8] M. A. Khorrami, S. El-Ghazaly, S. Q. Yu, H. Naseem, "A novel THz plasmonic switch," *2012 IEEE Int. Microwave Symp. Dig.*, Montreal, Canada, Jun. 2012.

[9] V. W. Brar, M. S. Jang, M. Sherrott, J. J. Lopez, and H. A. Atwater, "Highly confined tunable mid-infrared plasmonics in graphene nanoresonators", *Nano Lett.,* Apr. 2013.

[10] H. Yan, X. Li, B. Chandra, G. Tulevski, Y. Wu, M. Freitag, W. Zu, P. Avouris and F. Xia, "Tunable infrared plasmonic device using graphene /insulator stacks", *Nature Nanotech.,* vol. 7, pp. 330-334, May 2012.

[11] H. We, Z. Wang, X. Tian, M. Kall, and H. Xu, "Cascaded logic gates in nanophotonic plasmon networks," *Nature Communications*, vol. 2, p. 387, Jul. 2011.

[12] F. A. Parsan, W. K. Al-Assadi, S. C. Smith, "Gate Mapping Automation for Asynchronous NULL Convention Logic Circuits," *IEEE Trans. on Very Large Scale Integ. (VLSI) Syst.*, vol. 22, no.1, pp. 99-112, Jan. 2014.

[13] F. A. Parsan, S. C. Smith, "CMOS implementation comparison of NCL gates," Circuits and Systems (MWSCAS), 2012 IEEE 55th International Midwest Symposium on, Aug. 2012.

[14] J. Chen, M. Badioli, P. Alonso-Gonzalez, S. Thongrattanasiri, F. Huth, J. Osmond, M. Spasenovic, A. Centeno, A. Pesquera, P. Goldignon, A. Z. Elorza, N. Camara, F. J. Garcia-de-Abajo, R. Hillenbrand, and F. H. L. Koppens, "Optical nano-imaging of gate-tunable graphene plasmons," *Nature,* vol. 487, pp. 77-81, Jul. 2012.

[15] W. Gao, G. Shi, Z. Jin, J. Shu, Q. Zhang, R. Vajtai, P. M. Ajayan, J. Kono, and Q. Xu, "Exciation and active control of propagating surface plasmon polaritins in graphene," *Nano Lett.,* vol. 13, pp. 3698-3702, Jul. 2013.

[16] J. Schiefele, J. Pedros, F. Sols, F. Calle, and F. Guinea, "Coupling light into graphene plasmons through surface acoustic waves," *Phys. Rev. Lett.*, vol. 111, p. 237405, Dec. 2013.

[17] Y. V. Bludov, A. Ferreira, N. M. R. Peres, and M. I. Vasilevskiy, "A primer on surface plasmon-polaritons in graphene," *Int. J. Mod. Phys. B*, vol. 27, p. 1341001, Apr. 2013.

[18] M. A. Khorrami, S. El-Ghazaly, "Design and analysis of a silicon-based terahertz plasmonic switch," *Optics Express*, vol. 21, no. 21, pp. 25452-25466, Oct. 2013.

[19] A. Rusina, M. Durach, M. I. Stockman, "Theory of spoof plasmons in real metals," *Appl. Phys. A,* vol. 100, no. 2, pp. 375-378, Aug. 2010.

[20] Ansoft HFSS, Ansys Inc., Pittsburg, PA.

UNIVERSITY OF
ARKANSAS.

College of Engineering
Department of Electrical Engineering

May 17, 2014

To whom it may be concerned,

I certify that Mr. Mohammadali Khorrami is the first author of the paper titled "Broadband excitation and active control of terahertz plasmons in graphene," presented in *IEEE International Microwave Symposium* in 2014. Mr. Khorrami completed the majority (more than 51 percent) of this research and writings of this paper.

Dr. Samir El-Ghazaly
Distinguished Professor
Electrical Engineering
Office: 3169 Bell Engineering Center
Phone: (479) 575-6048
Email: elghazal@uark.edu

APPENDIX II:

Copyright Clearance Center

RightsLink®

Home   Create Account   Help

IEEE
Requesting permission to reuse content from an IEEE publication

Title: Compact terahertz Surface Plasmon switch inside a Two Dimensional Electron Gas layer

Conference Proceedings: Microwave Symposium Digest (MTT), 2012 IEEE MTT-S International

Author: Ali Khorrami, Mohammad; El-Ghazaly, S.; Shui-Qing Yu; Naseem, Hammed

Publisher: IEEE

Date: 17-22 June 2012

Copyright © 2012, IEEE

Thesis / Dissertation Reuse

The IEEE does not require individuals working on a thesis to obtain a formal reuse license, however, you may print out this statement to be used as a permission grant:

Requirements to be followed when using any portion (e.g., figure, graph, table, or textual material) of an IEEE copyrighted paper in a thesis:

1) In the case of textual material (e.g., using short quotes or referring to the work within these papers) users must give full credit to the original source (author, paper, publication) followed by the IEEE copyright line © 2011 IEEE.
2) In the case of illustrations or tabular material, we require that the copyright line © [Year of original publication] IEEE appear prominently with each reprinted figure and/or table.
3) If a substantial portion of the original paper is to be used, and if you are not the senior author, also obtain the senior author's approval.

Requirements to be followed when using an entire IEEE copyrighted paper in a thesis:

1) The following IEEE copyright/ credit notice should be placed prominently in the references: © [year of original publication] IEEE. Reprinted, with permission, from [author names, paper title, IEEE publication title, and month/year of publication]
2) Only the accepted version of an IEEE copyrighted paper can be used when posting the paper or your thesis on-line.
3) In placing the thesis on the author's university website, please display the following message in a prominent place on the website: In reference to IEEE copyrighted material which is used with permission in this thesis, the IEEE does not endorse any of [university/educational entity's name goes here]'s products or services. Internal or personal use of this material is permitted. If interested in reprinting/republishing IEEE copyrighted material for advertising or promotional purposes or for creating new collective works for resale or redistribution, please go to http://www.ieee.org/publications_standards/publications/rights/rights_link.html to learn how to obtain a License from RightsLink.

If applicable, University Microfilms and/or ProQuest Library, or the Archives of Canada may supply single copies of the dissertation.

VI.   CONCLUSION AND FUTURE WORKS

A.   CONCLUSION:

In this work, the plasmon propagations along two-dimensional electron gas layers of biased hetero-structures are analyzed both analytically and numerically. To this end, Maxwell and electronic transport equations are being solved simultaneously. In the analytical model, several simplifying assumptions have been taken into account to make the analysis possible. These include disregarding Ohmic contacts on the sides of the hetero-structure and the existence of homogenous materials surrounding the electron gas layer. In the proposed numerical simulation, finite difference time domain technique is employed to solve Maxwell equation. Additionally, finite difference scheme is utilized as discretizing electronic transport equations. In the multi-physics simulator, several presumptions, considered in the analytical model, have been eliminated. As example, the presence of Ohmic contacts and metallic grating on the top surface of the hetero-structure are included in the numerical solver.

As presented, the conventional understanding of wave propagation along biased 2D layers is changed by the developed model. This is due to the division of symmetrical plasmonic modes into new asymmetrical ones in the bias device, which has not been previously reported. The results of this research prove the possibility of steering and amplifying terahertz signals using these plasmonic structures. As an example, a compact and fast plasmonic switch is designed and simulated that can offer very high signal isolations in the interested frequency range.

In the second phase of this research, a silicon-based plasmonic switch is proposed and simulated in THz frequency range. The THz plasmonic modulator is implemented inside a corrugated n-type silicon substrate which is covered by a metal to achieve a Schottky contact. In this manner, the propagation of the plasmons along indented structure is controlled. To optimize the design, the employment of an intrinsic silicon substrate with a P-Intrinsic-N diode is

proposed. As will be described, employing highly p++ and n++-type doped areas inside the wafer leads to the formation of the P-I-N diode. The design begins with a finite element solution of the well-known drift-diffusion and Poisson equations using a numerical solver to compute the charge distribution in the diode. As mentioned, the electrical conductivity of the silicon can be obtained using Drude model and with the aid of the calculated charge density. Subsequently, plasmon propagation along the structure is characterized for each bias voltage using a full wave numerical solver. The results are stated in the form of scattering parameters in a wide frequency range.

In the last section of this research, an efficient methodology to launch 2D plasmons along graphene is proposed. To this end, plasmons along periodically grooved metallic surface are successfully coupled onto a graphene mono-layer. To analyze the proposed design, a fast and accurate transmission line representation of the plasmonic waveguides is utilized. For comparison, a full wave simulator is employed. It is observed that a wide band coupling of THz signal onto graphene is achievable which make this design very desirable in modern plasmonic systems.

B.   FUTURE WORKS:

There are several future paths to continue the research in every aspect of this work.

1. Design, simulation and fabrication of plasmonic devices inside two-dimensional conductors:

There are several challenges that need to be address before an efficient THz amplifier can be designed and fabricated. One of these bottlenecks is the lack of an appropriate plasmonic waveguide which can excite the growing mode inside the THz source and extract the generated field effectively. The availability of global modeling can help engineers to employ the

appropriate waveguides and matching networks into the design of THz plasmonic amplifiers to transform the success of THz emission observations from biased hetero-structures into advanced THz plasmonic amplifiers with acceptable level of voltage gain. Moreover, the presented multi-physics analysis can open a new venue in the simulation of modern active plasmonic devices. Therefore, it is expected that new sets of plasmonic active structures can be designed and employed in modern compact systems.

2. Silicon-based plasmonic modulator:

It is expected that the presented switch becomes popular in THz band due to high switching speed and ease of fabrication on the silicon platform. In the future, the number and locations of the doped areas inside the silicon wafer can even further improve the functionality of the device. Additionally, the design can be optimized by changing the doping densities of the employed wafer.